

**Investigations into the Tectonic Lineaments and Thermal
Structure of Lake Magadi, Southern Kenya Rift using
Integrated Geophysical Methods**

Akinola Adesuji Komolafe
March, 2010

Investigations into the Tectonic Lineaments and Thermal Structure of Lake Magadi, Southern Kenya Rift using Integrated Geophysical Methods

by

Akinola Adesuji Komolafe

Thesis submitted to the International Institute for Geo-information Science and Earth Observation in partial fulfilment of the requirements for the degree of Master of Science in Geo-information Science and Earth Observation, Specialisation: Earth Resources Exploration

Thesis Assessment Board

Prof. Dr. F.D. Van der Meer (Chairman)

Prof. Dr. S. Kroonenberg (External Examiner)

Dr. T. Woldai (First supervisor)

Dr. M.F. Noomen (Second Supervisor)

Observer :

Drs T.M. Loran (Program Director)



**INTERNATIONAL INSTITUTE FOR GEO-INFORMATION SCIENCE AND EARTH OBSERVATION
ENSCHDEDE, THE NETHERLANDS**

Disclaimer

This document describes work undertaken as part of a programme of study at the International Institute for Geo-information Science and Earth Observation. All views and opinions expressed therein remain the sole responsibility of the author, and do not necessarily represent those of the institute.

Abstract

In this research, the tectonic lineaments and thermal structure around Lake Magadi, southern Kenya rift were investigated in order to explore its geothermal potential using integrated geophysical methods. Surface lineaments around this Lake and their influence on the hot springs manifestations along its margins have not been previously investigated. Also, depth to the heat source which could provide information on the thermal structure and geodynamic activities in the area has not been delineated using aeromagnetic data despite the vast expression of geothermal resources on the surface. The structural information of the area was derived from the enhanced AsterDEM and Aster images, supplemented by the existing lineaments map of the area. Five N-S Faults in the south of study area, within Magadi basin, close to the known hot springs were identified for ground investigation using combined Electrical Resistivity Tomography (ERT) and Ground Magnetic Survey. These were further probed to greater depths with aeromagnetic data using 2D Euler deconvolution. The heat source (Curie point) depth was delineated by analysing the aeromagnetic data using power spectral method.

The subsurface constituents of the investigated structures revealed a funnel-shaped fluid-filled (mostly saline hydrothermal) zone with a relatively low resistivity values of less than $1\Omega\text{m}$, separated by resistive structures to the west and east, to a depth of 75m along the ERT profiles. The ERT shows an upward flow of saline hydrothermal fluid to the surface through the fault splays. The gradual downward increase in resistivity values within the ERT profiles show the salinity differences from the near surface to the subsurface. Ground magnetic profiles revealed subsurface faulting/tectonic activities up to a depth of 400m and the presence of fluid-filled zones within the basin which are marked by the absence of magnetic sources. These complimentary methods confirm the fluid-filled high micro crack porosity in the upper crust and also show that the N-S faults structures in the south of the lake serve as fluid conduits which support the upward flow of the hydrothermal fluid along its margin. A deeper investigation into the lineaments from the aeromagnetic data showed that the surface faults extend into a depth of 7.5 km in the subsurface. These faults are probably the parallel faults which bound the basin/graben to the west and to the east.

The spectral analysis of the aeromagnetic data revealed the emplacement of Magadi Curie point (heat source) at the depth of 12.1km. This estimation is consistent with the existing crustal model proposed by other researchers. This depth marked the transition point between the ductile and brittle crust. The shallowness of this depth implies a high heat flow around Lake Magadi; this is supported by the surface manifestations of hot springs along its margins. The correlation of the heat source, subsurface tectonic activities and seismic hypocenters showed that the seismogenic zone exist directly on top of the magma intrusion (heat source) and forms the commencement of geodynamic activities.

Keywords: Lake Magadi, Curie Point, Electrical Resistivity Tomography, Ground Magnetic Survey, Aeromagnetic, AsterDEM, Seismogenic, Geothermal, geodynamics and Tectonics Lineaments

Acknowledgements

Firstly, I am indeed grateful to the Almighty God for the sustenance, strength and the successful completion of my Msc program. Many thanks to the Netherlands Fellowship Program (NFP) for making my dream a reality.

My profound gratitude goes to my Supervisors, Dr. T. Woldai and Dr. M.F. Noomen for their technical guidance, constructive comments, critical reading and directions. I want to thank the Applied Earth Science (AES) Course Director, Drs T.M. Loran and the Chairman of the department of Earth System Analysis, Prof. Dr. F.D.Vander Meer for their efforts in ensuring a successful running of the Msc program. I am grateful to Dr. M. van der Meijde for his constructive criticisms and his guidance during the geophysical data processing and interpretation. I thank the trio of Dr. F.J.A. van Ruitenbeek, Drs. J.B. de Smeth and Dr. E.J.M. Carranza of Earth Resource Exploration stream for their company and valuable instructions during this program.

I cannot but appreciate my PhD advisor, Mr Zack Kuria for field work guidance and hospitality, and also the full support during the research phase. I appreciate the concerted efforts of the staff of the geophysics and geology department of the Kenya Electricity Generating Company (Kengen), University of Nairobi and Kenya Ministry of Mineral Resources in ensuring the availability of their geophysical equipments during the field work. Thanks to Dr. Sally Barrit for providing the aeromagnetic data of the study area.

Undoubtedly, my unreserved gratitude goes to my Sweet Heart, Love and World, Mrs Ronke Justina Komolafe (Msc) and my Daughter, Peace Oluwakemi Komolafe for their patience and unbroken link during my Msc Program. I am highly indebted to my extended family for their supports during my struggle. Thanks to Mr. Okhumale Emmanuel, Managing Director, Easytracks Communications Ltd and Mr. Ayoola Olalusi, Managing Director, Pathway and Company Limited for their encouragements and supports during my stay in Netherlands. Many thanks to the Pastors and Members of Deeper Life Bible Church, Netherlands for their spiritual and moral supports during my Msc study.

To all my instructors and colleagues in the department of Applied Earth Science, I say thank you.

Komolafe Akinola Adesuji

To my dearest wife and daughter

Table of contents

1.	Introduction.....	1
1.1.	Problem Statement.....	2
1.2.	Objectives.....	2
1.2.1.	General Objectives	2
1.2.2.	Specific Objectives	2
1.3.	Research Questions	2
1.4.	Hypotheses.....	3
1.5.	Datasets and Research Setup.....	3
1.5.1.	Datasets.....	3
1.5.2.	Software	3
1.5.3.	Setup of Research	3
1.6.	Organization of the Thesis	5
2.	Literature Review.....	6
2.1.	Study Area Location.....	6
2.2.	Geology and Tectonic Settings of the Kenya Rift	8
2.3.	Geology of Lake Magadi.....	9
2.4.	Role of Faults and Fractures on Crustal Fluids	12
2.5.	Geothermal System: Process and Model.....	13
2.6.	Applications of Resistivity Tomography in Fluid Conduits Mapping	14
2.6.1.	Electrical Resistivity Method	14
2.6.2.	Fluid Conduits Mapping with Resistivity	15
2.7.	Ground Magnetic Method	16
2.8.	Curie-Point Depth	17
3.	Remote Sensing Data Processing and Analysis	20
3.1.	Aster Image processing	20
3.2.	Digital Elevation Model Processing and Enhancements	20
3.3.	Structural Mapping.....	21
4.	Geophysical Imaging of Fluid Conduits around Lake Magadi	24
4.1.	Electrical Resistivity Survey.....	24
4.1.1.	Resistivity Meter	24
4.1.2.	Data Collection.....	25
4.1.3.	Resistivity Data Inversion	26
4.1.4.	Geo-resistivity structures along Resistivity Profiles.....	27

4.2.	Ground Magnetic Survey	30
4.2.1.	Instrument	30
4.2.2.	Data Collection.....	30
4.2.3.	Magnetic Data Corrections.....	31
4.2.4.	Data Enhancements and Analysis.....	32
4.2.5.	Magnetic Data Interpretations	36
4.3.	Aeromagnetic Data Analysis.....	40
4.3.1.	2D Interpretation of the Aeromagnetic Profiles.....	42
5.	Magadi Heat Source Depth Estimation	44
5.1.	Curie Point Depth Estimation from Aeromagnetic Data.....	44
5.1.1.	Spectral Analysis and Curie Point Depth Estimation.....	44
6.	Data Integration.....	46
6.1.	Subsurface Fluid Conduits Characteristics from Geophysical Imaging.....	46
6.1.1.	Linking surface Tectonic Lineaments to the Subsurface	47
6.2.	Lake Magadi Curie point depth: Implication on the Seismicity and Geothermal Resources	50
7.	Conclusions and Recommendation	52
7.1.	Conclusions	52
7.1.1.	Subsurface constituents of tectonic lineaments in the south of Lake Magadi.....	52
7.1.2.	Lake Magadi Geothermal Systems.....	52
7.1.3.	Geodynamic activities around Lake Magadi: Inference from the estimated heat source depth.	53
7.1.4.	Influence of N-S structures on the Geothermal Resources around Lake Magadi	54
7.3.	Recommendation	55
	References	56
	Appendices	60

List of figures

Figure 1.1. Research methodology flow chart.....	4
Figure 2.1. (a) Geographic location of Magadi area by Atmaoui and Hollnack (2003), (b) RGB colour composite of Aster bands 7-3-1 draped over SRTM DEM, showing the study and survey areas, and (c) field photo showing part of the study area and associated springs.	7
Figure 2.2. East African Rift System showing the location of Kenya Rift after Chorowicz (2005)	8
Figure 2.3. Simplified Geology map of the study area after Baker (1958).....	10
Figure 2.4. Upper crustal structure of Lake Magadi after Simiyu and Keller (1998)	11
Figure 2.5. Lineaments map of Lake Magadi overlaid on SRTM DEM. Modified after Sequar (2009)	12
Figure 2.6. Schematic representation of a typical geothermal system by Mary and Mario (2004)	13
Figure 2.7. Map of the Kenya Rift Valley showing location of the significant geothermal areas from Simiyu and Keller (2000).....	14
Figure 2.8. Radially averaged power spectrum from aeromagnetic data after Blanco-Montenegro et al. (2003).....	18
Figure 2.9 Example of average power spectrum of aeromagnetic anomaly map with depth to the top of magnetic sources (zt) estimated using lest squared method after El-Qady et al., (2005)	19
Figure 3.1. Shaded relief AsterDEM Image (30m resolution) draped over by Aster bands 7-3-1. The images show the structural trend of Lake Magadi.	21
Figure 3.2. (a) Extracted lineaments from remote sensing data overlaid on Aster Dem modified after Sequar (2009) (b.) Aster Dem hill shade (subset) showing major Faults (A, B, C, D and E) structures and ground survey lines within the study area.	22
Figure 3.3. Elevation Cross section along the magnetic traverse 1 showing the surface structures.....	23
Figure 4.1. a) Syscal R1 Plus Resistivity Meter, b) Field data acquisition with the instrument.	24
Figure 4.2. Hill shade AsterDEM showing the locations of resistivity profiles (R1, R2, R3 and R4) in the study area.	25
Figure 4.3. Field photo showing :(a) the resistivity profile R1 close to Fault E (N20°S) and (b) across Fault D (Photo b (looking west)) striking N05°S. The profile (R1) is about 50m away from the springs (cold) in the southwest of Lake Magadi.....	26
Figure 4.4. (a) Field photo showing Profile R2 between Faults C and D (Photo looking north). (b) photo showing the western most basaltic rock (looking south) where profiles 3 and 4 were taken by Sequar (2009) during 2008 field work. The arrow in both photos is pointing north	26
Figure 4.5. Inverted 2D resistivity section for profile1 across fault D and towards Fault E in the southeast of Lake Magadi.	28
Figure 4.6. Inverted 2D resistivity section for profile 2. The profile crosses Fault D almost perpendicular to its strike direction.	28
Figure 4.7. Inverted 2D resistivity section for profile 3 between Faults A and Fault B in the southwest of Lake Magadi.	29

Figure 4.8. Inverted 2D resistivity section for profile 4 across Fault B towards Faults A in the southwest of Lake Magadi.	29
Figure 4.9 (a): Geometrics 856 Proton Precession Magnetometer (b): Field photo showing data acquisition with the instrument.	30
Figure 4.10. Field photo showing the magnetic profile extent from Fault A to Fault D (on a west-east direction); the black arrow is pointing north.	31
Figure 4.11 (a): Field photo showing the hot springs along the lake margin between Faults A and B. (b): Hill-shaded AsterDEM showing the magnetic profiles across the major faults in the study area.	31
Figure 4.12. Ground magnetic data (total magnetic field intensity) obtained from the traverses 1, 2, 3 and 4 after correction.	32
Figure 4.13. Gridded residual ground Total Magnetic field Intensity (TMI) for the four profiles (in blue) showing hot springs and faults locations.	33
Figure 4.14. Colour-shaded Vertical derivative of the magnetic field intensity showing the shallow magnetic sources.	33
Figure 4.15. Colour -shaded Analytical signal maps of the four profiles.	34
Figure 4.16. Euler Convolution input and step process [modified after El Dawi et al. (2004)]	35
Figure 4.17. 3D Euler's depths solutions (structural index of 1) plotted on the colour shaded analytical signal map.	36
Figure 4.18. (a). Geologic map of the magnetic survey area. (b). Processed ground magnetic data with 2 D Euler solutions obtained along traverse one with inclination and declination angles of -26.2° and 0.03° respectively. Plus (+) signs are Euler solutions for 1.0 structural index.	38
Figure 4.19. Processed ground magnetic data with 2D Euler solutions obtained along traverse two with inclination and declination angles of -26.2° and 0.03° respectively. Plus (+) signs are Euler solutions for 1.0 structural index.	39
Figure 4.20. Processed ground magnetic data with 2D Euler solutions obtained along traverse three with inclination and declination angles of -26.2° and 0.03° respectively. Plus (+) signs are Euler solutions for 1.0 structural index.	39
Figure 4.21. Processed ground magnetic data with 2D Euler solutions obtained along traverse four with inclination and declination angles of -26.2° and 0.03° respectively. Plus (+) signs are Euler solutions for 1.0 structural index.	40
Figure 4.22. (a) Colour-shaded Aeromagnetic Total Magnetic Intensity (TMI) grid data for Lake Magadi area. (b). Hill-shaded Aster Dem showing ground survey area and corresponding aeromagnetic lines selected for the analysis. R1, R2, R3 and R4 are the resistivity profiles 1, 2, 3 and 4 while P1, P2, P3 and P4 are the ground magnetic profiles 1, 2, 3 and 4 respectively.	41
Figure 4.23. (a) Extracted topography elevations of Lake Magadi area from Aster DEM along flight line 30 showing surface faults and grabens. (b) 2D Euler deconvolution solutions from aeromagnetic data along flight line 320. The plus (+) signs are structural index of 1 with inclination and declinations of -26.3° and 0.002° respectively.	42
Figure 4.24. (a) Extracted topography elevations of Lake Magadi area from Aster DEM along flight line 322 showing surface faults and grabens. (b) 2D Euler deconvolution solutions from aeromagnetic data along flight line 32. The plus signs are structural index of 1.	43

Figure 5.1. Log Power spectrum analysis of Lake Magadi generated from Aeromagnetic data45

Figure 6.1. Hillshaded AsterDEM Image showing the lineaments and seismic hypocenters distributions (from Ibs-von Seht et al (2001) around Lake Magadi. The brown dots are the re-projected hypocenters along the aeromagnetic flight lines.....47

Figure 6.2. (a): Hillshade aster DEM subset showing the surface lineaments and the extracted aeromagnetic flight line 32. (b): Scatter Plots showing the subsurface relationship between magnetic sources on flight line 322, the hypocenters and the Curie point (heat source). The magnetic sources are generated from 2D Euler deconvolution using structural index of 1 (i.e. contacts, faults) with inclinations and declination angles of -26.3° and 0.002° respectively. R1 and R2 are the resistivity profiles 1 and 2 respectively48

Figure 6.3. (a): Hillshade aster DEM subset showing the surface lineaments and the extracted aeromagnetic flight line 320. (b): Scatter Plots showing the subsurface relationship between magnetic sources on flight line 320, the hypocenters and the Curie point (heat source). The magnetic sources are generated from 2D Euler deconvolution using structural index of 1 (i.e. contacts, faults) and inclinations and angles of -26.3° and 0.002° respectively. R3 and R4 are the resistivity profiles 3 and 4 respectively. The blue horizontal lines are the ground magnetic profiles location.....49

Figure 6.4. Magadi Crustal structure model derived from local earthquake tomography and hypocentral depth studies after Ibs-von Seht et al. (2001). The circles, dotted lines and dashed lines are projections of hypocenters, crustal velocities derived from seismic tomography and assumed depth ranges of active faults respectively51

List of tables

Table 2.1. Resistivity values of some earth materials after Yang (2002)16

List of Abbreviations

2D	Two Dimensions
3D	Three Dimensions
AMMP	African Magnetic Mapping Project
ASTER	Advanced Spaceborne Thermal Emission and Reflection Radiometer
CST	Constant Separation Traversing
DEM	Digital Elevation Model
ERT	Electrical Resistivity Tomography
FFT	Forward Filtering Transform
GPS	Global Positioning System
IGRF	International Geomagnetic Reference Frame
KRISP	Kenya Rift International Seismic Project
SRTM	Shuttle Radar Topography Mission
TMI	Total Magnetic Intensity
UTM	Universal Transverse Mercator projection
VES	Vertical Electrical Sounding
VNIR	Visible and Near Infrared
WGS	World Geodetic System

1. Introduction

The uprising of magma to the surface during the rifting process often results in different geodynamic activities such as the surface expressions of tectonic lineaments and manifestations of geothermal resources. These lineaments, such as faults and fractures play major roles in the study of the evolution and dynamism of the rift zones. Investigations into the tectonic lineaments and subsurface thermal structures are very crucial to the understanding of the geothermal activities and processes associated with these active regions. According to Blewitt et al.(2002), continuous accumulation of tectonic strain helps to maintain faults and fractures as conduits for fluids flow thereby sustaining the geothermal systems. The transportation of hydrothermal fluids in form of hot springs in these active regions are largely dependent on the existence of lineaments (faults and fractures) and deep seated thermal process (Babiker and Gudmundsson, 2004; Tüfekçi et al., 2010; Wheildon et al., 1994).

Hydrothermal fluids according to Mary and Mario (2004) are described as convecting water in the crust of the earth, which in a confined space, transfers heat through a pore space from a heat source to the free surface. These fluids, which are generated from the deep geothermal source, are sometime manifested in the surface in the form of hot springs and fumaroles through different conduits (faults and fractures) in the subsurface. Such faults and fractures, which are connected to one another to form networks, serve as major conduits through which fluids are transported to the surface. Evidently, critically stressed fractures and faults have been discovered to play important role in most geothermal fields (Blewitt et al., 2002; Noorollahi et al., 2007). This environment is generally associated with various tectonic/faulting occurrences due to magma intrusion and volcanism.

A typical example of geothermal environment with high geodynamic activity which is expressed by volcanism and earthquake activities is the area of Lake Magadi which is situated in the southern part of the Kenya rift (Ibs-von Seht et al., 2001; Kuria et al., 2009; Molnar and Aggarwal, 1971). Unlike some other geothermal regions where the reservoirs containing hot fluids have to be penetrated during exploitation, geothermal resources around Lake Magadi are clearly manifested on the surface in the form of hot springs and trona deposit along the lake margin and in the lake respectively. These surface manifestations of the hot springs have been attributed to the continuous tectonic activities and the presence of various faulting systems in the area (Jones et al., 1977; Maguire and Long, 1976). The potential of these resources anchors however, on the subsurface networks of fluid conduits and connectivity, and also depth to the heat source which provides information on the subsurface thermal structure. It is therefore important to investigate the geometry of the subsurface faults and fractures in order to know the distribution and the flow paths of hydrothermal fluids; this will help to understand its potentials.

In this research, various data sources emanating from satellite based remotely sensed data and geophysical data will be used to investigate the tectonic lineaments and geothermal potential of Lake Magadi, Southern Kenya Rift.

1.1. Problem Statement

Previous investigations have indicated active deformation in both south and north of Lake Magadi, southern Kenya rift (Atmaoui and Hollnack, 2003; Bosworth et al., 1992; Ibs-von Seht et al., 2008; Sequar, 2009). The Neotectonics and extension direction studies around the lake were designed to characterize the surface tectonic lineaments and crustal structure using remote sensing (Atmaoui and Hollnack, 2003; Sequar, 2009), borehole and geophysical data (Simiyu and Keller, 1998); but their subsurface components, especially fluids (mostly hydrothermal) infilling faults and fractures in the area has not been investigated. In Lake Magadi area, the presence of fluid-filled high micro crack porosity (fractures) in the upper crust was proposed by Ibs-von Seht et al. (2001) using seismic method. This was inferred from the low velocity anomaly experienced in the southern part of the area and also from the presence of hot springs. Also, the role of N-S faults in the south of Lake Magadi as major conduits for geothermal resources and the deposition of trona in the lake have been proposed by Jones et al. (1977) and Sequar (2009) using geochemical and remote sensing methods respectively. But the actual subsurface investigation of the influence of N-S faults structures on the hydrothermal fluids in the area has not been done. In addition, to date the Lake Magadi geothermal resources have not been explored in terms of depth to the heat source using aeromagnetic data despite the vast evidence of the geothermal manifestation on the surface.

This research therefore employs the use of integrated geophysical methods to understand the influence of these active tectonic lineaments (faults and fractures) on the hydrothermal fluids around Lake Magadi and also the delineation of the heat source. It is expected to link the surface tectonic lineaments (faulting systems) to the subsurface and to characterise the geothermal systems around Lake Magadi.

1.2. Objectives

1.2.1. General Objectives

The main objective of this research is to model the subsurface fluid conduits and thermal structure around Lake Magadi using integrated geophysical and remote sensing data.

1.2.2. Specific Objectives

1. To map the geometry of the subsurface fluid filled fractures in the south of Lake Magadi.
2. To determine depth to the heat source and characterised geothermal systems around Lake Magadi, integrating surface (remote sensing), subsurface (Magnetic and Resistivity) data and existing models.
3. To determine the effect of the deep heat source on the geodynamic activities around Lake Magadi.
4. To link the surface tectonic lineaments to the subsurface and contribute to the understanding of the role of the N-S structures on the surface manifestations of the hot springs and trona deposit.

1.3. Research Questions

- I. Can the proposed fluid bearing high micro cracks porosity in the upper crust be mapped?
- II. Can hot fluid path from geothermal source be delineated using geophysical methods?
- III. What is the effect of the deep seated heat source on the geodynamic activities around Lake Magadi?
- IV. What impact do the N-S faults structures in the south of Lake Magadi have on the geothermal resources?

1.4. Hypotheses

1. It is possible to delineate the geometry of fluid filled faults and fractures in the subsurface using integrated geophysical methods (Colella et al., 2004; Hunt et al., 2009).
2. Depth to the curie point from aeromagnetic data can provide information on the subsurface thermal structure (Espinosa-Cardena and Campos-Enriquez, 2008).
3. The intrusion of Magma into the mid-crust in the south of Kenya Rift (Magadi area) has been suggested by Ibs-von Seht et al., (2001) and Maguire and Long (1976) to be responsible for the geodynamic activities around lake Magadi, southern Kenya rift .
4. Faults and fractures acts as the subsurface conduits for the flow of fluids from the subsurface to the surface.

1.5. Datasets and Research Setup

1.5.1. Datasets

The following datasets were available for processing and analysis in this research:

1. 3 Aster Image Scenes: acquired in 2007 with resolution of 15m (VNIR), 30m (SWIR) and 90m (TIR).
2. Mosaiced Aster DEM
3. 4 Resistivity profiles Data: 2 profiles acquired during the field work plus the existing 2 profiles acquired last year by Sequar, 2009 (not reported).
4. 4 magnetic profiles data: 2 profiles acquired during the field work plus the existing 2 profiles acquired last year by Sequar, 2009 (not reported).
5. Aeromagnetic Data: acquired by Compagnie Generale de Geophysique (CGG) in 1987
6. Seismic Hypocenters (Ibs-von Seht et al., 2001)

1.5.2. Software

The software used in this research are listed below:

- Geosoft Oasis Montaj 7.1
- Euler Deconvolution 1.00 freeware by Cooper (2004)
- Surfer 8
- Earth imager
- Envi 4.4
- ArcGIS 9.3
- Erdas Imagine 9.3

1.5.3. Setup of Research

In order to answer the research questions, the following methods were followed:

1. Literature review: A review of previous work in Lake Magadi area and Kenya Rift was undertaken to understand the contributions of various researchers on geodynamics activities in the area. Also, applications of geophysical methods in the investigations of fluid conduits were studied.
2. Digitization of the existing scanned geologic map from Baker (1958)

3. Remote sensing data processing: Data such as Aster Image and Aster DEM were processed for the identification of area for ground geophysical investigation.
4. Field work (between 15th – 30 September, 2009): involving both geophysical (Magnetic and Resistivity) data collection
5. Geophysical (ground and airborne) data processing, analysis and interpretation.
6. Data Integration: This involved integration of subsurface fluid conduits model from the geophysical data, heat source depth, seismic hypocenters, with the existing crustal models to characterize Magadi geothermal system and determine effects of heat source on the geodynamic activities.

The overall detail methodology of this research is explained in the flow chart below.

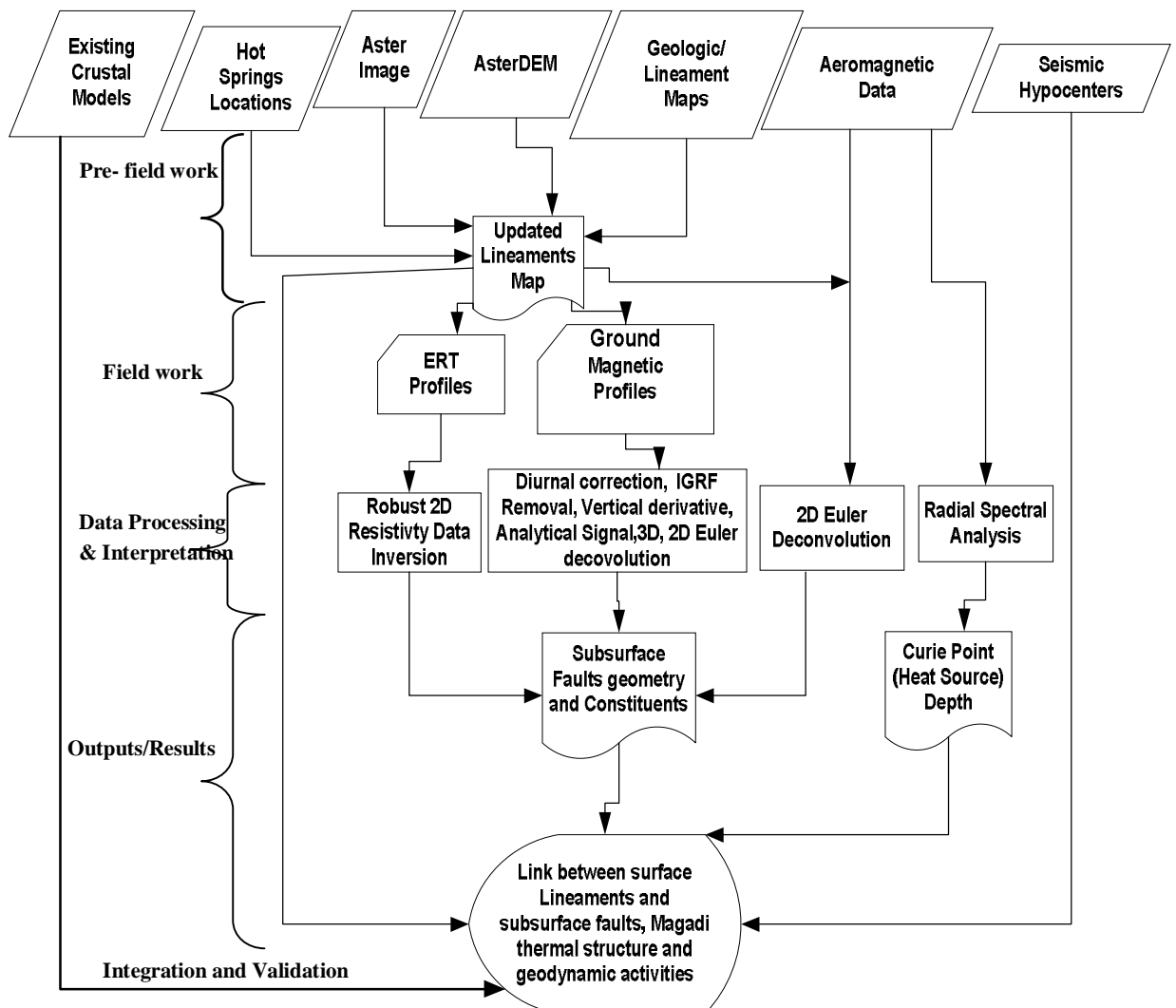


Figure 1.1. Research methodology flow chart

1.6. Organization of the Thesis

This thesis is made up of seven chapters as stated below:

- Chapter Two is the literature review on the geology of the study area, existing crustal model, role of faults and fractures on crustal fluids, geothermal process and model, principles and applications of geophysical methods in mapping fluid conduits.
- Chapter Three emphasizes on the pre-field work; remote sensing data processing and analysis, selection of area for ground investigation.
- Chapter Four centres on the geophysical data acquisition, processing, analysis, results and interpretations.
- Chapter Five focuses on the estimation of the depth to the heat source around Lake Magadi from aeromagnetic data.
- Chapter Six involves the integration of the results and existing model and discussions.
- Chapter Seven comprises of the conclusions from the research, limitations and recommendations

2. Literature Review

This section deals with the literature review on the geology of the study area, role of faults and fractures on crustal fluids, geothermal process and model, principles and applications of geophysical methods in mapping fluid conduits.

2.1. Study Area Location

Lake Magadi area is the southernmost part of Kenya Rift, 120km southwest of Nairobi and 20km north of the Tanzanian border. It is located within latitudes 1°40'S and 2°10'S, and longitudes 36°00'E and 36°30'E, characterized by a flat plain known as the rift floor (Atmaoui and Hollnack, 2003) (Figure 2.1). The approximately 100km² square kilometers size lake is recharged by saline hot springs (between 26 °C- 86°C) along the lake margins (Jones et al., 1977) (Figure 2.1). Most of these hot springs lie along the north-western and southern shorelines of the lake.

The lake is made up of trona deposit ($\text{Na}_2\text{CO}_3 \cdot \text{NaHCO}_3 \cdot 2\text{H}_2\text{O}$) up to 40m thick and covers an area of 75km² resulting from the concentration of different water sources, especially hydrothermal fluid (Jones et al., 1977). According to Eugster (1970) after a chemical analysis of collected waters, Magadi trona results from the evaporated concentration and mixing of waters from three sources namely; dilute surface inflow, relatively deep hot and concentrated groundwater reservoir, and cold concentrated surface brine. A further water analysis by Jones et al. (1977) revealed five distinct hydrologic stages in the evolution of the water compositions; i) the dilute stream flow, ii) dilute ground water, iii) saline ground water (or hot springs reservoir), iv) saturated brines, and v) residual brines. The saline (alkaline brine) hot springs are supplied by the active alkaline volcanoes in the area through hydrothermal systems circulation (Kodikara, 2009). For the purpose of this research, sites which are close to the hot springs located in the southern part of the Lake were selected (Figure 2.1).

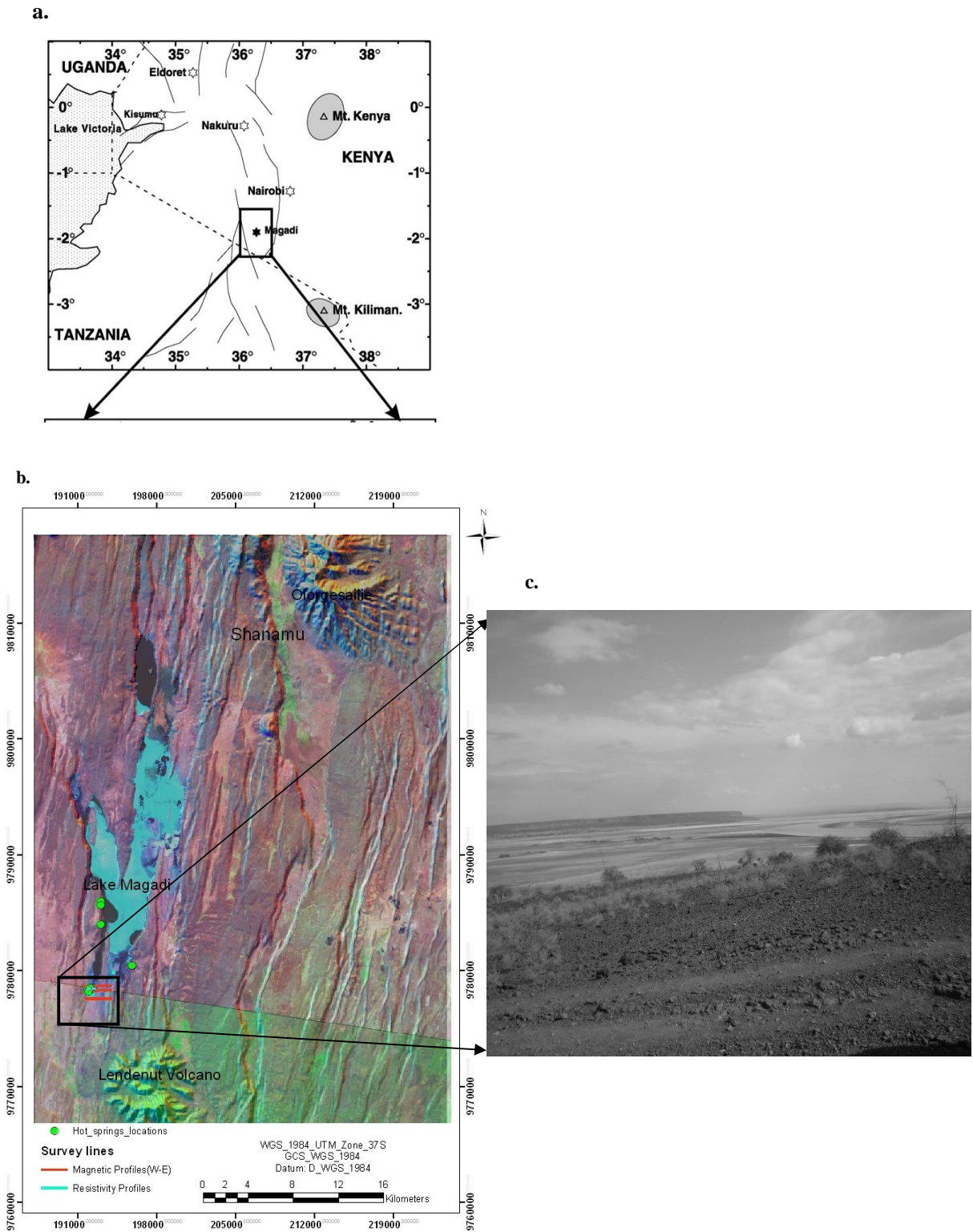


Figure 2.1. **(a)** Geographic location of Magadi area by Atmaoui and Hollnack (2003), **(b)** RGB colour composite of Aster bands 7-3-1 draped over SRTM DEM, showing the study and survey areas, and **(c)** field photo showing part of the study area and associated springs.

2.2. Geology and Tectonic Settings of the Kenya Rift

Kenya rift (also called Gregory rift) is the eastern branch of the continental East African Rift System (EARS) which extends to about 3000km from Afar triangle to southern Mozambique (Atmaoui and Hollnack, 2003; Chorowicz, 2005) (Figure 2.2).

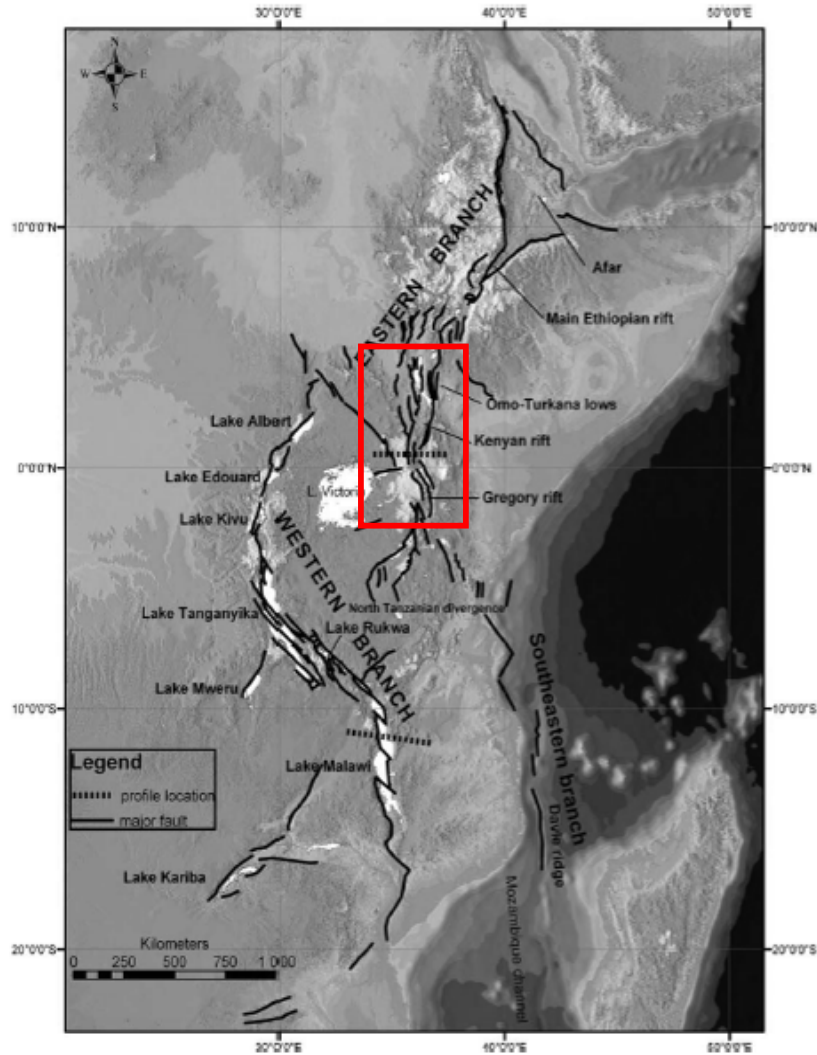


Figure 2.2. East African Rift System showing the location of Kenya Rift after Chorowicz (2005)

Geologically, the rift is made up of Cenozoic volcanic and sedimentary rocks. Baker et al. (1971) reported that the Cenozoic rocks are divided into four litho-stratigraphic units, mainly: Miocene basalts, Miocene phonolites, Pliocene and Quaternary volcanic rocks and sedimentary rocks. The crustal structures of the Kenya rift have been investigated using integrated seismic, magnetic and gravity data (Braile et al., 1994; Maguire et al., 1994; Mechie et al., 1994; Prodehl et al., 1997). A 5km- deep sediment, volcanic filled basin and thinning crust of about 8km in a 100km- wide zone beneath the rift valley were discovered by Braile et al. (1994) using a 2D seismic velocity model. An integrated seismic-refraction/teleaseismic survey by Keller et al. (1994a), undertaken to study the deep structure beneath the Kenya rift revealed that the rift is associated with sharply defined lithospheric thinning and very low upper mantle velocities down to depths of over 150 km. Mechie et al. (1994)

and (1997), after a detail study of the structures of the rift from south to north showed crustal variations along the rift axis from 35km in the south beneath the Kenya dome around Lake Naivasha to 20km in the north beneath the Turkana region. This variation in crustal thickness along the rift axis has been attributed to tertiary rifting episode. Investigations during Kenya Rift International Seismic Project (KRISP) revealed increase in the crustal extension to the north and the presence of low primary velocities anomalies which are possibly caused by magma rising from below and get trapped in the uppermost mantle (Keller et al., 1994b; Mechie et al., 1994).

Baker (1987) reported three major stages of rifting, accompanying by intense alkaline volcanism in its tectonic development: (1) the pre-rift stage (30-12Mya), forming deformation and minor faulting (2) the half-graben stage(12-4 Mya), forming of the main boundary faults, and (3) the graben stage(<4 Mya) with an increase and inward migration of faulting. The volcanism and rifting of the Kenya Rift began 40 -45 Ma and ~ 25Ma ago in the north and propagated to the south. According to Atmaoui and Hollnack (2003), with time, there is a north - south rift propagation and a shift in volcanism and tectonic activities from the rift margins towards the axial part of the rift floor, which is accompanied by high fault density. From this, it is therefore expected that the tectonic activity is mainly concentrated in the axial part of the southern Kenya rift (Lake Magadi Area). They also investigated the tectonic extension direction of southern Kenya rift (Lake Magadi) using structural analysis of open fractures and size characteristics of faults and indicated an E-W to ESE-WNW normal faulting extension direction as against the NE-SW extensional stress proposed by Bosworth et al. (1992). Neotectonics studies of the Rift reveals four sets of faults: normal N-S fault, dextral NW-SE fault, strike slip ENE-WSW fault and sinistral NE-SW fault (Le Turdu et al., 1999; Sequar, 2009).

In terms of seismicity, Kenya rift shows a relatively low seismic activity compared to the whole East African rift systems. Apart from a magnitude of 6.8 recorded in 1928 in the central part of the rift, no events of magnitude more than 5 have been reported (Ibs-von Seht et al., 2008). However, a constant rate of approximately 10 ($M < 3$) events per day for the southernmost part of the rift have been reported by Ibs-von Seht et al. (2001). The strongest event from the southernmost Kenya rift as discovered by Ibs-von Seht et al. (2001) and Atmaoui and Hollnack (2003) had a magnitude of 4.2, accompanied with a surface crack of several kilometers length in the epicenter region. This makes the Lake Magadi area the most seismically active region within the Kenya rift.

2.3. Geology of Lake Magadi

Smith and Mosley (1993) defined the geology of Lake Magadi as being made up of mostly Achaean to early Palaeozoic crystalline basement rocks and rifted related volcanic and sediments. This can be grouped into three (3) categories as explained by Atmaoui and Hollnack (2003); 1).Precambrian metamorphic rocks, 2) Plio-to Pleistocene volcanic rocks and 3).Holocene to recent lake and fluvial sediments (Figure 2.3). The oldest rocks in the area are the quartzite, gneisses and schist of the basement formation which is of Archaean age. The extrusion of alkali trachytes within the lake as explained by Baker (1958) and Baker et al. (1971) occurred in the Pleistocene age. In the southern and northern ends of the Lake Magadi area, there is a deposition of irregular interbedded chert rocks which consists of silicified bedded clays on top of Alkali trachytes (Atmaoui and Hollnack, 2003; Sequar, 2009). This was later unconformably deposited on by a thin layer of lake beds known as the Oloronga beds and followed by series of sub-parallel faulting system that resulted in the formation of

the lake Magadi rift floor. The formation of the quaternary sediments exists within a fault-bounded basin.

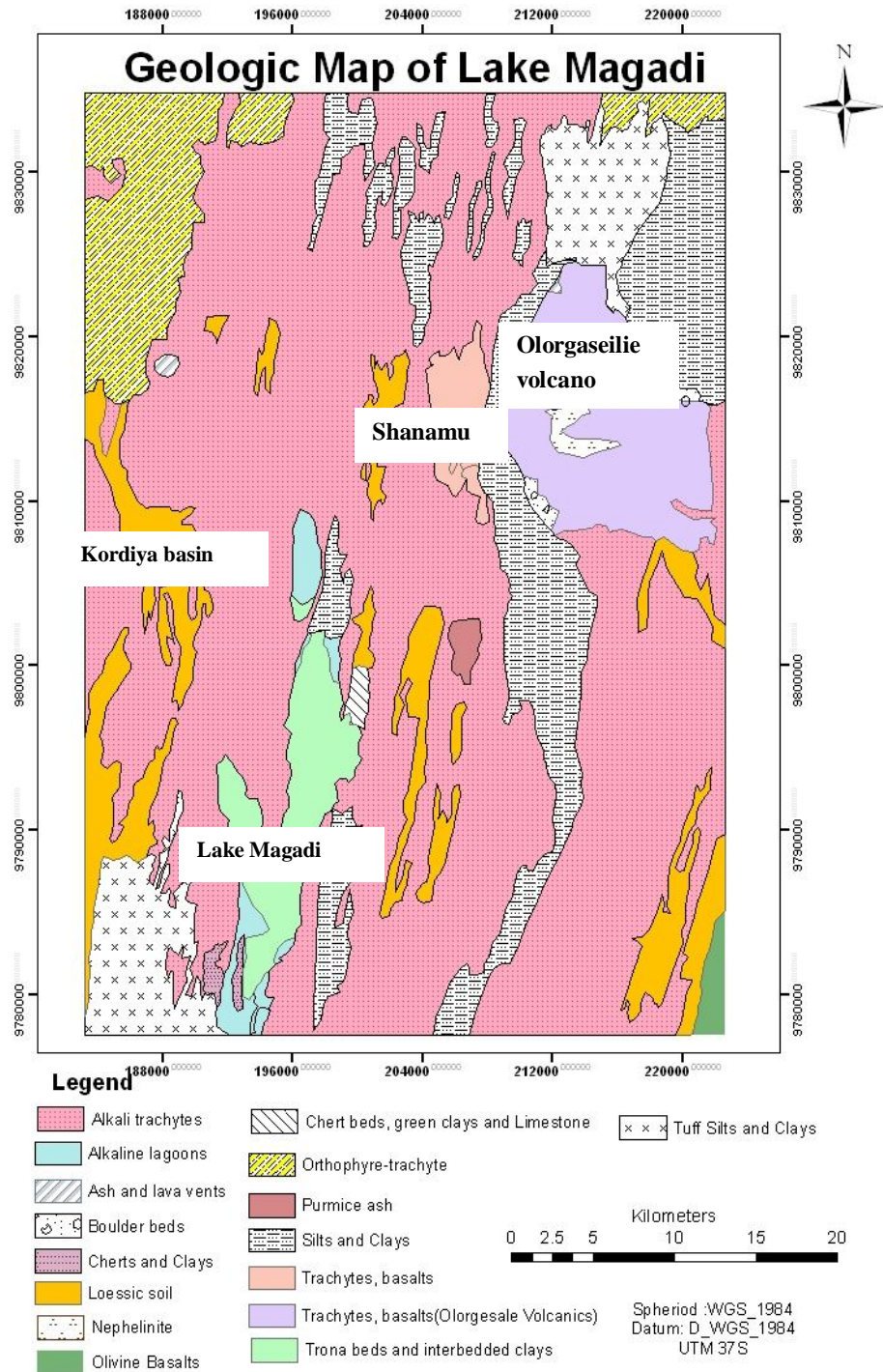


Figure 2.3. Simplified Geology map of the study area after Baker (1958)

An integrated seismic, drill hole data and gravity model by Simiyu and Keller (1998) revealed sediments and volcanic complex at the rift floor adjacent to Nguruman escarpment (Figure 2.4). Their model explained the crustal structure of Lake Magadi as having basement rocks at the bottom which are exposed at the western (Tanzanian craton) and eastern (Mozambique belt) flanks and are overlain by Pliocene to Miocene volcanic and sediments rocks. The Rift has been discovered to exist in the boundary between the Achaean Tanzanian craton and neoproterozoic Mozambique belt, which is characterized by a complex fault zone (Smith and Mosley, 1993).

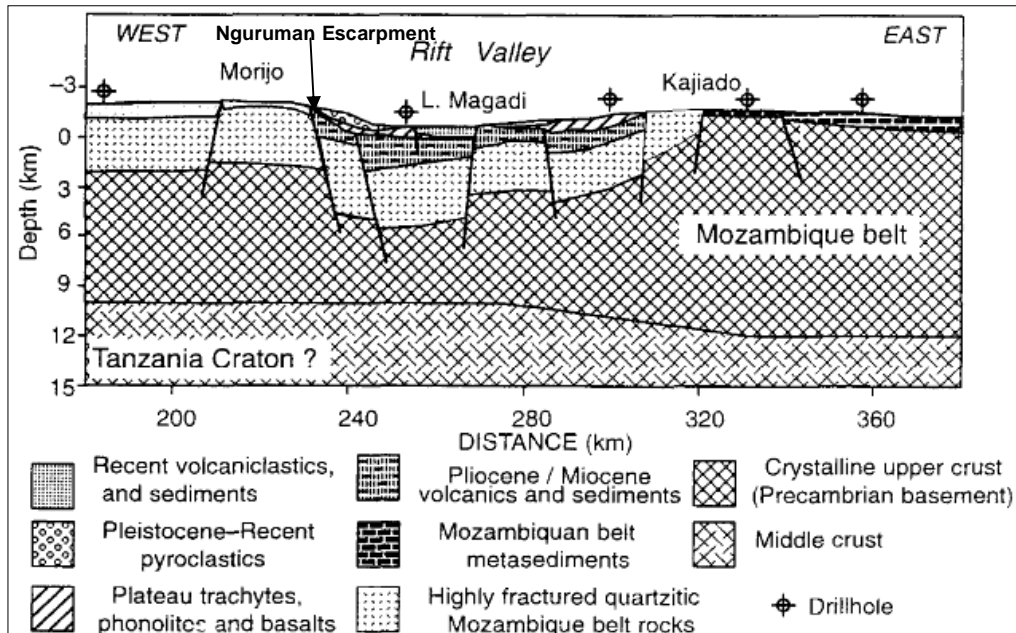


Figure 2.4. Upper crustal structure of Lake Magadi after Simiyu and Keller (1998)

The tectonic settings and structures of Lake Magadi are influenced by three factors: (1) stable Tanzanian Craton (2) Aswa shear zones and (3) southern fringes of the Kenya dome (Le Turdu et al., 1999). The four major fault sets associated with the Kenya rift (normal N-S fault, dextral NW-SE fault, strike slip ENE-WSW fault and sinistral NE-SW fault) are revealed at Lake Magadi (Figure 2.5).

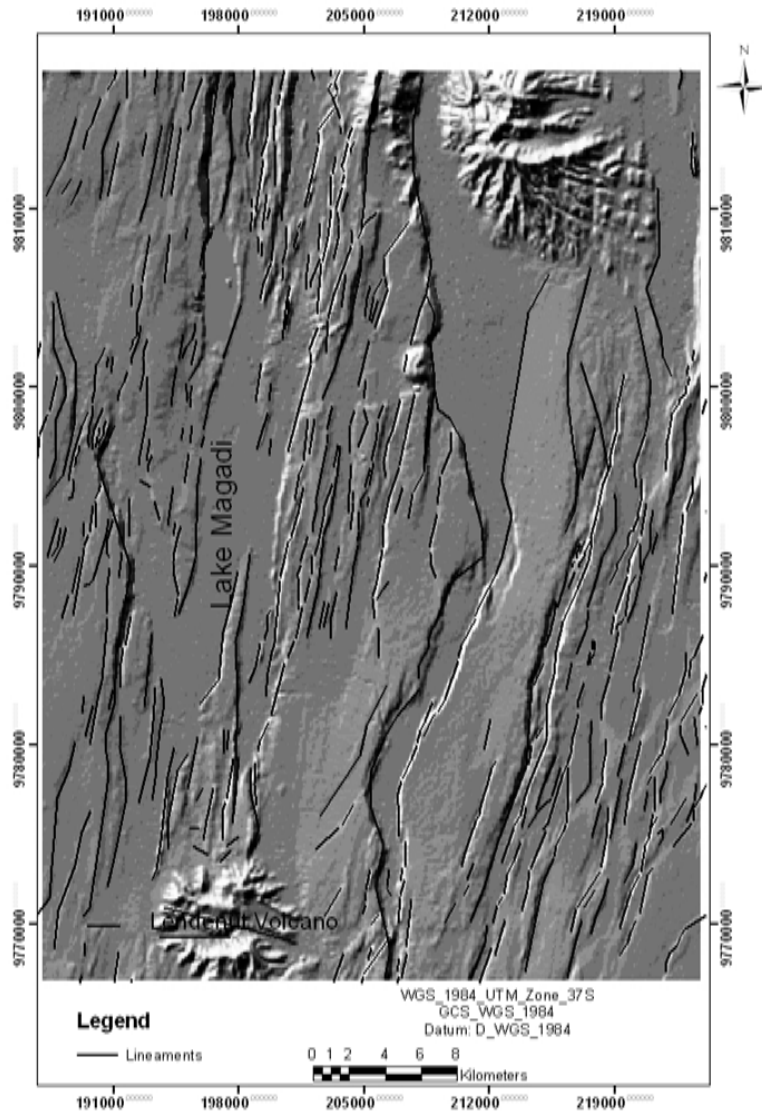


Figure 2.5. Lineaments map of Lake Magadi overlaid on SRTM DEM. Modified after Sequar (2009)

2.4. Role of Faults and Fractures on Crustal Fluids

The roles of faults and fractures on crustal fluids have been of major interest in earth sciences, including geology, seismology, hydrogeology and petroleum geology (Gudmundsson et al., 2001). The static and dynamic effects of different stress on rock often produce change in rock mass such as fractures, faults and in general permeability which in turn control the flow of fluids in the earth crust. According to Lerner and Cengage (2003), fractures and faults are planes of tensile or shear failure at microscopic to regional scales in brittle rocks. These faults and fractures are developed mostly in competent rocks within the earth crust. In case of fractures, they are usually developed when the stress applied exceeds the elastic limit of the rock (Lerner and Cengage, 2003). These two deformations are of great importance in crustal fluid distributions and control.

The movement of crustal fluids (in this case, hydrothermal) to the surface from the reservoir rock

depends of the pressure, temperature and most importantly the presence of active faults and fractures in the subsurface which are extended to the surface.

2.5. Geothermal System: Process and Model

Literally, geothermal energy can be described as the heat generated within the earth which could be exploited for use. Geothermal resources, according to Mary and Mario (2004) are generally associated with tectonically active region which are generated as a result of temperature differences between the different parts of the asthenosphere (below the lithosphere) where convective movement are formed. This slow convective movement is said to be maintained by the radioactive elements and heat from the deepest part of the earth. The less dense deep hotter rocks tends to rise with the movement towards the surface while the colder but heavier rocks close to the surface tend to sink, re-heat and rise again.

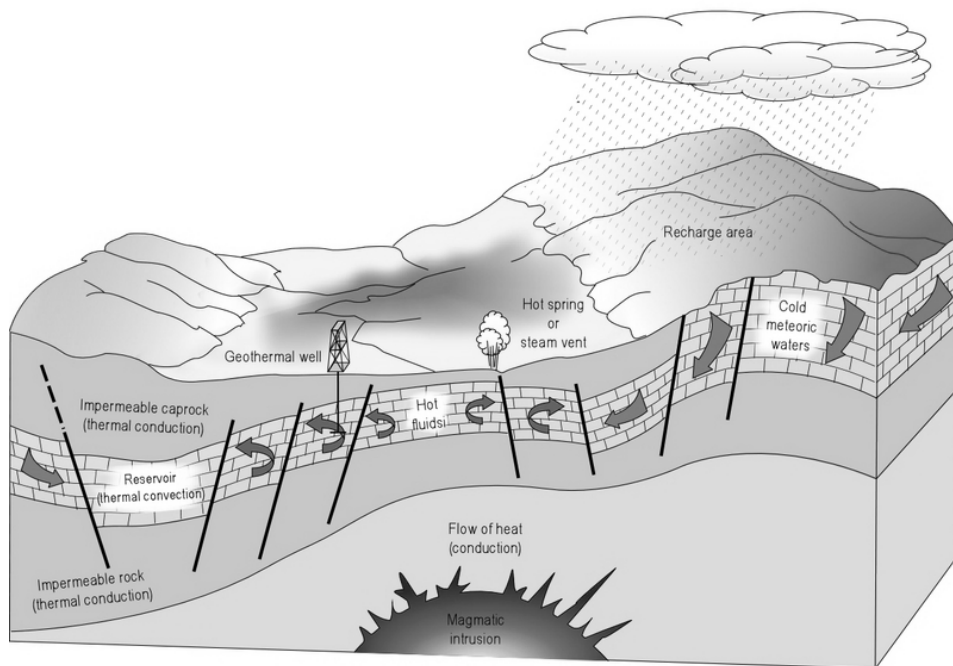


Figure 2.6. Schematic representation of a typical geothermal system by Mary and Mario (2004)

Generally, hydrothermal system is made up of the heat source, the reservoir, the recharge area and the connecting paths such as faults and fractures through which fluids percolates to the reservoir (the host rock) and in most cases are escaped to the surface as fumaroles and hot springs. The heat source is generally magmatic intrusion that has reached shallow depths (5-10km) (Mary and Mario, 2004). The reservoir rocks are permeable rocks through which fluids circulates and extracts heat from the heat source. This is often overlain by impermeable rocks and also connected through medium such as faults and fractures to a surficial recharge area from which meteoric water replaces or partly replace the fluids which escapes from the reservoirs through springs or by drilling (Figure 2.6). Large amounts of chemicals are carried along as the geothermal water percolates through the host rock; this dissolution of rock minerals mostly contributes to the salinity of most hot springs.

Geothermal activities are associated with most of the Kenyan rift valley. The warm and hot springs are mostly connected to the lakes through various fluid conduits (Mwaura, 1999). In the Kenya rift, geothermal manifestations at different location have been indentified (Simiyu and Keller, 2000) (see

Figure 2.7), the most active and currently producing is the Olkaria geothermal field, the northern part of the Kenya rift. The latter exists within an old caldera complex cut by N-S normal faults in the surface. The surface manifestations are in the form of hot springs. The warm ground which are common in the area, are associated with N-S normal faulting as reported also in the southern part of the rift (Magadi) (Simiyu and Keller, 2000). Lake Magadi water is mostly derived from underground hot water inflow with a continuous recharge from the surface waters (Jones et al., 1977; Mwaura, 1999)

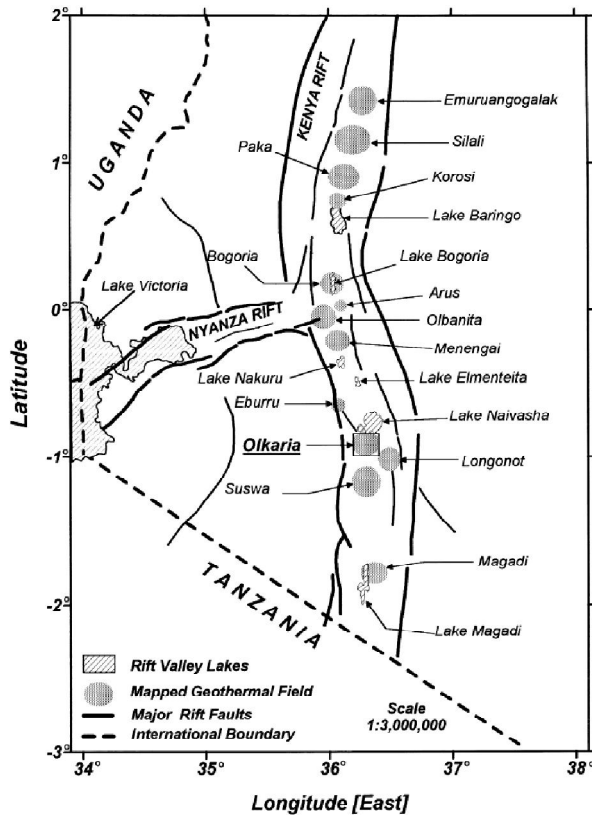


Figure 2.7. Map of the Kenya Rift Valley showing location of the significant geothermal areas from Simiyu and Keller (2000).

2.6. Applications of Resistivity Tomography in Fluid Conduits Mapping

2.6.1. Electrical Resistivity Method

Electrical resistivity is a geophysical method that measures or image subsurface electrical resistivity structures using direct or low frequency alternating current with series of electrodes injected into the ground. In general, the electrodes consist of both current and potential for injecting the current and measuring the potential difference respectively. Conventionally, the bulk resistivity (apparent resistivity) distributions of the subsurface are calculated from the measurement based on the electrode configuration (Kearey and Brooks, 1984) and are later inverted to true resistivity of the subsurface layers.

Two types of resistivity procedures are normally applied; the Vertical Electrical Sounding (VES) and the horizontal profiling (often called Constant Separation Traversing, CST). These two field procedures are used for probing vertical and lateral resistivity distribution respectively, depending on

the types of array or configuration in use. Although the convectional resistivity survey known as electrical resistivity tomography (ERT) combines both lateral and vertical resistivity measurements in a survey, each field procedures can be done separately to achieve both lateral and vertical resolution. Various types of configurations generally applied on the field in electrical resistivity surveying can be found in Keary and Brooks (1984) and Telford et al. (1976). Apart from direct electrical method, other geophysical methods utilize the electromagnetic waves to image the crustal resistivity distribution, many of which are generated by a transmitter. The method is used in various applications such as environmental, geotechnical investigation and hydrological surveys. This method was adopted in this research to model the subsurface fluid conduits around Lake Magadi.

2.6.2. Fluid Conduits Mapping with Resistivity

Resistivity of a material is its ability to resist the passage of current through it. Electrical resistivity imaging of the earth crust provides information about its structure and composition, and can be used in geothermal environment for delineating the subsurface structure and their fluid content. Subsurface resistivity depends on the: porosity and connectivity of pores, moisture (water content), dissolved electrolytes, temperature and resistivity of minerals. Thus, rocks because of the embedment of highly resistant minerals such as quartz, calcites and feldspars are resistive, but could be less resistive when there is connectivity pores. Generally, crystalline igneous rocks have resistivity greater than 1000 ohm-m while sedimentary rocks are less resistive or intermediate resistivity; the fluid filled rocks can produce resistivity of 1ohm-m and below (Unsworth, 2002) (Table 2.1). These resistivities are greatly influenced by the presence of fluids within the pore space. According to Güner and Bayrak (2007) and Unsworth (2002), resistivity has good connection with the presence of interconnected aqueous or magmatic fluids within pores of the rock. This implies that, resistivity imaging of the subsurface can map both its physical state and fluid content. Thus, the higher fluid contents in the rock would produce low resistivity.

The relationship between the resistivity, porosity and water saturation (fluid) is expressed in Archie's equations stated as follows:

$$\rho_f = a \cdot \rho_w \cdot \rho^{-m} \cdot S^{-2} \quad \text{Equation (1)}$$

Where:

- ρ_f = Bulk resistivity of the rock
- a = texture factor, ranging from 0.5 to 1.5
- ρ_w = resistivity of the pore fluid
- Φ = porosity
- m = cementation factor, ranging from 1.3 to 2.6
- S =saturation of the pores

The above equation can also be re-written as:

$$\rho_f = F \rho_w \quad \text{Equation (2)}$$

Where F is called the formation factor of the rock, which is a function of the rock's porosity, cementation and texture. Thus, the resistivity of a fluid saturated rock depends on the amount of fluid and its distribution (degree of interconnection). Resistivity values of few common materials are stated below:

Materials	Resistivity(Ohm-m)
Saltwater	0.1 – 1
Clay	1 – 1,000
Fresh water	10 – 100
Alluvium	1 -1,000
Sandstone	1 -1,000
Limestone	10 – 10,000
Gravel	100 - 10,000

Table 2.1. Resistivity values of some earth materials after Yang (2002)

Resistivity values in a geothermal reservoir such as Lake Magadi are assumed to be much lower than in the surrounding rocks, because of the high-temperature fluids and also the existence of the faults and fracture which are potential medium through which electric current is transmitted (Garg et al., 2007). With resistivity tomography, it is possible to derive a high resolution two and three dimensions resistivity image of the subsurface geologic structures. Resistivity data can also be used to discriminate between hot and cold water in the subsurface (Hunt et al., 2009).

Resistivity Tomography has been applied by different authors for mapping fluid conduits, especially in a geothermal environment (Abiye and Tigistu, 2008; Bibby et al., 2009; Colella et al., 2004). Capability of resistivity data to map crustal fluid distribution was demonstrated by Mishina (2009) in Northeast Japan using magnetotelluric (MT) section. His resistivity model clearly revealed three fluid flow paths based on the distribution of the zones of low resistivity: (1) Fluid ascending from the top of the upper mantle through the lower crust to the surface, (2) second path produced small fluid reservoir from the first path and (3) third path represents another path from upper mantle through the lower crust forming a fluid reservoir. Risk et al (1999) reported the use of resistivity (large scale dipole – dipole array) for mapping fault structures and high temperature geothermal field in central Taupo Volcanic Zone, New Zealand. Their resistivity model clearly delineated the faults, the resistive and non resistive (geothermal resources) zones. Magnetotelluric resistivity model was adopted by Aizawa et al. (2008) to map the Asama, Tokyo 2004 volcanic eruption and magma fluid ascension to the surface. The resistivity model revealed resistivity structures of up to 3 km and various stages of intrusion of magmatic fluids to the surface. Resistivity survey in conjunction with other geophysical methods is therefore very crucial in the mapping of the fluid conduits such as faults and fractures.

2.7. Ground Magnetic Method

Magnetics is a geophysical technique that measures the magnetic field intensity of the Earth. It is capable of mapping subsurface structures such as faults, grabens, horsts and lithology. The aim of magnetic survey is to determine or measure the local magnetic contributions to the total magnetic field. This method is performed both on the ground and in the air (airborne). The ground magnetic surveys are always performed over a small area with relatively small spacing on the ground while the airborne are carried out in the air, covering a wide area and can penetrate deeper than the ground base (Kearey and Brooks, 1984). The principles of magnetic methods can be found in Keary and Brooks (1984) and Telford (1976).

Association of geological formations with magnetic minerals makes it possible for mapping with magnetic field data. According to Jessell (2001), lithology controls magnetic properties through mineralogy, and sharp variation in rock properties generally coincides with lithological contacts. Generally, igneous and metamorphic rocks show significant magnetic properties while sedimentary rock is non-magnetic (Clark and Emerson, 1991). Existence of faults and fractures in the geologic units creates magnetic variation and can cause anomaly in magnetic measurements. Abiye and Tigistu (2008) highlight the importance in mapping hydrothermal alteration zones. This is because most magnetic rocks must have been altered and converted from magnetite to pyrite which in turn results in lower magnetic anomaly than the unaltered zones. In general, the presence of fluid within the faults and fractures would reduce or have no magnetic response.

The subsurface structures geometry can be constructed from magnetic profiles data using various inversion processes. The anomaly due to the near surface and deep source can be enhanced using vertical derivative and upward continuation respectively. Depth to magnetic sources and geometry of the structures can be automatically estimated from Euler's deconvolution method as applied in this research. Magnetic method was used in this study to map the subsurface structures in the south of Lake Magadi, southern Kenya Rift.

2.8. Curie-Point Depth

Curie point is defined as the temperature (above 580°C) at which magnetic material loses its magnetic properties or susceptibility as a result of the high temperature (Stampolidis and Tsokas, 2002). This point is assumed to be the depth for the geothermal source (magmatic chamber) where most geothermal reservoirs tapped their heat from in a geothermal environment. Curie point temperature depths provide general information on both regional and local temperature distribution as well as geothermal gradients. According to Gürer and Bayrak (2007), Curie-point depth is one of the methods of examining data thermal structure of the crust using aeromagnetic data. Aeromagnetic data have been used widely to determine the depth to the Curie isothermal point using spectral analysis (El Dawi et al., 2004; Espinosa-Cardena and Campos-Enriquez, 2008; Stampolidis and Tsokas, 2002).

Airborne magnetic is applied over a large coverage area to delineate anomaly from a deep geothermal source. The total magnetic intensity anomaly can be associated with many geothermal reservoirs dominated mostly by hot fluid (Hochstein and Soengkon, 1997; Miyazaki, 1985). Magnetic method is able to detect depth at which the Curie temperature point is reached. At temperature up to 580°C, ferromagnetic materials which are potential magnetic sources lose nearly all magnetic susceptibility. With airborne magnetic data it is possible to differentiate between anomalies associated with near surface and deep subsurface. In general, for all magnetic survey above or at the surface, near surface magnetic anomaly is characterized by short wavelength while that of demagnetized Curie point has long wavelengths and low amplitude magnetic anomaly. The difference therefore can be used to determine the Curie point depth which is assumed to be the depth to deep heat source (Stampolidis and Tsokas, 2002).

Magnetic spectrum gives better information on the depth to magnetic sources. Statistical estimation of depth to magnetic sources in the crust was described by Spector and Grant (1970). Their model assumed that magnetic sources are made up of independent ensembles of rectangular prisms which are

characterized by frequency distribution of depth, width and length extent. Their assumption expects the value of the spectrum of the ensemble of sources to be the same as that of single prism.

Estimating the depth to Curie point (assumed heat source depth) helps to determine the transition of magnetic materials in the subsurface. The spectral analysis method provides relationship between the spectrum of magnetic anomalies and the depth of the magnetic source using Fourier transformation of spatial data (magnetic grid) into wave or frequency domain. Spectral analysis involves estimating depth to the bottom of the magnetized bodies which is the transition point for magnetic materials using log power spectrum. Radially averaged power spectrum of magnetic data according to Blanco-Montenegro et al. (2003) is expressed as function of wave number and is related to depth to the bottom of the deepest magnetic source in Equation 3.

$$K_{\max} = \frac{\log z_b - \log z_t}{z_b - z_t} \quad \text{Equation (3)}$$

Where z_t and z_b are depths to top and bottom of the magnetic sources respectively. K is a function of wave number which is expressed in radians per unit distance. The power spectrum according to Spector and Grant (1970) can be divided into two parts, 1) The deeper sources, which has small wave numbers and decays away rapidly and 2) the shallower sources with high wave number, which dominate the short wavelength end of the spectrum (Figure 2.8). The wave number value at maximum peak spectrum (due to deepest anomaly) K_{\max} is usually determined on the generated log power spectrum as shown in Figure 2.8. To obtain the value of the depth to the deepest anomaly therefore, a least squared method is usually adopted to determine the slope at each peak of the log spectrum (Figure 2.9).

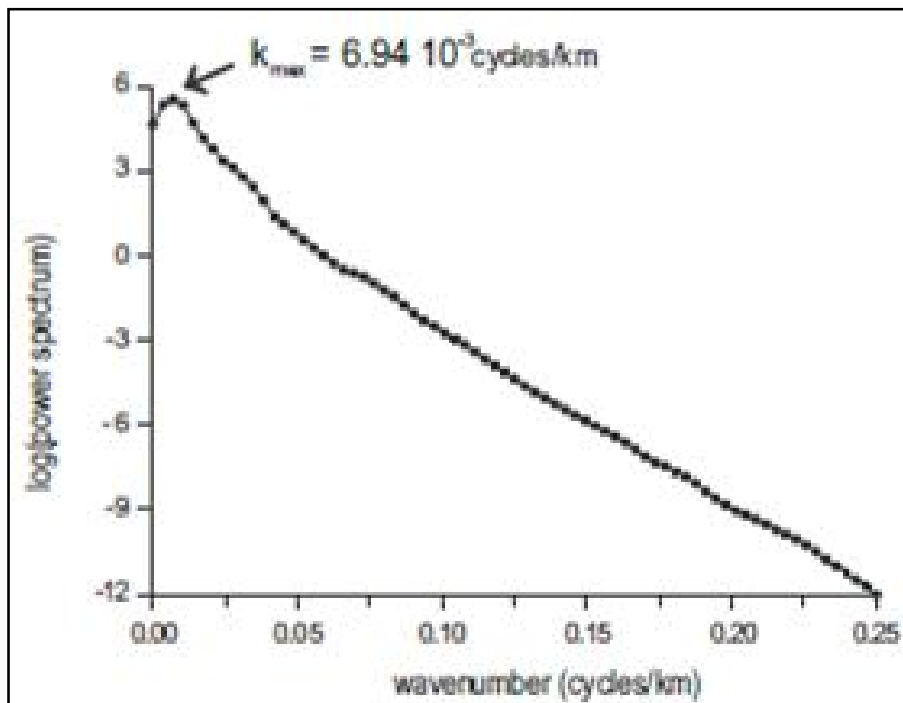


Figure 2.8. Radially averaged power spectrum from aeromagnetic data after Blanco-Montenegro et al. (2003)

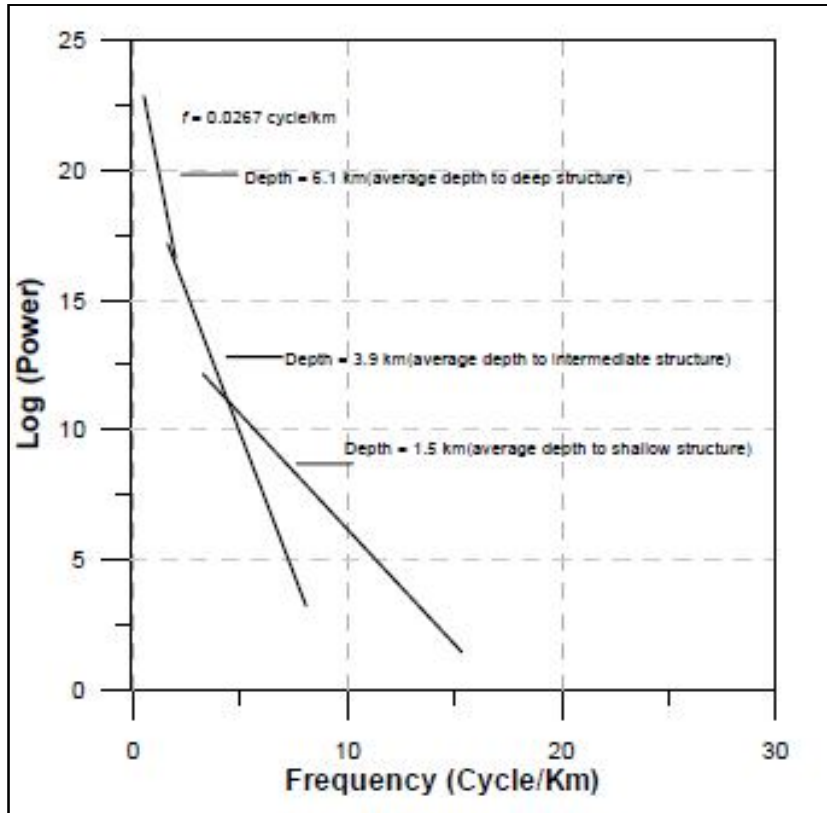


Figure 2.9 Example of average power spectrum of aeromagnetic anomaly map with depth to the top of magnetic sources (z_t) estimated using least squared method after El-Qady et al., (2005)

3. Remote Sensing Data Processing and Analysis

Processing and analysis of remote sensing data were necessary before the field work in order to understand the geology of the area (in conjunction with the existing geologic map) and also to delineate areas for ground investigation. The remote sensing data used for the purpose of this research are listed in section 1.5.1 of this thesis.

3.1. Aster Image processing

The Advanced Space-borne Thermal Emission and Reflection Radiometer (ASTER) data is a multi-spectral imaging system. It consists of 14 bands within the electromagnetic spectrum with 3 bands in the visible and near infrared (VNIR) having 15m spatial resolution, 6 bands in short wave infrared (SWIR) with 30m spatial resolution, and 5 bands in the thermal infrared (TIR) with 90m spatial resolution. Because of its better and enhanced spatial resolution especially in the visible and near Infrared, Aster band ratios and colour composites are useful in geologic and structural mapping.

The various Aster image scenes were co-registered to the same reference system (WGS 84 zone 37S), layer stacked and re-sampled to the 15m spatial resolution of the VNIR. The layer stacked image was subsetting to cover the study area. Aster image colour composites, band 7-3-1 were applied for lineament delineation as demonstrated by Thurmond et al. (2002) and Yang et al. (2008).

3.2. Digital Elevation Model Processing and Enhancements

Digital elevation model (DEM) can be described as representation of topography of the Earth (Teichrieb and Kelner, 2007). It reveals the surface expressions of the Earth's geomorphology and very useful in delineating structural information on the Earth's surface. AsterDEM was used in conjunction with the Aster image to identify the major fault structures of interest for geophysical measurements.

After removing the bad pixel values (very low negative values) from the datasets in Envi software, the study area was subsetting. The subsetting AsterDEM was further enhanced using shaded relief with 45° sun elevation angle of 225° and 315° solar azimuths. The Aster 3D DEM hill shaded relief was draped on Aster image RGB combination 7-3-1 for faults identification (Yang et al., 2008) (Figure 3.1).

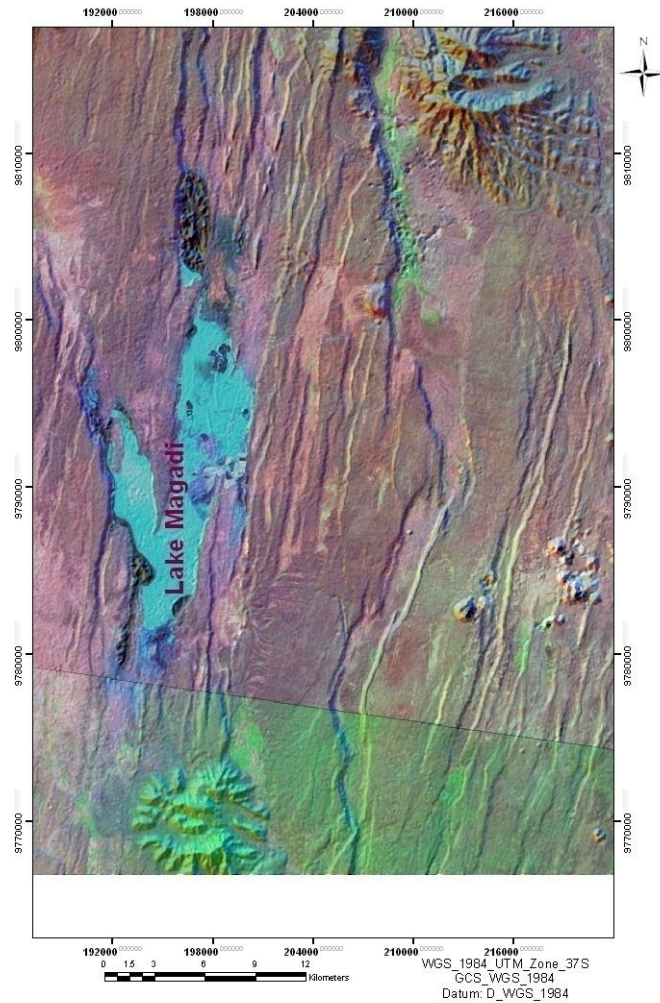


Figure 3.1. Shaded relief AsterDEM Image (30m resolution) draped over by Aster bands 7-3-1. The images show the structural trend of Lake Magadi.

3.3. Structural Mapping

For the structural mapping of the study area, Aster image and AsterDEM were integrated. Outcome of the interpreted structures from the remote sensing data, with the existing lineaments map was used to generate a spatial distribution of faults and fractures in the area (Figure 3.2a). In the study area, five fault systems referred to as A, B, C, D, and E (from west to east) assumed to be the major fluid conduits in the south of the lake, within the basin were identified for ground investigation (Figure 3.2b).

Major faults around Lake Magadi are the normal N-S fault, dextral NW-SE fault; strike slip ENE-WSW fault and sinistral NE-SW fault (Atmaoui and Hollnack, 2003; Sequar, 2009) (Figure 3.2a). The N-S faults are well pronounced in the area and are suggested to be the oldest faults in the Lake Magadi area while the youngest are the NE - NW faults. A detailed Lake Magadi fault characterization can be found in the research work by Atmaoui and Hollnack (2003) and Sequar (2009).

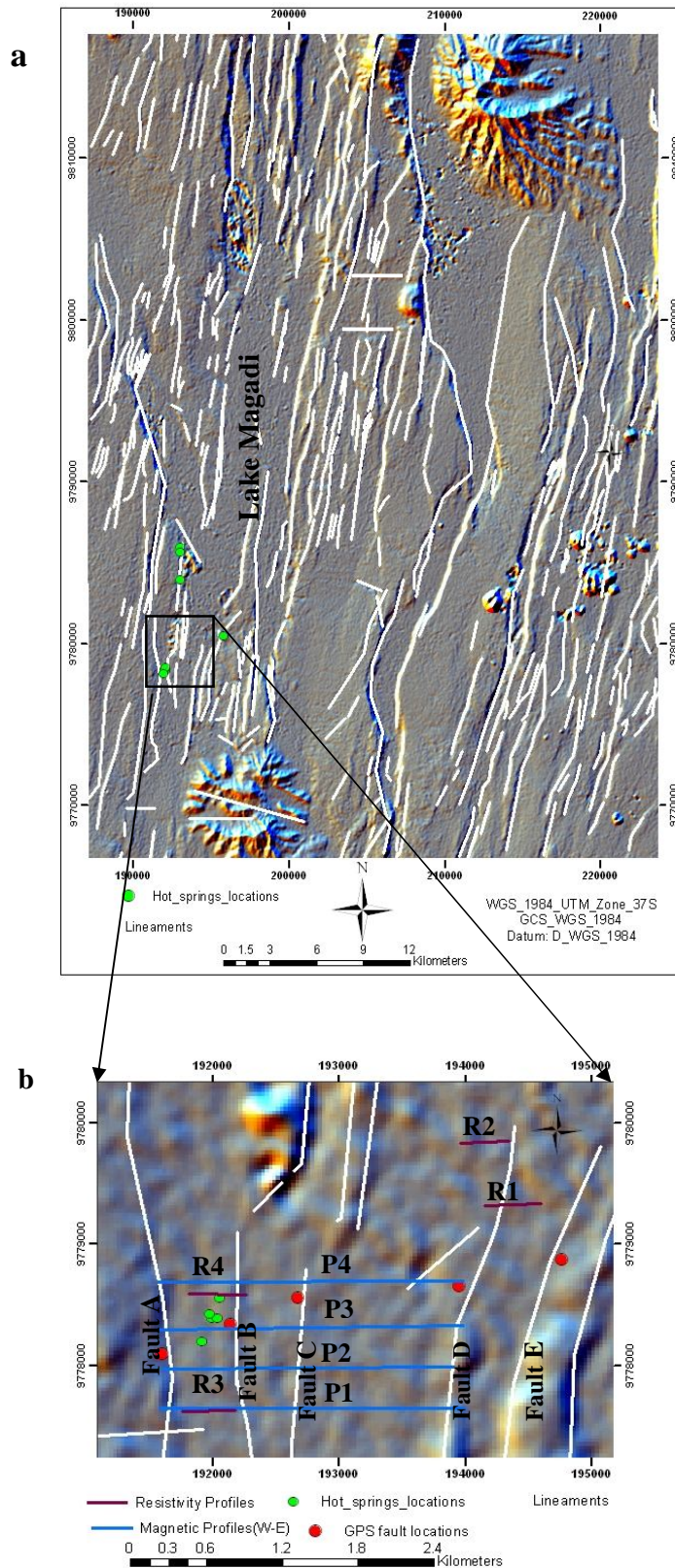


Figure 3.2. (a) Extracted lineaments from remote sensing data overlaid on Aster Dem modified after Sequar (2009) (b.) Aster Dem hill shade (subset) showing major Faults (A, B, C, D and E) structures and ground survey lines within the study area.

In the study area, the basin is bounded by three faults that are striking N05°S (for Faults (A and D respectively) and N20°S (for Fault E), separated by a distance of about 2.3km and 2.7km (Figures 3.2). Fault B and C strikes approximately N05°S and have about 500m separation from each other apart. They were mapped during the field work and marked using GPS (see Figure 3.2b). The topography surface expressions within the four magnetic profiles were re-drawn using elevation values obtained on the field (Figure 3.3, Appendix 03). The elevation values along each profile (with 25m station separation) were plotted to further enhance the orientation of the surface structures in the south of Lake Magadi. The profiles, as confirmed by the field work reveal that the lake is bounded by basaltic rocks which are of high elevation both to the west and east of the study area (Figure 3.3). The basin is characterized by sediments, comprising of the alkaline trachytes, mud, clay and silt. The chert deposit forms linear structures trending approximately north-south. They are supposed to have been deposited within the fault zones in the lake basin (Atmaoui and Hollnack, 2003).

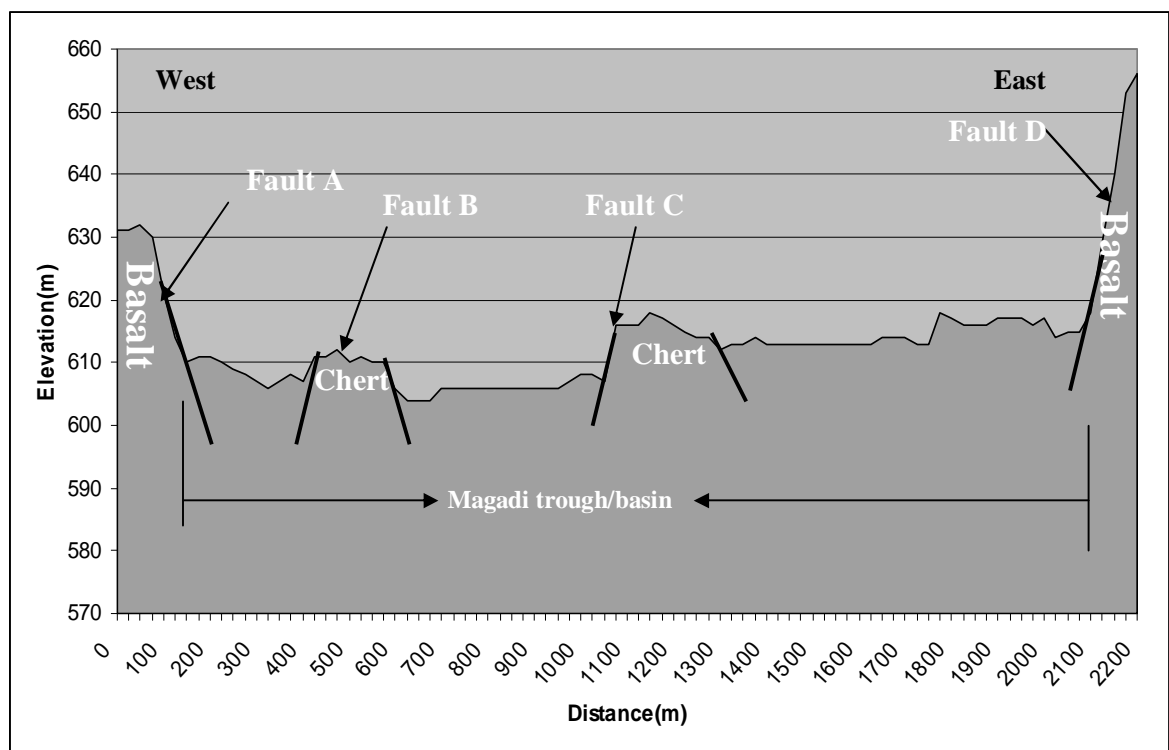


Figure 3.3. Elevation Cross section along the magnetic traverse 1 showing the surface structures

The identified N-S structures in the south of Lake Magadi that have been proposed to be the fluid conduit for the hot fluids flow to the surface and the deposition of trona in the lake were investigated in the field using ground geophysical techniques.

4. Geophysical Imaging of Fluid Conduits around Lake Magadi

In order to map the fluid conduits, a field work for ground investigation was proposed. The field work was carried out within two weeks, from 15th to 30th September, 2009. During the field work, ground geophysical data were collected. Magnetic data were collected across the major faults namely; A, B, C, D (from west to east) in the south of Lake Magadi near the hot springs while resistivity data were collected across Faults D towards Fault E (see Figure 3.2b). Two (2) sections (data) were collected for both resistivity and magnetic data; these were combined with the existing data in the same area for processing and analysis. The resistivity profiles (R1 and R2) were conducted between two faults in the southeast covering 450m and 360m length respectively while the magnetic profiles were made across the four major faults of approximately 2.3km long (see Figures 3.2b). The geographical locations of each station interval along the profiles were recorded using extrex GPS with accuracy of 8m.

4.1. Electrical Resistivity Survey

4.1.1. Resistivity Meter

Resistivity equipment used in this research is Syscal R1 Plus Resistivity Meter (Figure 4.1). The resistivity meter is an IRIS instrument designed for medium- depth investigation. It is made up of a power source which transmits up to 600V output voltage and a receiver unit. The equipment generates current from the power source, measures the resultant voltage and displays the apparent resistivity value.

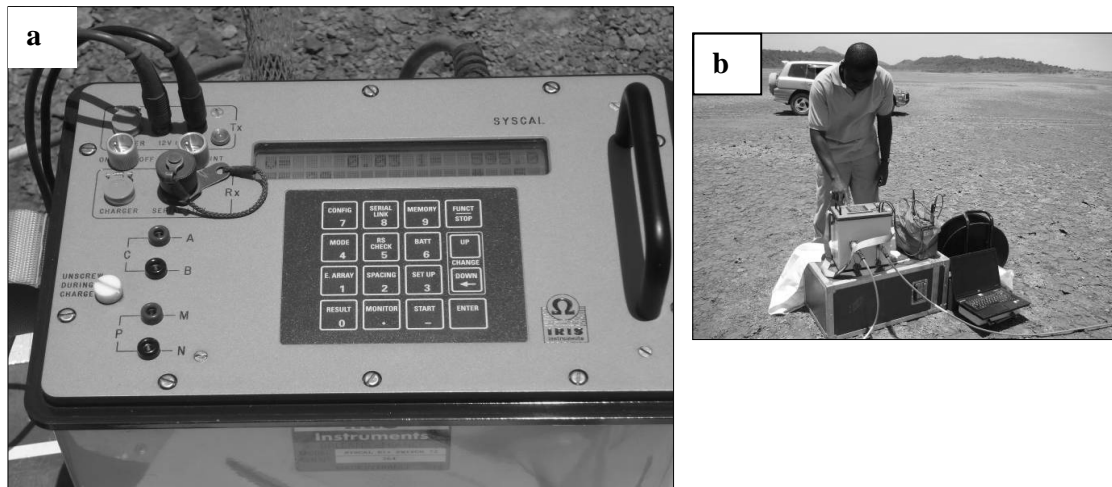


Figure 4.1. a) Syscal R1 Plus Resistivity Meter, b) Field data acquisition with the instrument.

It consists of internal switching board of 72 electrodes with 200W power source. It is meant to automatically measure the subsurface resistivity via the injected electrodes with roll along capability. The equipment has two strings which are connected to the 36 electrodes on both sides through heavy duty seismic cables with either 5 or 10m electrode spacing. Syscal R1 Plus Resistivity Meter combines both horizontal profiling and vertical electric sounding using wenner and Schlumberger array

respectively. It is generally used in engineering and civil engineering works such as pollution mapping, depth-to-rock determination, bedrock mapping and groundwater exploration.

4.1.2. Data Collection

2D resistivity profiles data (see Figure 4.2) separated by 500m were collected during the field work against the intended four (4) parallel profiles planned. This was as a result of the non-availability of the equipments throughout the full period of the fieldwork. Profile R1 was executed within the sediment basin in the southeast of Lake Magadi, between Faults D and E (striking N05°S and N20°S respectively), while the second profile (R2) exists between the Faults C and D (Figures 4.2, 4.3(a and b) and 4.4b). The Wenner array electrode configuration was adopted in this research for both lateral and vertical resolution. The length of the single profile achieved during the survey was 360 meters using 4 cables (18 electrodes each) with 5 meter separation. In order to increase the lateral extent of the profile, roll along was performed for the profile 1 covering a distance of 450m with the depth of investigation of 75 meters while the normal single profile (360m distance) was achieved for profile 2 due to the data download problem encountered on the field. The 2 profiles (R3 and R4) were collected during the 2008 field work (Figures 4.2 and 4.4b) using the same resistivity equipment. These profiles had a lateral distance of 450m in the east-west direction and are separated by 1km.

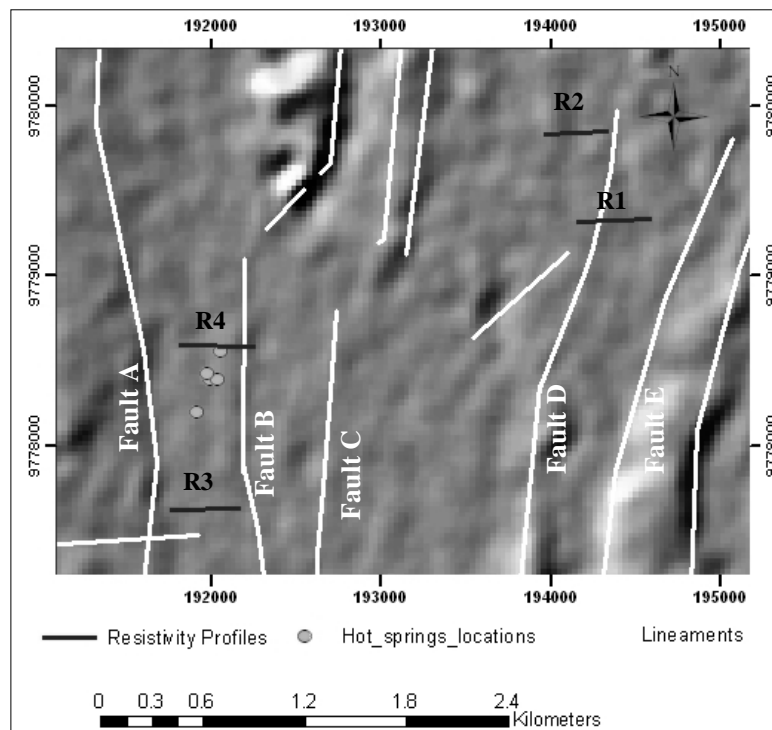


Figure 4.2. Hill shade AsterDEM showing the locations of resistivity profiles (R1, R2, R3 and R4) in the study area.

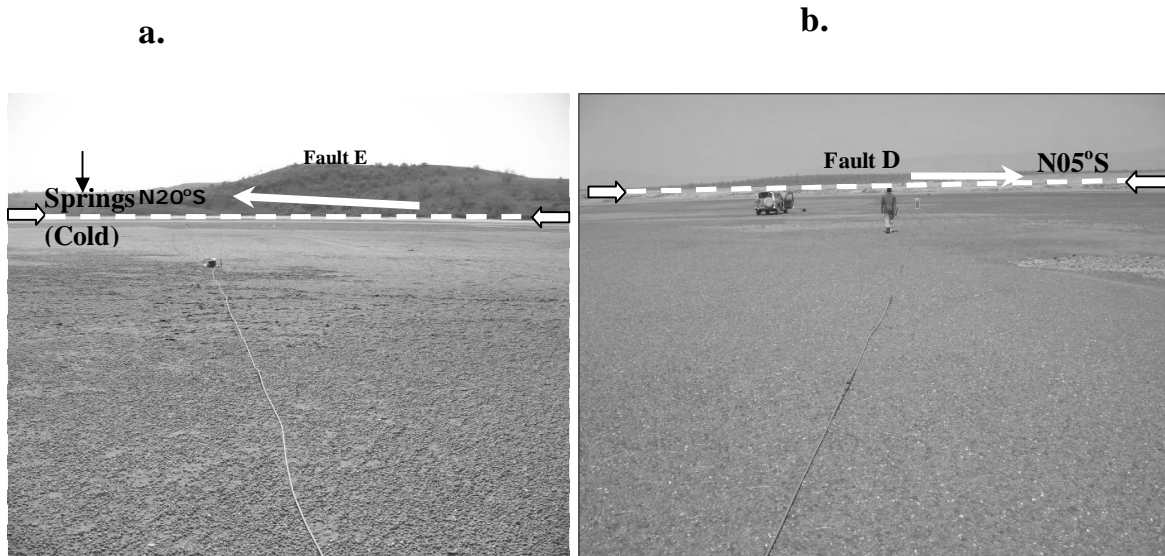


Figure 4.3. Field photo showing :**(a)** the resistivity profile R1 close to Fault E (N20°S) and **(b)** across Fault D (Photo b (looking west)) striking N05°S. The profile (R1) is about 50m away from the springs (cold) in the southwest of Lake Magadi

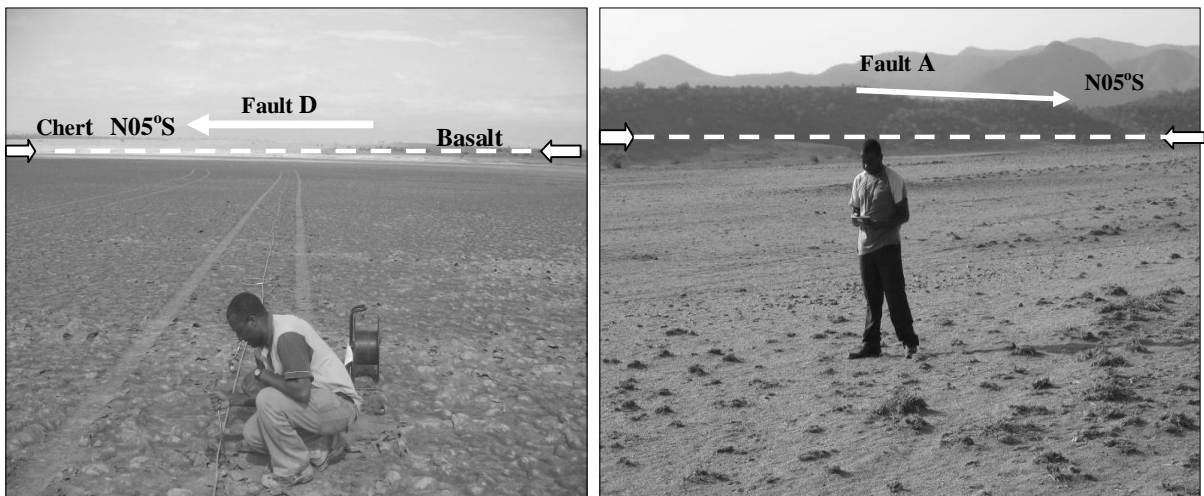


Figure 4.4. **(a)** Field photo showing Profile R2 between Faults C and D (Photo looking north). **(b)** photo showing the western most basaltic rock (looking south) where profiles 3 and 4 were taken by Sequar (2009) during 2008 field work. The arrow in both photos is pointing north

4.1.3. Resistivity Data Inversion

After the data acquisition, the measured apparent resistivity data were uploaded from the resistivity instrument into the laptop for further processing and analysis.

In principle, the measured data during resistivity survey is the bulk resistivity of the sub-surface which is also known as apparent resistivity. Since most investigations are not aimed at knowing the bulk subsurface parameters but the subsurface layers resistivity distribution, there is need for an efficient and accurate inversion method. Resistivity inversion can simply be defined as the process of reconstructing subsurface resistivity distribution from the measured apparent resistivity or voltage data

(AGI, 2008). The inversion of resistivity data has dominated the convectional curve matching process for determining the subsurface true resistivity. Application of the inversion program to the measured apparent resistivity enables clear interpretation of the Earth's resistivity structure (Boonchaisuk et al., 2008). Different 2D resistivity inversions methods have been proposed by different authors (Pelton, 1978; Tripp et al., 1984)

The exported apparent resistivity data for the four profiles (see Appendix 01) were inverted in the Earth Imager software; an inversion program developed by the United States based Advanced Geosciences Inc. (AGI). The software automatically calculates the subsurface true resistivity using various inversion settings. In this research, the inversion technique adopted was the Robust Inversion. The latter technique is based on the assumption of exponential distribution of data errors; it has been found to be very effective inversion methods for noisy data (AGI, 2008).

The inversion procedures were generated for different numbers of iterations in order to achieve a better and accurate subsurface image, with relatively low root mean square error (RMSE). The results of the resistivity inversion and their interpretations are discussed in the following section.

4.1.4. Geo-resistivity structures along Resistivity Profiles

The main objective of deploying resistivity method was to image the geometry of the subsurface fluid conduits (faults and fractures) with their fluid content. Inverted 2D resistivity profiles in the south of Lake Magadi have revealed the fluid distribution and migration path within the active faults and fractures. The descriptions of each resistivity profiles, their resistivity distributions and geological implications are explained below.

Profile One (R1)

Total lateral extent of 450 m with 5 meters electrode spacing apparent resistivity was inverted to a penetrating depth of 75 m as shown in Figure 4.5.

The 2D Resistivity model is characterized by relatively low resistivity distributions with the highest resistivity value of 2.0 ohm-m (Figure 4.5). The highly fluid saturated saline alkaline trachytes with mud and clay which are predominantly seen on the surface show a very low resistivity (0.10 - 0.33 ohm-m) with thickness of approximately 10m. This very low resistivity zone commences at 45m station along the profile (west – east) with a lateral extent of about 305m towards the Fault E. Below is a low resistivity (0.15 – 0.33 ohm-m) attributed to a saline fluids, probably hydrothermal. These are clearly manifested on the surface very close to Fault E in the study area (see Figure 4.3a and Appendix 04c). The saline nature of Magadi springs and brine has been reported by Jones et al. (1977) and Eugster (1970; 1986). There is an increase in the resistivity profile from near surface to the bottom of the profile. This could be attributed to the salinity differences beneath Lake Magadi. The salinity as revealed by Jones et al. (1977) results from the concentration of both surface (meteoric) waters and saline groundwater (or hot water). This and also the presence of clay must have resulted in the very low resistivity values in the area. Weathered chert rock within the fault zone D shows a relatively high resistivity (0.65 – 2.0 ohm) with a possible fault splay which extends to depth of about 65m.

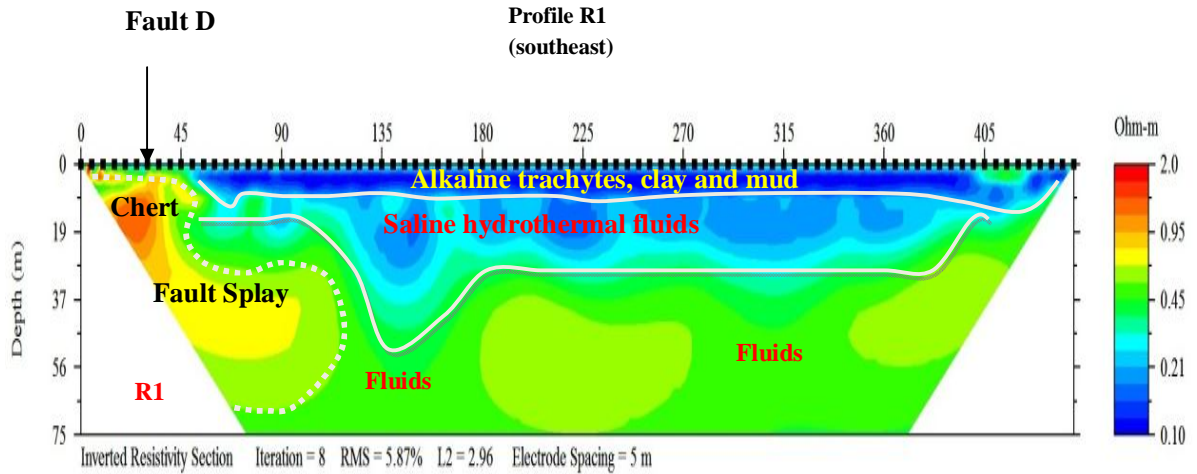


Figure 4.5. Inverted 2D resistivity section for profile1 across fault D and towards Fault E in the southeast of Lake Magadi.

Profile Two (R2)

In Figure 4.6, the alkaline trachytes, clay and mud show low resistivity similar to that in profile R1. Continuous vertical variations in the bulk resistivities as revealed in the model could be attributed to salinity differences as indicated also in profile R1 (Jones et al., 1977; Wilson et al., 2006). The relatively high resistivity (2.1 – 5.8 ohm-m) at Fault D coincides with the chert rock linear alignment (N-S) in the study area. The chert rock separates the saline fluid-filled sediments both to the west and east of the Fault D and it is assumed to have been deposited within the fault zone (Atmaoui and Hollnack, 2003; Sequar, 2009). The resistive structure (1.0 – 5.8 ohm-m), which are covered by the sediments shows some degree of fractures in the subsurface.

The alkaline trachytes and clay show approximately the same thickness as profile R1. The profile also show decrease the saline concentrations as the resistivities gradually increases. Generally, the two models show similar geo-electric structure in terms of alkaline sediment thickness, saline fluids and fractures.

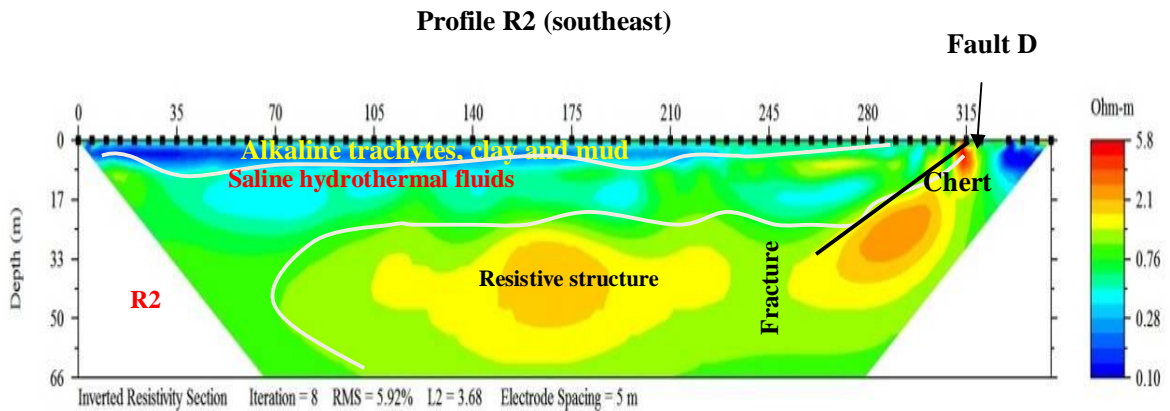


Figure 4.6. Inverted 2D resistivity section for profile 2. The profile crosses Fault D almost perpendicular to its strike direction.

Profile Three (R3)

Inverted 2D resistivity model of profile R3 shows approximately funnel shaped feature with low resistivity (Figure 4.7). This funnel shaped feature which extends to surface is bounded on both sides by high resistivity structures; it coincides with the hot springs location (see Appendix 04a and b), which exists between Faults A and B (Figures 4.2 and 4.7). The low resistivity is characteristic of a typical geothermal environment where saline hot fluid circulates within reservoir and finds its way to the surface through a connecting path (Bibby et al., 2009; Hunt et al., 2009). The geo-electric structure shows the subsurface faults which can be classified as normal fault with splays both to the west and east. The upward inclination of the fluids both to the west and east within the resistive body shows probably that the fluid path follows the direction of the conduits (faults) to the surface.

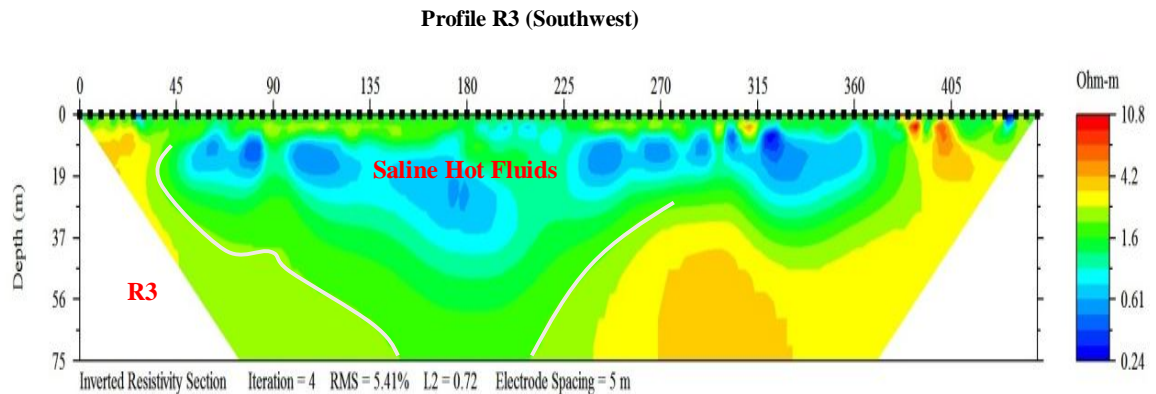


Figure 4.7. Inverted 2D resistivity section for profile 3 between Faults A and Fault B in the southwest of Lake Magadi.

Profile Four (R4)

The depth of investigation of the inverted resistivity is 75 metres with well defined geological units comprising faults splay both to west and east (Figure 4.8). The geo-electric structures show similar unit with the profiles (1, and 3) in terms of fault inclination and funnel shaped structure. The low resistivity observed is probably due to the presence of the hot-springs which in principle increases its conductivity. The hot fluid (0.18 – 1.0 ohm- m) upward movement with funnel shape structure follows the path between a fault zones (about 125m wide). The fault zone exists between the high resistivity rock bodies. In general, the saline hydrothermal fluid shows a sharp resistivity contrast with the surrounding rocks. The high resistivity in the near surface can be attributed to the volcanic rock outcropping within the hot springs from the field observations.

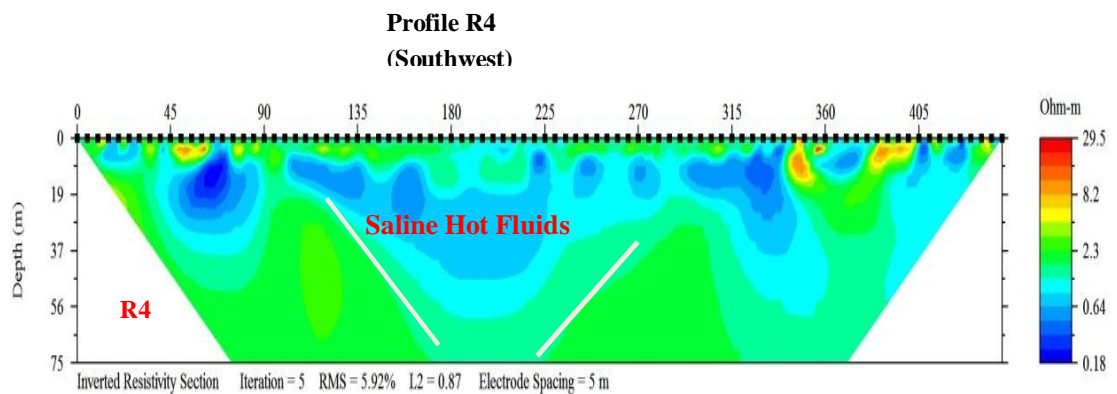


Figure 4.8. Inverted 2D resistivity section for profile 4 across Fault B towards Faults A in the southwest of Lake Magadi.

4.2. Ground Magnetic Survey

4.2.1. Instrument

The instrument used for the magnetic survey is the Geometrics 856 Proton Precession Magnetometer. It measures the absolute value of total magnetic field to a resolution of 0.1 nT with accuracy of 0.5 nT. It is used in various field applications such as faults and geological mapping, mining and location of magnetic materials. It is made up of six digit display of the magnetic field and three digit displays of station, line number and signal strength (Figure 4.9). Geometrics 856 Proton Precession Magnetometer uses 9 D cell industrial grade batteries and it is connected to magnetic coils mounted on the pole for measurement.

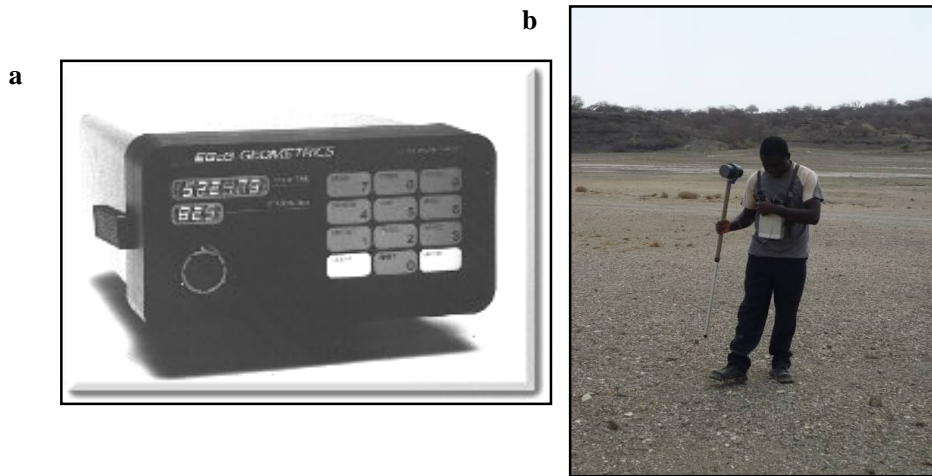


Figure 4.9 (a): Geometrics 856 Proton Precession Magnetometer (b): Field photo showing data acquisition with the instrument.

4.2.2. Data Collection

Ground magnetic data were collected perpendicularly to the strike of the four (4) structures in the south of Lake Magadi (see Figures 3.2, 4.10 and 4.11). The two profiles (P1 and P2) collected covered a lateral distance of 2.3 km running west–east direction across the hot springs which are located along the lake margins (Figure 4.11a). The profiles cover the area marked by Faults A and D. The latter faults are defined by steep fault scarp (Figure 4.11b). The 2 parallel magnetic traverses (P1 and P2) were separated by a distance of 330m from the two existing magnetic profiles acquired during the 2008 field work. The latter profiles were taken to bridge the wide separation existing between the profiles and for close detection of the possible anomaly in the area. The four profiles P1, P2, P3 and P4 are separated by 330, 330 and 360 meters respectively (Figure 4.11).

Magnetic measurement was taken at every 25m station along the traverse (west-east direction) with the base station readings taken at every one hour for diurnal correction at the same position where the previous data was taken.

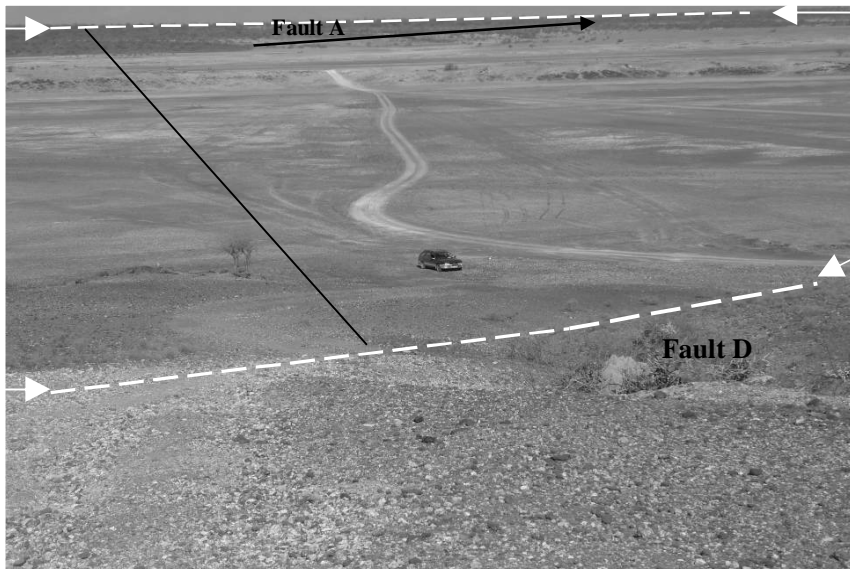


Figure 4.10. Field photo showing the magnetic profile extent from Fault A to Fault D (on a west-east direction); the black arrow is pointing north.

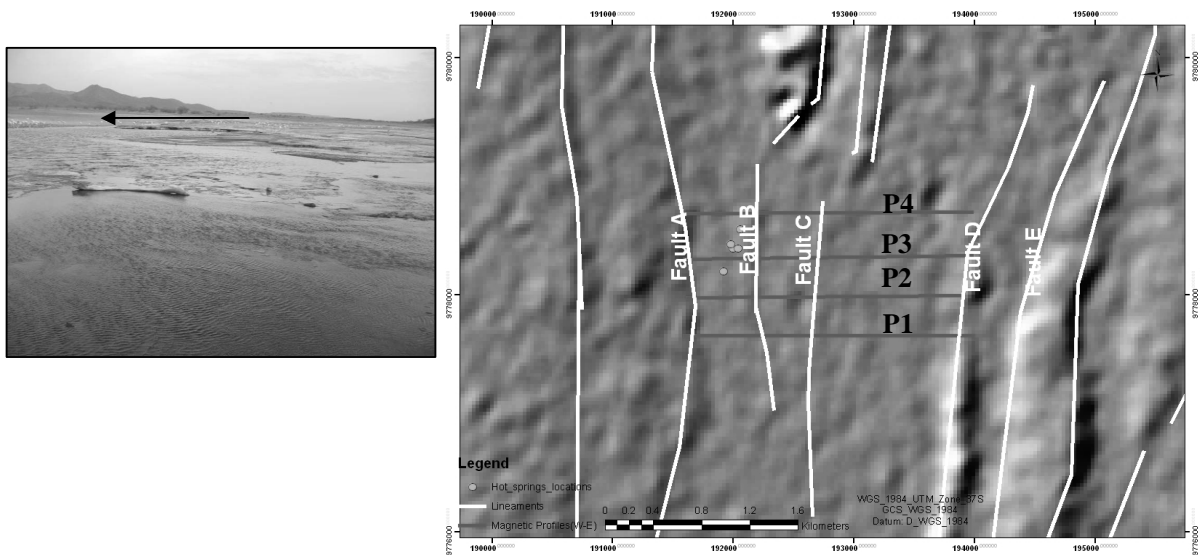


Figure 4.11 (a): Field photo showing the hot springs along the lake margin between Faults A and B. (b): Hill-shaded AsterDEM showing the magnetic profiles across the major faults in the study area.

4.2.3. Magnetic Data Corrections

The acquired data, plus the existing ones were collated and processed for effective interpretation of the subsurface fluid conduits (faults and fractures) geometry.

4.2.3.1. Diurnal Variation Correction

Variation of Earth's magnetic field with time, due to the rotation of the earth and with respect to the solar wind, which may last several hours to one day, is called diurnal variation (Riddihough, 1971). In order to correct for drift or diurnal effect in the magnetic readings, a base station within the four magnetic profiles, assumed to be free from magnetic noise were selected. Repeated readings were taken every one hour of the magnetic measurement for the drift correction. After the data collection,

the diurnal effect was calculated and the magnetic data were filtered. Noise due to secular change or epoch was considered negligible because consistent measurements were taken at the base station every one hour (Adepelumi et al., 2008).

4.2.3.2. Calculation and Removal of the Geomagnetic Field

Magnetic survey involves measurement of the sum of magnetic field produced by both local and regional magnetic fields. The regional magnetic field, often referred to as geomagnetic field needed to be subtracted from the acquired total magnetic field to obtain the magnetic field anomaly caused by the local source.

After subtracting the diurnal effect from the original magnetic data observed, the geomagnetic field was calculated using the mathematical model of earth magnetic field called the International Geomagnetic Reference Frame (IGRF) model 2005 in Geosoft Oasis Montaj software. This model is calculated based on the dates, elevation and geographical locations (latitudes and longitudes) of the observed magnetic data with the generated average geomagnetic field of 33430nT, inclination of -26.2° and declination of 0.03° . The IGRF values were subtracted from the observed magnetic values for each station to determine the residual magnetic field due to anomalous contribution from local magnetic sources in the area.

4.2.4. Data Enhancements and Analysis

The corrected magnetic data were presented both in 2D profiles and grid forms for visualization and further enhancements. For 2D visualization, the total magnetic field intensity for the four profiles were plotted against the separation distance as shown in Figure (4.12), after which the possible noisy (spikes) data were removed. In addition to profiles plots, the total magnetic intensity (TMI) data were gridded using minimum curvature gridding method with 50m cell size, having the four faults and hot-springs locations overlaid (Figure 4.13). For effective interpretation of the obtained magnetic data, further enhancements were carried out using various filtering techniques.

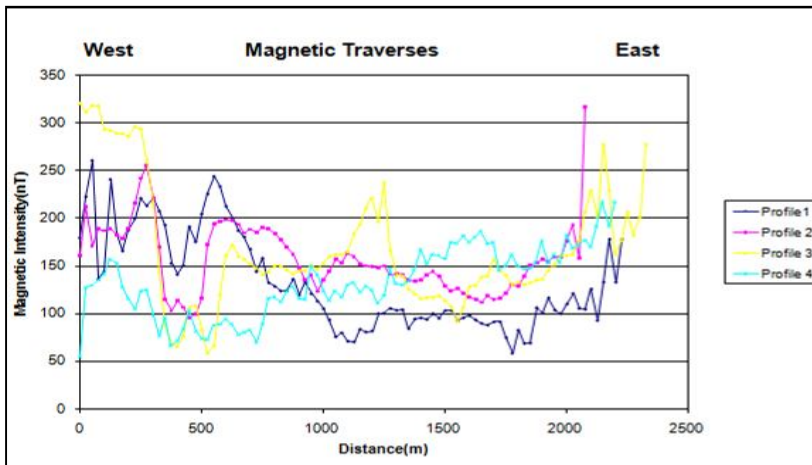


Figure 4.12. Ground magnetic data (total magnetic field intensity) obtained from the traverses 1, 2, 3 and 4 after correction

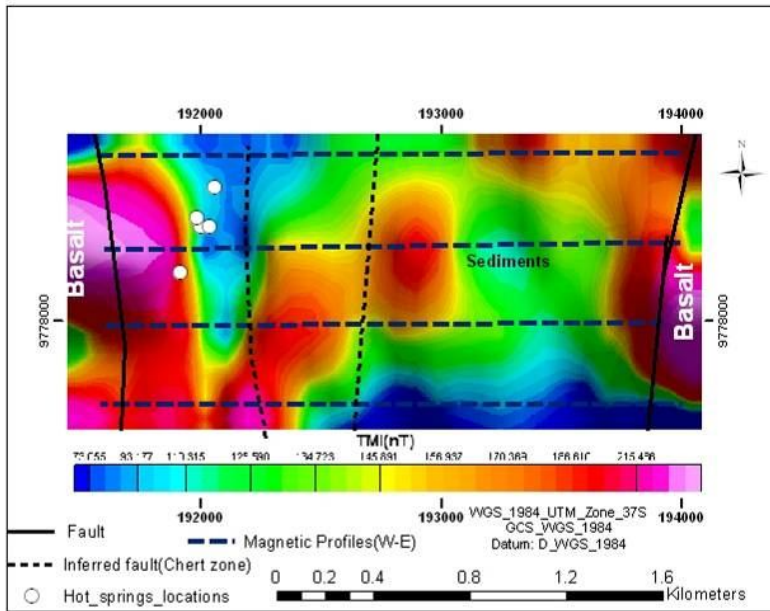


Figure 4.13. Gridded residual ground Total Magnetic field Intensity (TMI) for the four profiles (in blue) showing hot springs and faults locations.

4.2.4.1. Vertical Derivatives

Vertical derivatives of magnetic data generally aid the interpretation process as it enhances and sharpens geophysical anomalies. This filtering method is effective in enhancing anomaly due to shallow sources; it narrows the width of anomalies and very effective in locating source bodies more accurately (Cooper and Cowan, 2004). Vertical derivative was done by applying low-pass filters to remove high-wavelength, thereby enhancing low-wavelength component of the magnetic spectrum. The vertical derivative of the total magnetic Intensity was derived in Geosoft oasis software as shown in Figure 4.14.

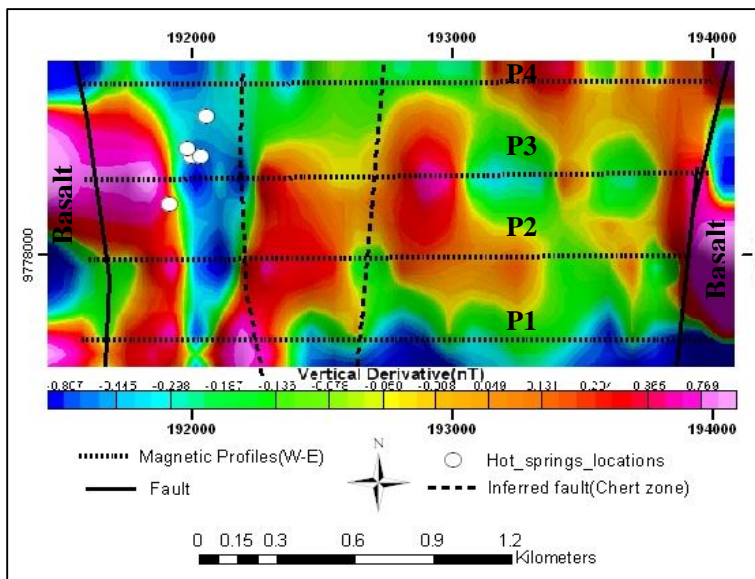


Figure 4.14. Colour-shaded Vertical derivative of the magnetic field intensity showing the shallow magnetic sources.

4.2.4.2. Analytical Signal

Absolute analytic signal according to Roest et al. (1992) can be defined as the square root of the squared sum of the vertical and horizontal derivatives of the magnetic field (Equation 4)

$$AS = \sqrt{\delta x.\delta x + \delta y.\delta y + \delta z.\delta z} \quad \text{Equation (4)}$$

where the dz is the vertical derivative, dx and dy are the horizontal derivative and AS is the analytical signal. The advantage of this method of magnetic data enhancement is that its amplitude function is an absolute value and does not need assumption of the direction of source body magnetization (Jeng et al., 2003). Analytical signal can be used to locate the edges of remanently magnetized bodies, reveal anomalous texture and highlight discontinuities (MacLeod et al., 1993). The analytical derived from the obtained magnetic data enhances the edges of the major structures in the study area (Figure 4.15).

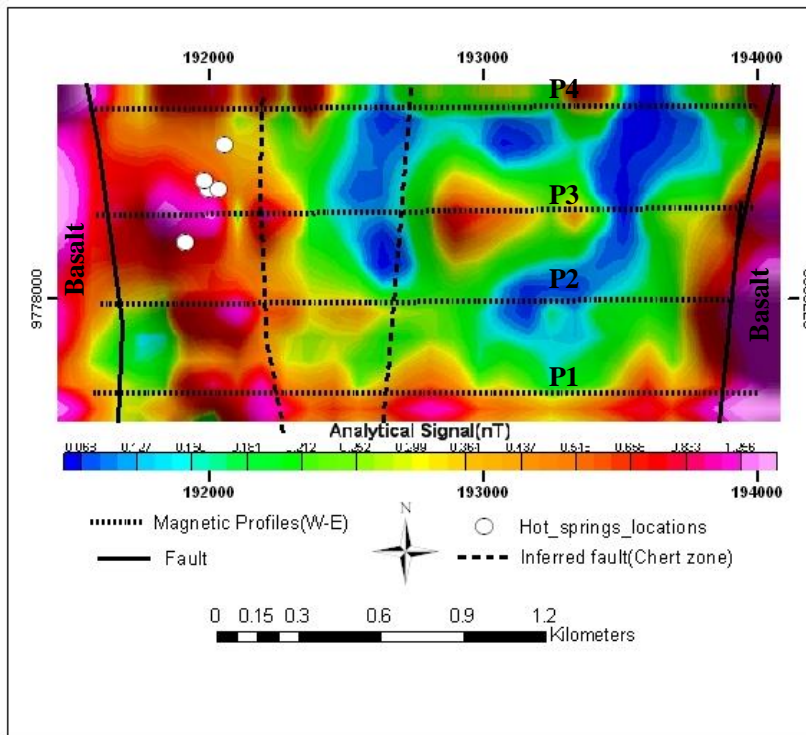


Figure 4.15. Colour -shaded Analytical signal maps of the four profiles

4.2.4.3. Euler Deconvolution

Euler deconvolution is an inversion method for estimating location and depth to magnetic anomaly source. It relates the magnetic field and its gradient components to the location of the anomaly source with the degree of homogeneity expressed as a structural index and it is the best suited method for anomalies caused by isolated and multiple sources (El Dawi et al., 2004). The structural index (SI) is a measure of the fall-off off the field with distance from the source. Euler deconvolution is expressed in Equation (5) as:

$$(x - x_o)\delta T / \delta x + (y - y_o)\delta T / \delta y + (z - z_o)\delta T / \delta z = N (B - T) \quad \text{Equation (5)}$$

Where (x_o, y_o, z_o) is the source position of a magnetic source whose total field T is measured at x, y, z. B is the regional value of the total field. N is expressed as the structural index (SI), a measure of the

rate of change with distance of the potential field; it depends on the geometry of the source (El Dawi et al., 2004).

Estimating depth to magnetic anomaly using Euler deconvolution involves; i.) Reduction to the pole and ii.) Calculation of horizontal and vertical gradients of magnetic field data, calculated in frequency domain, iii.) choosing window sizes and iv.) structural index, e.g. contact, dike and point (Figure 4.16).

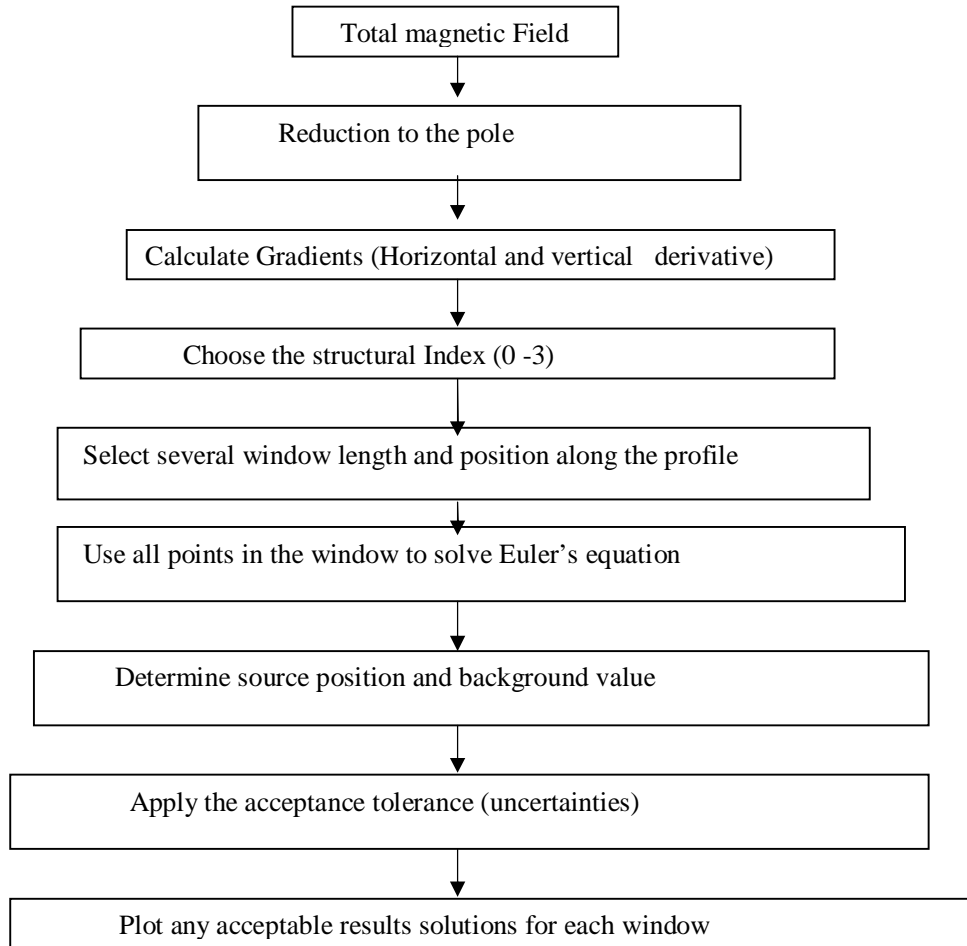


Figure 4.16. Euler Convolution input and step process [modified after El Dawi et al. (2004)]

In general, the desired structural indices are chosen with the window size for depth determination. This is set based on the anomaly of interest. In this research, both 3D and 2D Euler deconvolution were adopted for both the gridded and profiles data respectively.

2D Euler Deconvolution

Two- dimensional Euler deconvolution was generated from the software developed by Cooper (2004) for constraining the subsurface geometry along the profile lines. The software requires magnetic parameters such as the geomagnetic field, survey locations, inclinations and declination angles. Two columns with a space delimited ASCII file are required for input; the first column is the magnetic station locations while the second column is the corrected magnetic field values. The results of the IGRF in section 4.2.3.2 was used as the inputs for this process, i.e. geomagnetic field

intensity of 33430nT, inclination of -26.2° and declination of 0.03° . Similar to the 3D Euler deconvolution, the structural indices and the Euler window size must be selected. In this research, a window size of 13, 110m X-separation and 55m Y separation were adopted. To better constrain the subsurface geology, 1.0 structural index (steep contact) which is an indication of faults contacts were plotted for all the traverses; these are shown in Figures 4.18- 4.21 respectively.

3D Euler Deconvolution

3D Euler deconvolution was performed on the total magnetic intensity (TMI) grid data using standard Euler deconvolution. This was done to locate depths to the lithology contacts on the gridded map. The best clustering Euler depths was achieved using solution window size of 4, 1.0 structural index (SI) (steep contact) and 15% depth tolerance. The results were plotted on the analytical signal map for effective interpretations (Figure 4.17).

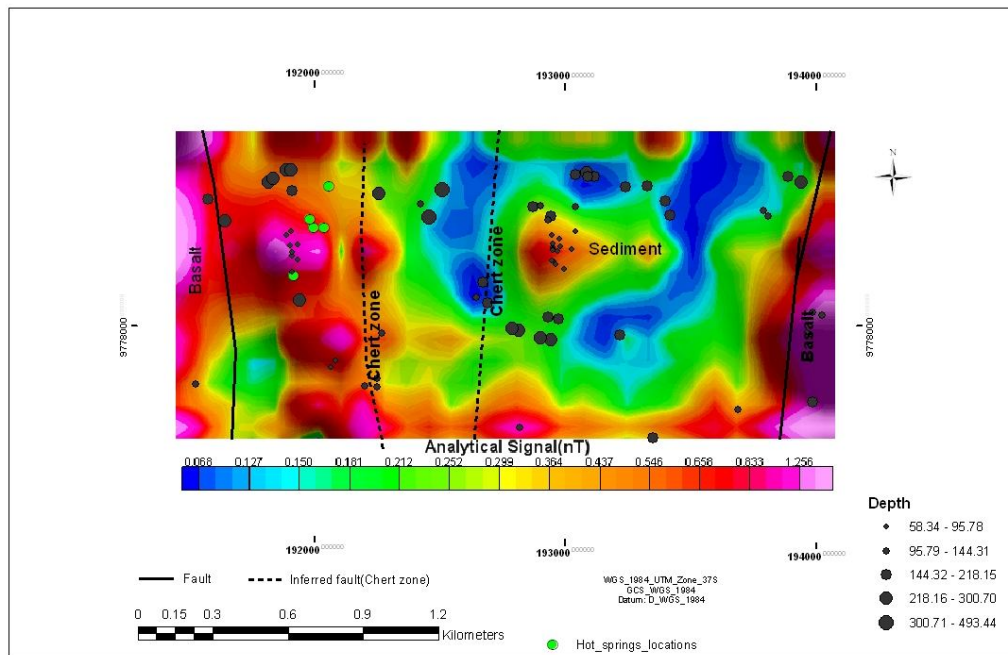


Figure 4.17. 3D Euler's depths solutions (structural index of 1) plotted on the colour shaded analytical signal map.

4.2.5. Magnetic Data Interpretations

4.2.5.1. Interpretation of magnetic grids

The detail 2D analysis and interpretations of each profile are explained in Section 4.2.5.2. From the TMI grid data, the high intensity magnetic signals at the eastern and western margins of the profiles mark the faults with basaltic rocks (see Figure 4.13) while the eastern margin of the profile 3 shows a decay of the magnetic intensity corresponding to the end of the basalts and marking the onset of the chert zone. The basin is characterized by low magnetic signatures which can be attributed to the presence of fluids. The two chert zones shows reasonably high magnetic anomaly in the TMI grid (see Figure 4.13).

In the vertical derivative map (Figure 4.14), the hot springs which are clearly manifested in the surface between the north-south trending Fault A and Fault B in the south west show low (negative) magnetic anomaly. The map also shows the lateral continuity N-S faults along the axial rift zone. The high magnetic signal within the basin coincides with the Fault zones (B and C) (see Figures 4.12 and 4.13). The analytic signal map (see Figure 4.15) shows that the survey area is inside a basin surrounded by the west, east Faults A and D. In this map, the edges of the magnetic anomaly are better enhanced and it clearly shows the zones of discontinuities between each geologic unit, especially the major faults in the area. Majority of the hot springs occurs within a boundary between high and moderate magnetic intensity rocks. The location of hot spring is characterised by very low and negative anomaly as revealed in the vertical derivative map (Figure 4.14). The basaltic rocks outcropping at the hot springs are buried by the sediments further south (Figure 4.13); these are probably responsible for the high magnetic anomaly which are evident in the analytical signal map (Figure 4.15). Within the basin is a localised high magnetic anomaly which can be attributed to the presence of volcanic rock. From the depth estimation, the basin, which comprises sediments and volcanics, has the highest estimated depth between 300 and 493 metres. The depth of the western and eastern basalts from the Euler's depth extends to depth of about 300m.

4.2.5.2. 2D Interpretation of the magnetic data along the traverses

Qualitative interpretation of the magnetic traverses shows that the basin is bounded by N-S trending faults both to the west and to the east. The 2D magnetic profiles (Figures 4.18 – 4.21) show the magnetic anomaly observed over the four faults in the south of Lake Magadi. The differences in magnetic anomaly signatures possibly indicate structurally controlled subsurface features (Adepelumi et al., 2008; Telford et al., 1976).

Figure 4.18(b) shows magnetic anomaly along traverse P1. Here, four distinct trends are recognized, which coincide with the location of the identified faults within the basin. The traverse begins with a high and low magnetic anomaly (station 0 – 200m), which is attributed to the highly faulted basaltic dyke that bounds the basin to the west (Figure 4.18 a and b). This signature is followed to the east by generally low signatures (station 200 – 380m). This very low magnetic anomaly coincides with the hot and cold springs locations within the basin. The same result was experienced in Ethiopian Rift by Abiye and Tigistu (2008). The lack of magnetic sources exists mostly between the faults, an evident of the presence of fluids as experienced in the field. The discontinuity between the basalt and sediments basin show the existence of faults between the rock units. A gentle rise in the anomaly towards the east (station 380 -500m) shows the commencement of the chert zone within fault B followed by low signatures characterized by sediments (station 500 -700m). The high magnetic response within the chert zone could be attributed to the presence of chert vein as experienced in the field. At the end of the low anomaly, there is a little rise but undulating signatures (station 700m) which commence the chert zone (Fault C), followed by a relatively low anomaly (up to station 1700m). The eastern- most basaltic rock along the traverse shows a rise in magnetic anomaly. General fluctuation of the magnetic response along the profile and the scattering of the Euler solutions possibly indicate that series of intense tectonic/faulting activity associated with shearing might have taken place within the basin (Adepelumi et al., 2008; Telford et al., 1976).

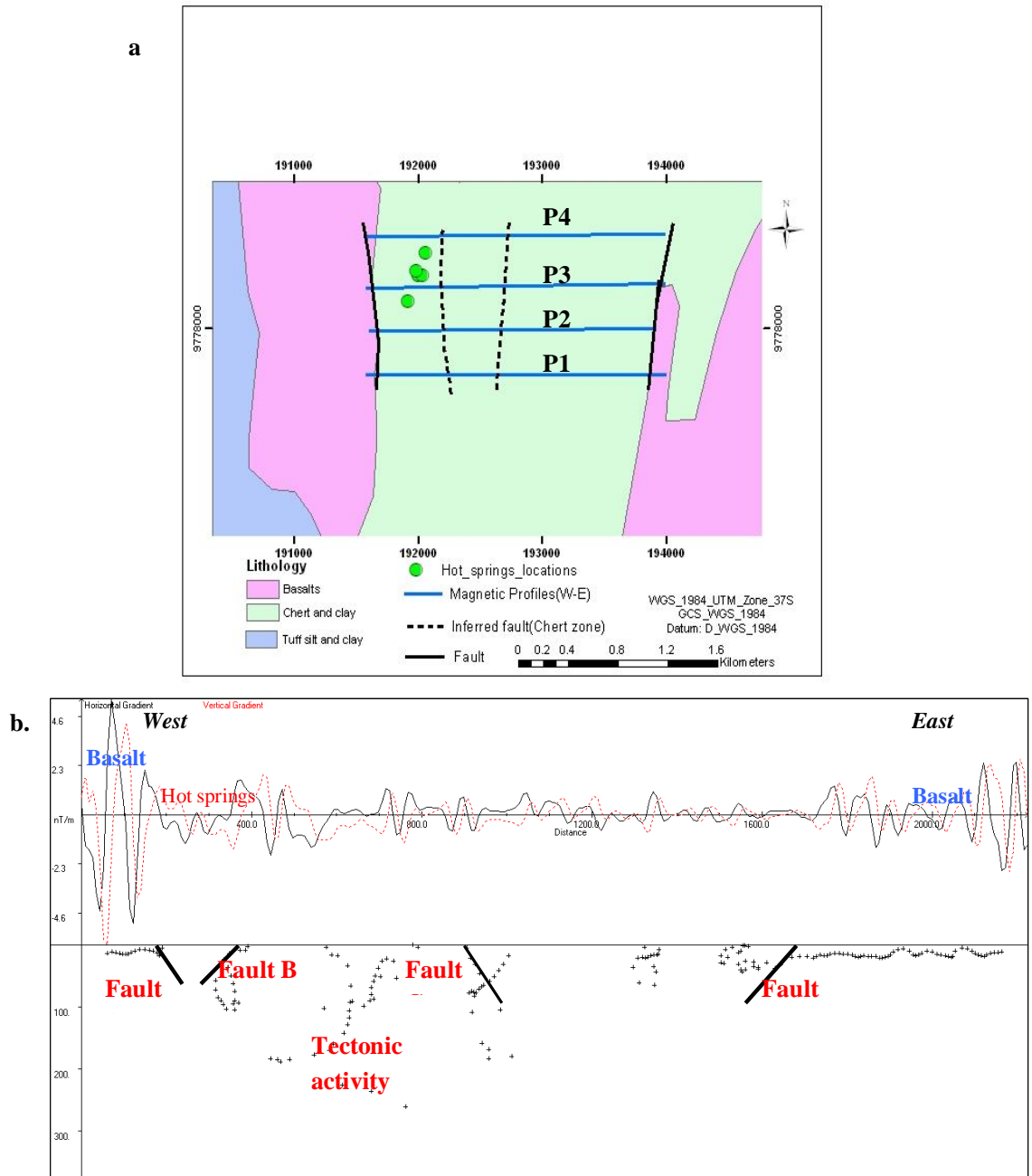


Figure 4.18. **(a)**. Geologic map of the magnetic survey area. **(b)**. Processed ground magnetic data with 2 D Euler solutions obtained along traverse one with inclination and declination angles of -26.2° and 0.03° respectively. Plus (+) signs are Euler solutions for 1.0 structural index.

Traverse P2 and P3 (Figures 4.19 and 4.20) shows similar variation in magnetic signatures as traverse P1. Traverse P3 has a well defined three faults, corresponding to Faults B, C, and D. The variation in magnetic amplitudes and the much scattering in the Euler solution could be attributed to an intense shearing activity and localized anomaly beneath the profiles, which is also visible in the analytical map. These scatterings are not seen in the fourth profile (Figure 4.21). Profile four shows consistent high and low magnetic responses along the transverse. These undulating signatures and the Euler deconvolution solutions clearly show the subsurface faulting/contacts pattern within the geological

units. The subsurface fault geometry as revealed in traverse four shows a general normal faulting system associated with Magadi N-S faults. Generally in all the traverses, Faults A and D show both eastern and western dip respectively. These faults are major structures bounding the basin in the southern part of Lake Magadi.

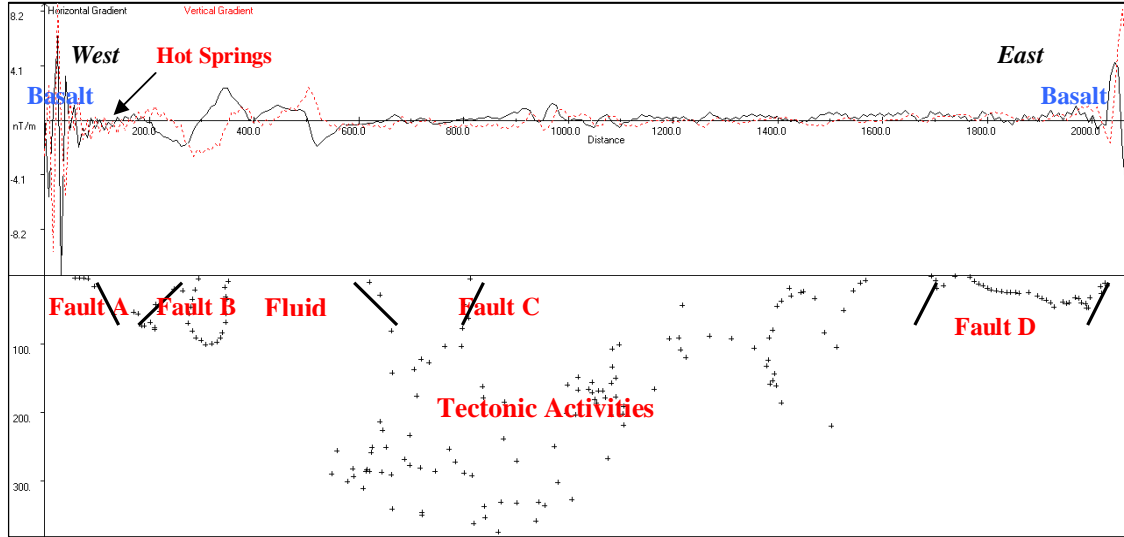


Figure 4.19. Processed ground magnetic data with 2D Euler solutions obtained along traverse two with inclination and declination angles of -26.2° and 0.03° respectively. Plus (+) signs are Euler solutions for 1.0 structural index.

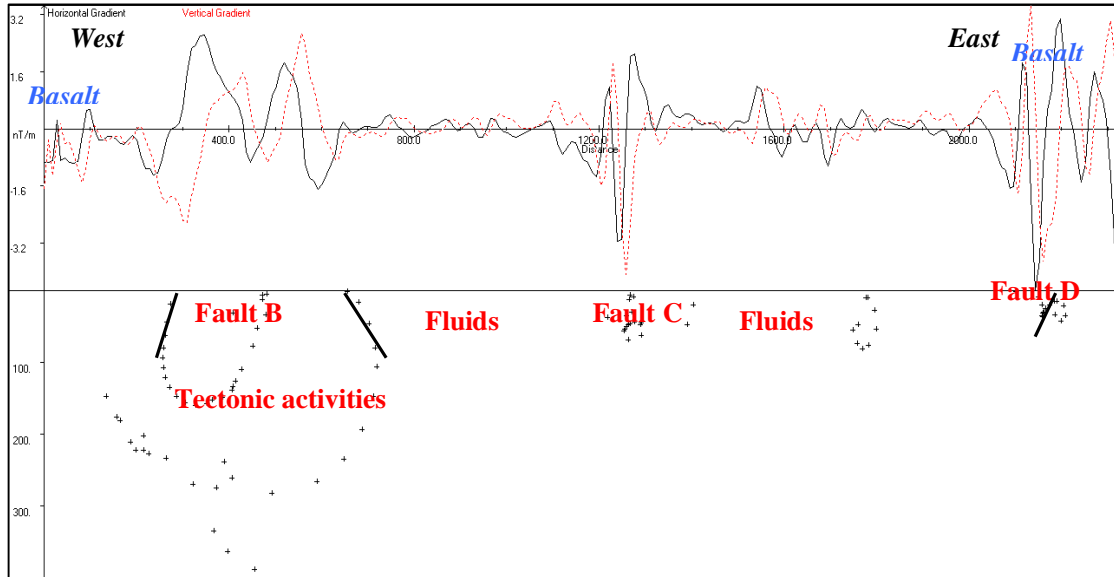


Figure 4.20. Processed ground magnetic data with 2D Euler solutions obtained along traverse three with inclination and declination angles of -26.2° and 0.03° respectively. Plus (+) signs are Euler solutions for 1.0 structural index.

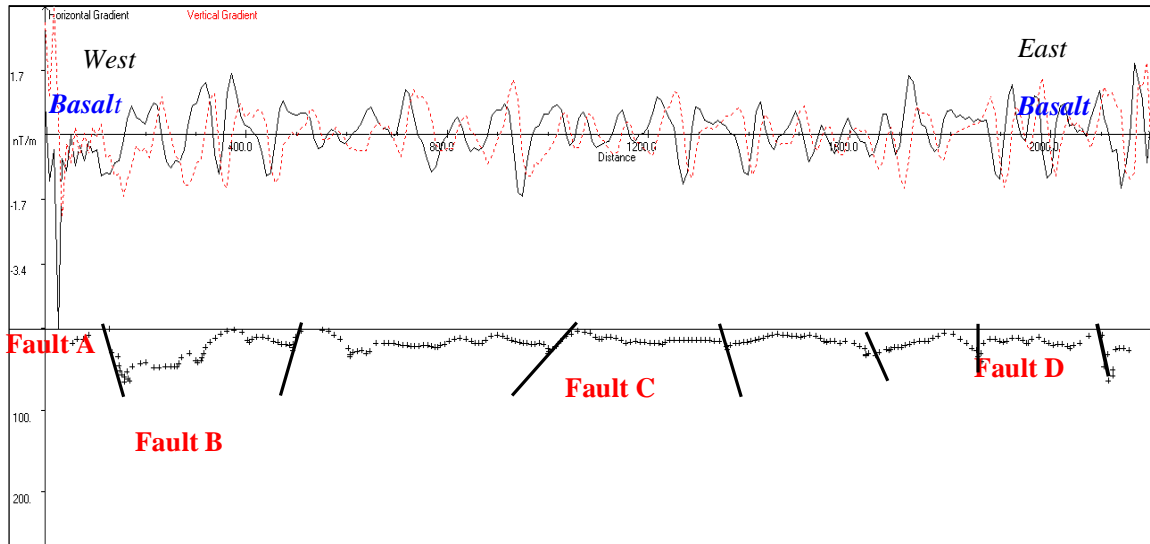


Figure 4.21. Processed ground magnetic data with 2D Euler solutions obtained along traverse four with inclination and declination angles of -26.2° and 0.03° respectively. Plus (+) signs are Euler solutions for 1.0 structural index

4.3. Aeromagnetic Data Analysis

Deep tectonic/faulting activities around Lake Magadi were further investigated using aeromagnetic data. Magnetic data on flight lines 320 and 322, covering about 7.7 km long corresponding to the ground magnetic line 2(P2) and the resistivity profile 2 (R2) were extracted from the total magnetic intensity map of the aeromagnetic data as shown in Figure 4.22a and b. The aeromagnetic data was part of the African Magnetic Mapping Project (AMMP) which was intended to compile airborne magnetic data for some parts of Africa. Aeromagnetic data in the study area was acquired by the Compagnie Generale de Geophysique (CGG) in the year 1987 with 2km line spacing, flight direction of 90° (W-E) and flying height of 2896 m above sea level (Sequar, 2009).

The data processing (levelling correction and geomagnetic field removal) was done by AMMP. The magnetic grid was created using 1km cell size with AMMP grid projection system, re-projected to WGS 84, UTM 37S projection later to conform to the projection used in this research. Lake Magadi study area was clipped from the entire gridded data as shown in Figure 4.22).

The extracted aeromagnetic data were processed and inverted using 2D Euler deconvolution software developed by Cooper (2004) and following the same procedures adopted in the ground magnetic processing in section 4.2.4.3. The magnetic data was used to construct the subsurface geology and to correlate it with the seismic hypocenters as related to the geodynamic activities in the study area. In this case, the results from IGRF 2005 model calculated from the magnetic data were the magnetic intensity of 33414, inclination of -26.3° and declination of 0.002° with structural index of 1 (steep contacts). These were used as inputs to the Euler's software to construct the subsurface magnetic sources along the selected profile lines.

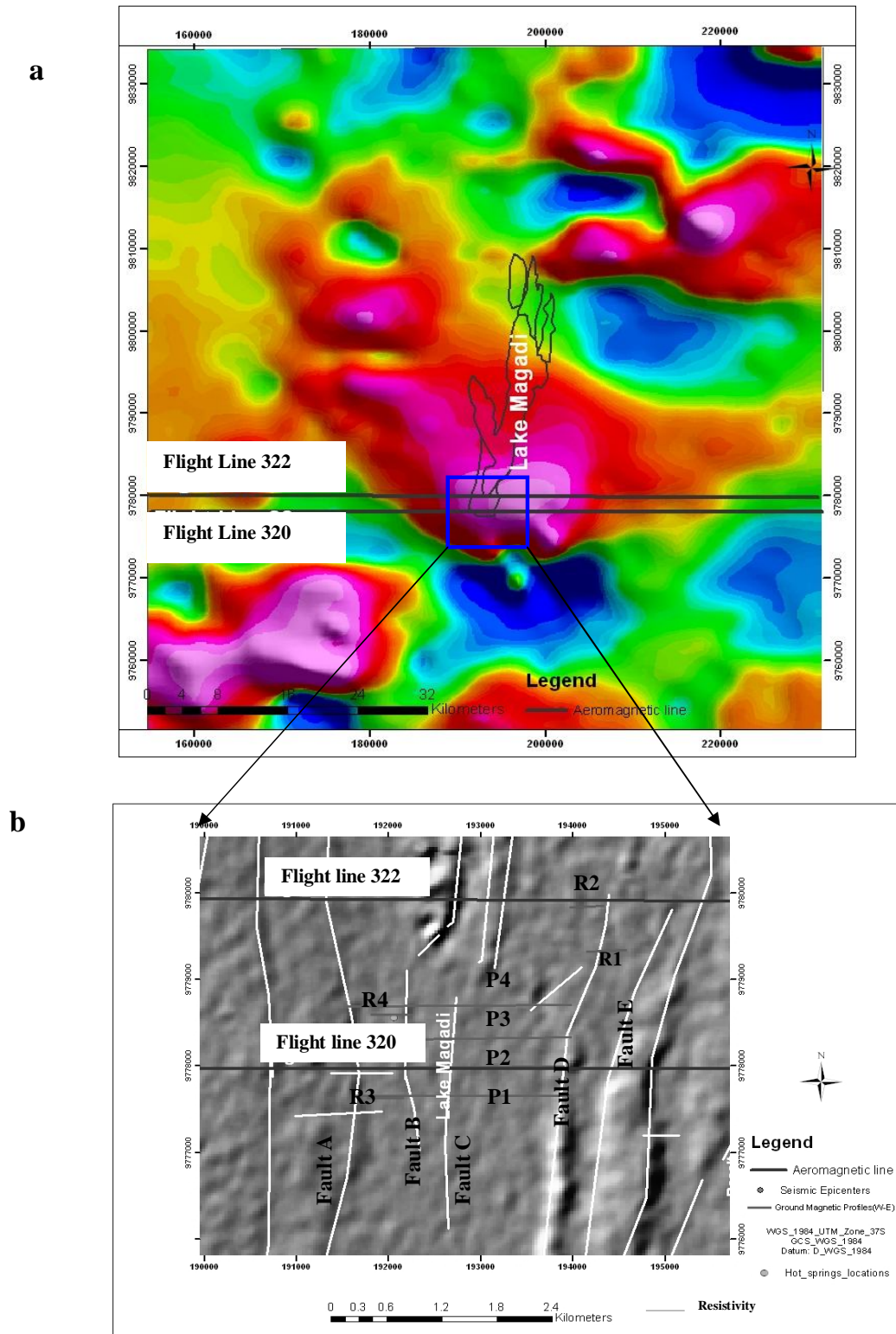


Figure 4.22. **(a)** Colour-shaded Aeromagnetic Total Magnetic Intensity (TMI) grid data for Lake Magadi area. **(b)** Hill-shaded Aster Dem showing ground survey area and corresponding aeromagnetic lines selected for the analysis. R1, R2, R3 and R4 are the resistivity profiles 1, 2, 3 and 4 while P1, P2, P3 and P4 are the ground magnetic profiles 1, 2, 3 and 4 respectively.

4.3.1. 2D Interpretation of the Aeromagnetic Profiles.

The processed aeromagnetic data for lines 320 and 322 are shown in Figures 4.23 and 4.24. The flight lines which are 2km separated from each other shows similar subsurface geometry, both in frequency and amplitudes. Most of the Euler solutions are concentrated along the rift axis while the basin is marked by the absence of magnetic sources. These observations are in line with the results experienced in the northern part of the Kenya rift by Mariita and Keller (2007). The magnetic sources from 2D Euler correspond approximately to the top of the magnetic sources. These sources reflect rock beneath the thick sediment within the axial part of the rift basin/trough. The sub-vertical alignment and scattering of the Euler solutions reveals the existence of tectonic activities (Adepelumi et al., 2008; Kuria et al., 2009; Mushayandevvu et al., 2001) which extends to the depth of 7.5 km (Figures 4.23b and 4.24b). The magnetic sources correspond largely to the tectonic structures (faults). These tectonic structures, approximately at a depth of 7.5km, correspond to the established surface N-S faults A, D and E in the south of Lake Magadi, which bounds the basin in the surface as seen in the topographic profiles (Figure 4.23a and 4.24b).

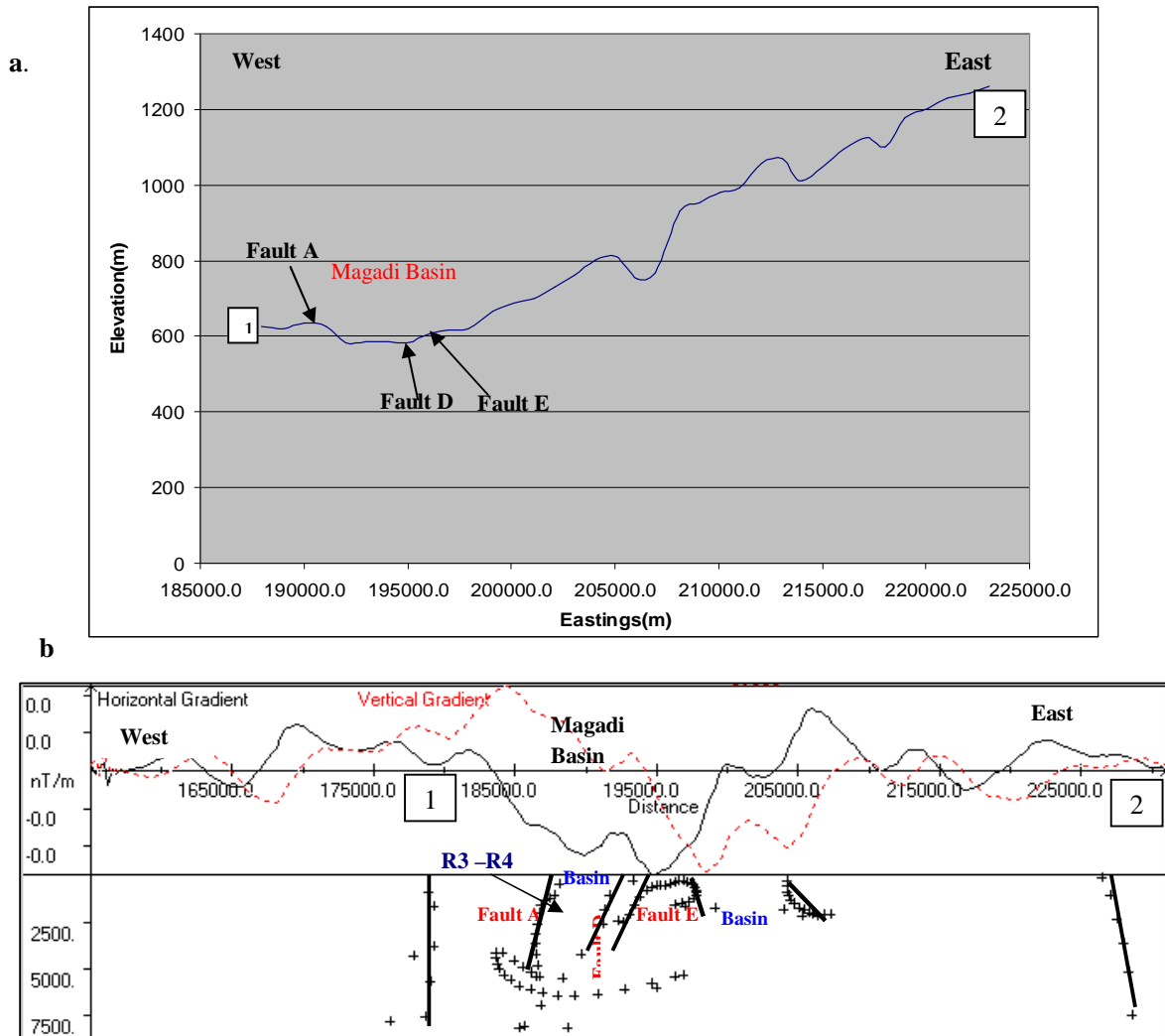


Figure 4.23. (a) Extracted topography elevations of Lake Magadi area from Aster DEM along flight line 330 showing surface faults and grabens. (b) 2D Euler deconvolution solutions from aeromagnetic data along flight line 320. The plus (+) signs are structural index of 1 with inclination and declinations of -26.3° and 0.002° respectively.

The lack of magnetic signal between the faults in the subsurface could be as a result of the presence of hydrothermal fluids within the basin, which are delineated from ERT profiles (Figures 4.5- 4.8). This zone exists between Faults A, D and E and coincides with the ERT profiles (R1-R4). Faults B and C are mostly shallow; they are not clearly manifested in the aeromagnetic profiles, but are visible in the ground magnetic profiles.

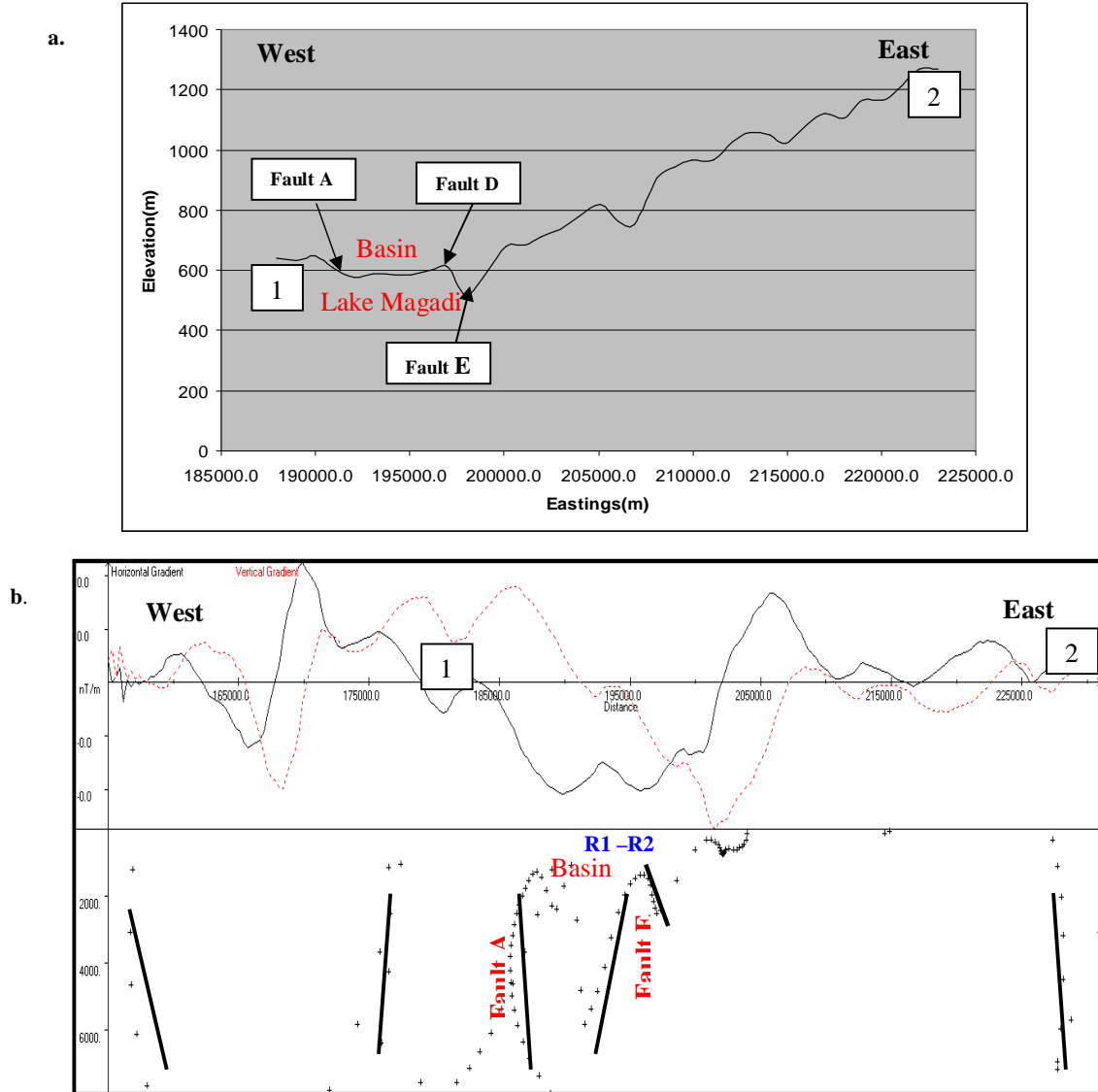


Figure 0.1 .(a) Extracted topography elevations of Lake Magadi area from Aster DEM along flight line 322 showing surface faults and grabens. (b) 2D Euler deconvolution solutions from aeromagnetic data along flight line 322. The plus signs are structural index of 1

5. Magadi Heat Source Depth Estimation

5.1. Curie Point Depth Estimation from Aeromagnetic Data

Curie point depth in this thesis is used to infer transition depth of magnetite. Generally, rocks are usually non-magnetic at temperature greater than the Curie point of magnetite (Stampolidis and Tsokas, 2002). The assumed magma chamber acts as the hydrothermal source in most geothermal environment. To date the Lake Magadi geothermal resources have not been explored in terms of depth to the heat source and reservoir using aeromagnetic data. This estimate is expected to give a clue to the heat flow mechanism and geothermal potential in the area.

The total magnetic intensity (TMI) grid of the aeromagnetic data in Figure 4.22a, with window size of (85km x 75km) was used for the estimation of the Curie point depth using spectral analysis technique.

5.1.1. Spectral Analysis and Curie Point Depth Estimation

Spectral analysis technique was adopted in this thesis to analyze the depth to the Curie point around Lake Magadi. The analysis of the Curie point depth was attempted based on spectral analysis using the same method as Blanco-Montenegro et al. (2003). This method relates the depth to the top and bottom of the magnetic sources as stated in the Equation 3, Section 2.8.

The spectral analysis was done using interactive filtering technique in Oasis Montaj MAGMAP extension, which is frequency domain processing of most potential field data. After preparing the magnetic grid (in space domain), it was then transformed to wave number (frequency) domain using forward filtering transform (FFT) filters. The Fourier transformation of a space domain function is defined as:

$$f(x, y) = 1/4\pi \int_{-\infty}^{\infty} \int_{-\infty}^{\infty} \overline{f}(\mu, \nu) \cdot e^{i(\mu x + \nu y)} d\mu d\nu \quad (\text{Space domain}) \quad \text{Equation (5a)}$$

$$\overline{f}(\mu, \nu) = \int_{-\infty}^{\infty} \int_{-\infty}^{\infty} f(x, y) \cdot e^{-i(\mu x + \nu y)} dx dy \quad (\text{Wave number domain}) \quad \text{Equation (5b)}$$

Where μ and ν are wave numbers in the x and y directions respectively which are measured in radians per metres (Geosoft, 2005). The transformation procedures involved application of different filtering functions such as upward and downward continuation. In this study, the upward continuation was applied to remove the effect of shallow sources since the analysis was aimed at estimating depth to deeper magnetic sources.

After the filtering application, the inverse filter was applied to the space domain grid data which transformed it to wave number or frequency domain, from which power spectrum was generated.

5.1.1.1. Radial Power Spectrum and Depth Estimation

The power spectrum is a 2D function of the energy and wave number. Radial power spectrum plot was generated from the transformed aeromagnetic data using Oasis Montaj software. The software automatically computes the depth corresponding to the power spectrum by plotting 5 point data from spectrum file (Geosoft, 2005). The result of the computed radial power spectral and depths to the top magnetic sources around Lake Magadi is shown in Figure 5.1.

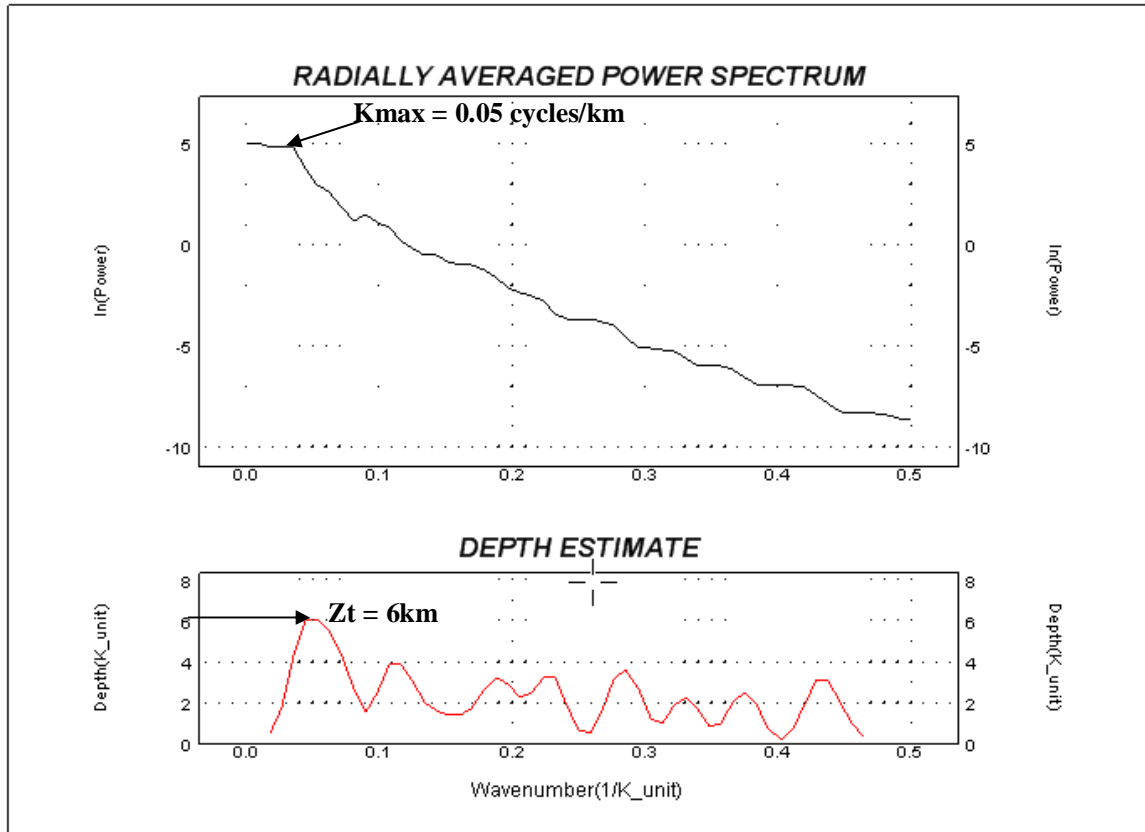


Figure 5.1. Log Power spectrum analysis of Lake Magadi generated from Aeromagnetic data

The result shows that the depth to top of the deepest magnetic source around Magadi is about 6km. Estimating heat source (Curie point) depth therefore was done by determining the depth to the bottom (Z_b) of the deepest anomaly using the Equation (3) in Section 2.8. The relation requires the depth to the top (Z_t) and the peak wave number value (K_{max} in cycle/km) which are derived from the generated power spectrum in Figure 5.1 as 6 km and 0.05 cycle/km respectively.

The depth to the bottom of the deepest magnetic material was estimated from the Equation (3) to an approximately 12.074 km. This depth is the assumed Curie point for Lake Magadi area. The estimated top to the magnetic sources and Curie point depths corresponds with the existing crustal models by Ibs-von Seht et al. (2001) and Simiyu and Keller (1998).

6. Data Integration

6.1. Subsurface Fluid Conduits Characteristics from Geophysical Imaging

This section discusses the integration of the resistivity and magnetic data in mapping the geometry of the fluid conduits and the fluid paths in the south of Lake Magadi, southern Kenya Rift.

Subsurface investigations in this research reveals the potential presence of fluids (mostly saline hydrothermal) within the five major faults in the south side of Lake Magadi. These faults, which are mostly north-south striking, serves as the conduits which support the hot springs flow in the lake margin and the trona deposits in the lake (Jones et al., 1977). Within the faults are the general funnel shaped structures, with very low resistivity ($< 1 \text{ ohm-m}$) in most of the resistivity model (See Figures 4.5 – 4.8); this shows that Magadi area is host to mostly high saline ground water and hot springs reservoir (Risk et al., 1999). In the study area, the resistivity distribution increases from the near surface to the deep subsurface (See Figures 4.5 and 4.6). These variations could be attributed to the saline concentration differences as revealed by Jones et al. (1977). Jones et al. (1977) showed the existence of two distinct units below the lake from a borehole investigation; the shallow which coexisted with bedded salts and highly concentration of salts, and the deeper which is lacustrine sediments or fractured lava with less concentration. The concentration sequence originates from the surficial dilute ground water in trachytes, hot springs and deepest brine. The salinity also could attribute to the weathering process. The strong influence of Magadi inflow waters by weathering of volcanic rocks, which are generally characterized by Na and $(\text{Ca} + \text{Mg})/\text{HCO}_3$ have been discovered by Eugster (1970) .

The highly fractured zones with fluid in the resistivity models support Ibs-von Seht et al. (2001)'s findings from seismic velocity model which attributed the low velocity anomaly to the presence of fluid –filled fracture in the upper crust. This faulted and fractured Pliocene/Miocene volcanics and sediments from the Simiyu and Keller (1998) model extends to approximately depth of 6km beneath Lake Magadi (See Figure 2.4). The multiple scattering of Euler solution in the ground magnetic profiles also confirmed this highly fractured and faulted zone in the subsurface. Location of the fluid filled zone within the basin is marked by the absence of magnetic source in the 2D Euler's deconvolution solutions of the ground magnetic profiles. These fluids zones exist between the investigated tectonic lineaments. The existence of the fluid –filled fractures in the upper crust is said to reduce the seismic activities in the southern part of Lake Magadi (Ibs-von Seht et al., 2001; Ibs-von Seht et al., 2008) because they lubricate the fault zones and reduce stress. This is confirmed by comparing this ERT profiles with the one acquired by Sequar (2009) in the northern part of the study area (see Appendix 02). The resistivity profiles in the north (see Appendix 02), where there are intense seismic activities (see Figure 6.1) shows mostly the sediments as the major component of the faults and fractures in the subsurface while the southern area is fluid dominated.

This tectonic activity in the lake Magadi upper crust contributes to the upward flow of hydrothermal fluids from the hot geothermal reservoir to the surface. Both resistivity and magnetic results shows that the existence of the investigated structures in the south of Lake Magadi plays important role in creating a flow path through which the hydrothermal fluids (hot or cold) are transported to the surface. The change in the direction of the fluid path could result from tectonic activities; it follows the subsurface faults splay (minor fault at the extremist of the major fault) to the surface (Figures 4.5 –

4.8). This implies that the flow of the fluids have been highly supported by the existence of the N-S fault structures in the study area (Sequar, 2009); this is obvious from the field observation, as there are existence of springs in the north direction toward the lake, within the five structures bounding the basin. This low resistivity zones could be as a result of continuous deformation due to an extensive network of the fluid fractures, which maintains the electrical connection (Unsworth, 2002).

6.1.1. Linking surface Tectonic Lineaments to the Subsurface

A plot of magnetic sources of aeromagnetic flight lines (Figure 6.1), from the 2D Euler deconvolution solutions with structural index of 1 (steep contacts i.e. faults) (Figure 4.23 and 4.24) against subsurface depth was generated as shown in Figures 6.2b and 6.3b. This deeper investigation of the established surface lineaments with aeromagnetic data reveals that the tectonic activities along and beneath Magadi basin extends deeply to the subsurface (approximately 7.5km). The plots shows that Faults A and D and E are surface expressions of the deep subsurface faulting activities. The alignments of the magnetic sources at the rift axis show that these faults bind the graben to the west and to the east. These tectonic zones which extends to the top of the basement agrees with Simiyu and Keller (1998) and Ibs-von Seht et al (2001)'s model (Figure 6.4).

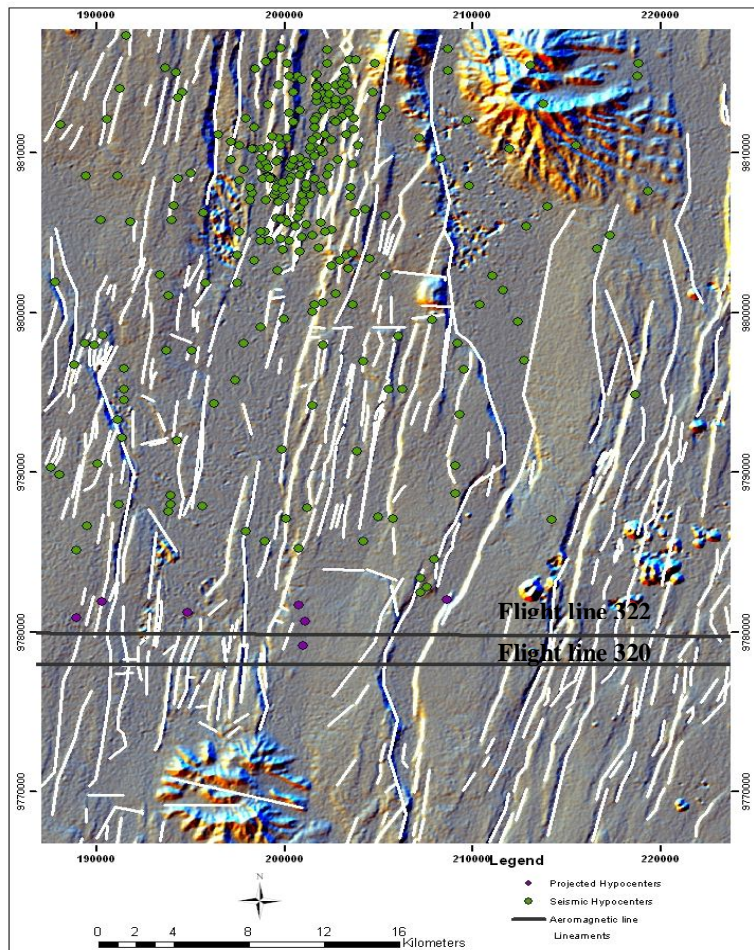


Figure 6.1. Hillshaded AsterDEM Image showing the lineaments and seismic hypocenters distributions (from Ibs-von Seht et al (2001) around Lake Magadi. The brown dots are the re-projected hypocenters along the aeromagnetic flight lines.

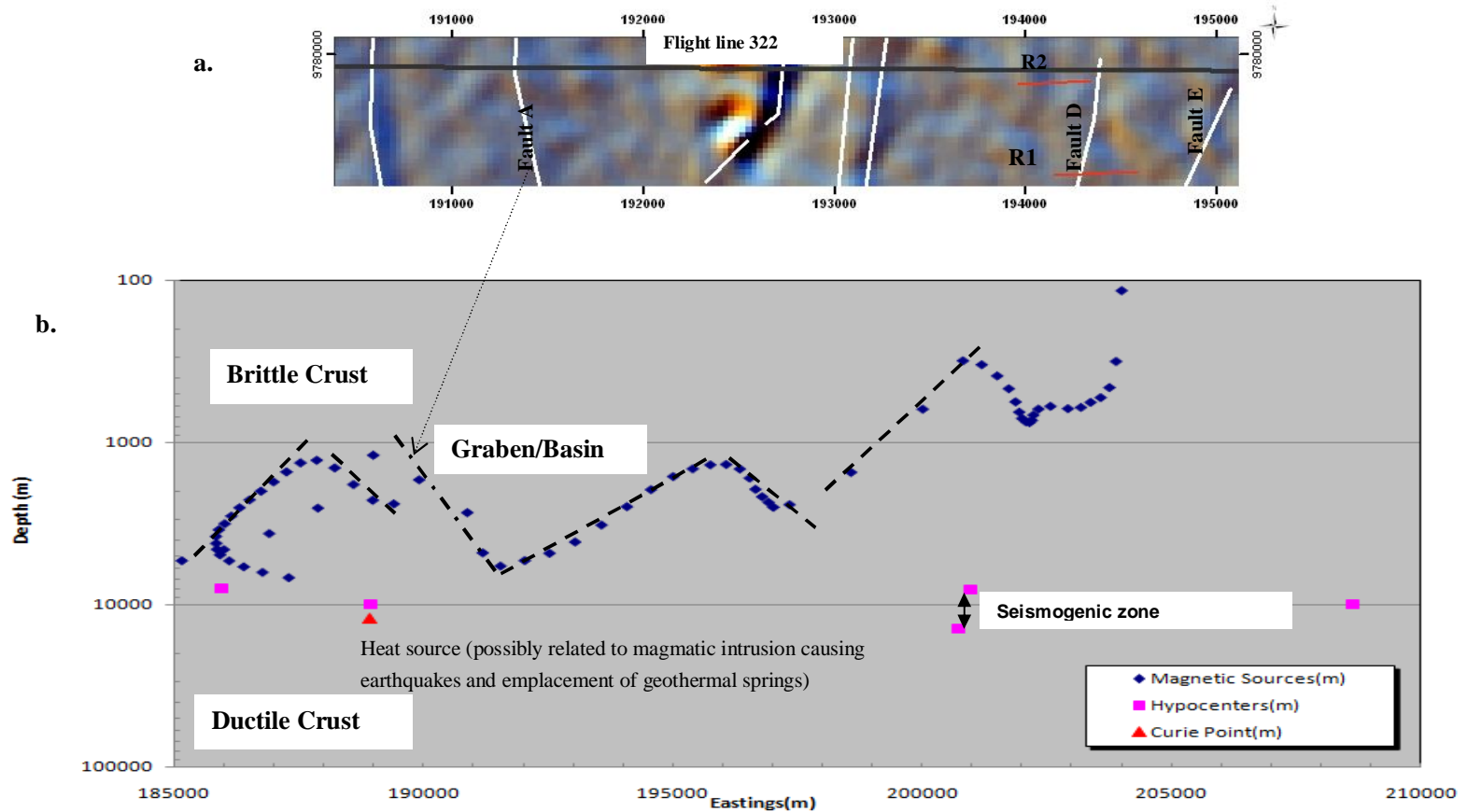


Figure 6.2. (a): Hillshade aster DEM subset showing the surface lineaments and the extracted aeromagnetic flight line 322. (b): Scatter Plots showing the subsurface relationship between magnetic sources on flight line 322, the hypocenters and the Curie point (heat source). The magnetic sources are generated from 2D Euler deconvolution using structural index of 1 (i.e. contacts, faults) with inclinations and declination angles of -26.3° and 0.002° respectively. R1 and R2 are the resistivity profiles 1 and 2 respectively

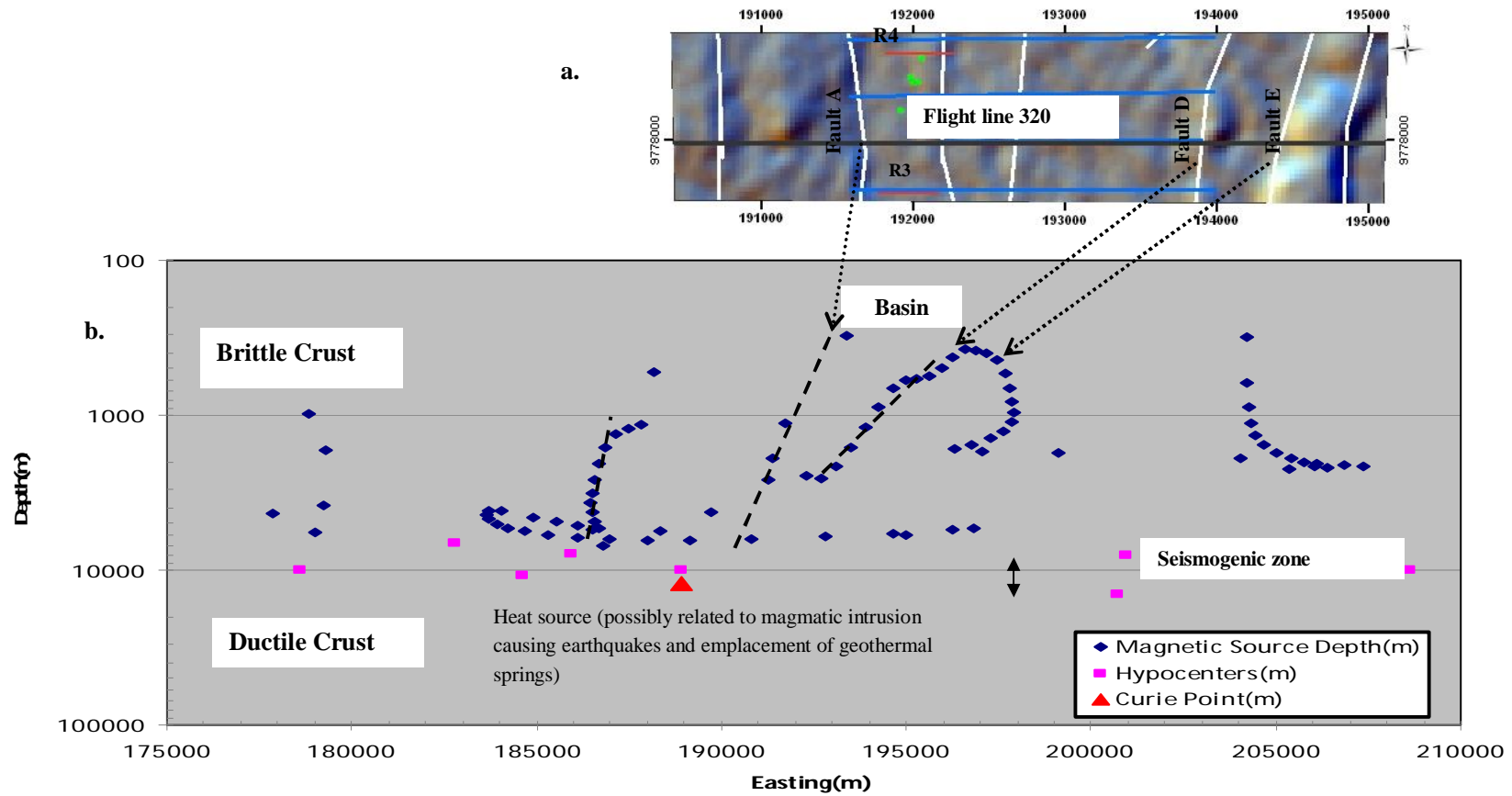


Figure 6.3. (a): Hillshade aster DEM subset showing the surface lineaments and the extracted aeromagnetic flight line 320. (b): Scatter Plots showing the subsurface relationship between magnetic sources on flight line 320, the hypocenters and the Curie point (heat source). The magnetic sources are generated from 2D Euler deconvolution using structural index of 1 (i.e. contacts, faults) and inclinations and angles of -26.3° and 0.002° respectively. R3 and R4 are the resistivity profiles 3 and 4 respectively. The blue horizontal lines are the ground magnetic profiles location.

6.2. Lake Magadi Curie point depth: Implication on the Seismicity and Geothermal Resources

The penetration of the magma to the crust produces different geophysical phenomena such as crustal deformation; volcanic activity and seismicity (Mishina, 2009). In the southern part of Kenya rift, microseismic activity has been attributed to the geothermal processes, as a result of the magmas intrusion to the crust (Maguire and Long, 1976). Magadi earthquake swarm according to Ibs-von Seht et al., (2001) and (2008) can be linked to mid-crustal magma body in the centre of the rift and the movement of the magmatic fluids.

To further investigate these findings, the heat source depth (Curie point depth) generated from the aeromagnetic data was correlated with the seismic hypocenters (depth to the seismic events) and the magnetic sources, revealing subsurface faulting systems (see Figures 6.2b and 6.3b). The hypocenters used in this thesis were the output of the seismic experiments by Ibs-von Seht et al., (2001) at Lake Magadi area. Seismic hypocenters which are closed to the aeromagnetic lines 322 and 320 (about 5km) were re-projected to their corresponding latitude along the profile (see Figure 6.1) and are plotted with the sources against depth.

Comparing the estimated top and bottom of the deepest magnetic source (from spectral analysis and the scatter plots) with the existing crustal model by Simiyu and Keller (1998) (Figure 2.4); it is clear that the top and bottom depths coincides with the top of the crystalline upper crust (the Precambrian basement), which is of high magnetic property while the bottom falls within the middle crust, at the bottom of the basement, near the heat source. The heat source in Lake Magadi is inferred to be the magmatic body which is emplaced at approximately depth of 12.1km (Magadi mid-crust). The subsurface plots in Figures 6.2b and 6.3b is consistent with Ibs-von Seht et al. (2001)' crustal model (Figure 6.4) in terms of the heat source depth and active faults locations. According to Ibs-von Seht et al. (2001) and (2008), the brittle-ductile transition with positive mid-crustal P-velocity overlain by a negative anomaly is related to the movement of magma to the mid crust (Figure 6.4). Their model is consistent with the Curie point depth estimated in this research. From the scatter plots, it is noted that all the earthquake hypocenters are located between top of the magnetic sources and the bottom (that corresponds to Curie point depth); this defines the seismogenic layer, the onset of seismicity (Björnsson, 2008; Ito, 1999) (Figure 6.4). Generally, seismogenic zones often exist on top of the most ductile part of the earth (Ito, 1999). The curie depth that defines elevated temperature corresponds to magmatic intrusion which drives other processes such as stress accumulation, earthquake generation and emplacement of hydrothermal solutions. The shallowness of this zone must have resulted in the pronounced deformations, earthquakes generation and surface manifestation of hydrothermal fluids around Lake Magadi, southern Kenya rift. The intrusion of the magma to the mid-crust is attributed to the cause of earthquake swarms; this is because it focuses or releases strain energy in brittle or resistive part of the crust with small magnitude earthquakes (Gürer and Bayrak, 2007).

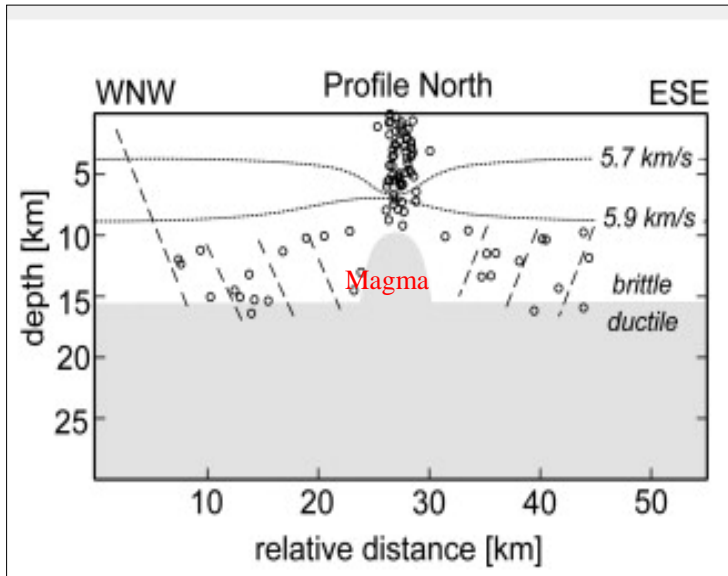


Figure 6.4. Magadi Crustal structure model derived from local earthquake tomography and hypocentral depth studies after Ibs-von Seht et al. (2001). The circles, dotted lines and dashed lines are projections of hypocenters, crustal velocities derived from seismic tomography and assumed depth ranges of active faults respectively

The shallowness of the estimated Curie point depth (12.1km) implies that the heat flow around Lake Magadi should be above the average value (Stampolidis and Tsokas, 2002). According to Espinosa-Cardeña and Campos-Enriquez (2008), the cause of a high heat flow in most geothermal regions is the tectonically induced magmatism.

Generally, at a certain threshold of increased temperature, rocks response to stress results in brittle to ductile deformation. This ductile condition reduces the open passages (pore fluids connection) through which fluids can be transported or connected to the convecting fluids at shallower depths (Bibby et al., 2009) and as such, heat flow is predominantly by conduction through a conductive medium to the fluid reservoir. Within the reservoir therefore, the heat is transported through a convection of geothermal fluids via a connected pores. This and the presence of active faults and fractures (supposed conduits) could be responsible for the surface manifestations of hot springs at Lake Magadi.

7. Conclusions and Recommendation

7.1. Conclusions

In this research, the subsurface geometry of the tectonic lineaments and thermal structures in the south of Lake Magadi area have been investigated using integrated geophysical methods and satellite remotely sensed datasets. Significantly, it has been able to define the subsurface constituents of the N-S faults and their impacts on the surface manifestations of the geothermal resources around the lake. It has also revealed the capability of aeromagnetic data in analysing thermal structures of the area using spectral method. Aeromagnetic data has not been used previously to estimate the depth to the heat source in the study area despite the vast evidence of the geothermal manifestation. This section therefore discusses the specific research objectives in section 1.2.1 by answering the earlier stated research questions (section 1.3).

7.1.1. Subsurface constituents of tectonic lineaments in the south of Lake Magadi

Regarding Research Question (i): Can the proposed fluid bearing high micro cracks in the upper crust be mapped?

From the interpreted geophysical data (resistivity and magnetic), the subsurface geometry of the Lake Magadi south N-S faults and their constituents have been delineated (see Sections 4.14 and 4.3.5.2). The relatively low resistivity values ($<1\Omega\text{m}$) from the ERT method that extends to a depth of 75m and the Euler solution scattering from the magnetic data, confirms the presence of saline fluids (mostly hydrothermal) filled fractures and fault zones. The presence of this zone is confirmed by the absence of magnetic sources in the magnetic profiles. This research has been able to confirm the findings of Ibs-von Seht et al.(2001) which proposed the presence of fluid filled fracture in the upper crust of Lake Magadi from the seismic method only.

7.1.2. Lake Magadi Geothermal Systems

Regarding Research Question (ii): Can hot fluid path from geothermal source be delineated using geophysical methods?

The capability of the integrated geophysical methods to investigate geothermal system has been demonstrated in this research. Most important part of this aspect is the heat source from which the surface manifestations of hot springs are generated from. The depth to the heat source (Curie point) calculated in this research is about 12.1km, which by reason of its shallowness could results in high heat flow in the study area and supports the evidence for occurrence of a geothermal resource. The determined Curie depth from Averaged Radial Power Spectrum is reliable; it is consistent with the existing model.

From the estimated heat source, compared with the existing crustal models, the geothermal systems in the study area can be characterised. The basic elements which characterize a geothermal system and their corresponding units as revealed by the geophysical data and existing models for Lake Magadi are:

1. The heat source which serves as the source of heat to the reservoir fluids. This heat source is typically magma chamber in the deep sub-surface. The source depth for Magadi area as estimated from the aeromagnetic data analysis in the research is 12.1km. This is an indicative of magma

- intrusion to the mid-crust (Figure 5.3). This shallow heat source, by implications could results in the high heat flow and the subsequent generation of hot fluids within the reservoir rock.
2. The impermeable rock directly overlay the heat source: This serves as the conductive medium through which heat is transferred to the reservoir rock through conduction process. The heat transfer rate varies from region to region and depends on the thermal conductivity of the impermeable rock. The depth to the top of the deepest magnetic material estimated from the aeromagnetic spectral analysis coincides with the top of the Precambrian basement from the existing crustal model; this is obvious because the basement is of high magnetic property. It can be concluded that the crystalline upper crust (the Precambrian basement) serves as conductive medium through which heat is transferred from the heat source to the reservoir rock.
 3. The hot fluid reservoir rock: a porous and permeable rock layer through which fluids circulate and find its way to the surface via connected medium such as faults and fractures. The layer from the existing crustal model is probably the highly fractured metasedimentary quartzitic rock; this extends the depth of 6km beneath the Lake Magadi.
 4. A caprock: basically an impermeable rock on top of the reservoir rock which in some cases prevents the upward movement of the hot fluid from the reservoir. The near surface rock units on top of the highly faulted and fractured metasedimentary quartzitic rock from the existing model is the highly faulted fluid saturated Pliocene to Miocene volcanic and sediments. This weak and highly fractured rock as revealed by resistivity and magnetic data allows the in-fill of hydrothermal hot fluids from the hot reservoir rock, which consequently resulted in the expression of the hot fluids in the surface at Lake Magadi area.
 5. Recharge area: the escarpments to the west and east of Lake Magadi are probably the recharge areas through which the meteoric water percolates the subsurface. The cold water interactions with the hot fluid could have resulted in the decrease in the temperature of the hot fluids expressed on the surface and the increase in the salinity of the fluids in the near surface.
 6. Connecting Paths: The existence of fault structures (mostly N-S) and fractures in the south of the lake, which are extended to the subsurface(up to 7.5km) as revealed by the aeromagnetic profiles probably serves as the connecting paths through which fluids flows within the reservoir and the subsequent transfer to the surface.

7.1.3. Geodynamic activities around Lake Magadi: Inference from the estimated heat source depth.

Regarding Research Question (iii): What is the effect of the deep heat source on the geodynamic activities around Lake Magadi?

Depth to the heat source estimated in this research and its correlation with the faulting systems and the seismic hypocenters provides information about the geodynamic activities around Lake Magadi. The estimated heat source, which is probably an indicative of magma intrusion, is relatively shallow and thus has several implications on the geothermal resources and tectonic activities in the area.

1. Geothermal Resources: The intrusion of the heat source (magma) into mid crust as revealed by the estimated depth (about 12km) shows that the heat flow around the study area is high enough to cause the surface geothermal manifestation. This is confirmed by the estimated heat flow values around Magadi. The heat flow emanating from the ground around Magadi was calculated by Crane and O'Connell (1983) to be 332 ± 66 MW, high enough to generate hot springs in the area. The shallowness of the magma and the existence of tectonic deformation in the study area probably control the distribution of geothermal resources.

2. Tectonic Activities: The heat source in this research defines the transition point between the ductile and brittle crust. The established relationship between the heat source, hypocenters and the magnetic sources revealed the seismogenic zone at the lake Magadi to the top of the estimated heat source depth (12km). This depth is probably the commencement of deformations, tectonic activities around Lake Magadi, southern Kenya rift. Directly on top of the seismogenic zone are various faulting activities within the brittle crust as revealed by the aeromagnetic profiles. This subsurface model is consistent with the existing model of Ibs-von Seht et al.,(2001), derived from seismic data. It shows that the uprising of the magma to the surface exert pressure in the brittle part of the crust which produces various tectonic activities.

Conclusively, the Curie depth that defines elevated temperature corresponds to magmatic intrusion which drives other processes such as stress accumulation, earthquake generation and emplacement of hydrothermal solutions. Magmatic intrusion to the crust therefore is sufficient to explain the thermal structure and evolution of Magadi basin/trough.

7.1.4. Influence of N-S structures on the Geothermal Resources around Lake Magadi

Regarding Research Question (iv): What impact do the N-S faults structures in the south of Lake Magadi have on the geothermal resources?

The ground magnetic survey as revealed in the Euler solutions provides information on the depth of the N-S faults investigated that extends to 400m. Most important is the extension of the Faults A, D and E to the deep surface (up to 7.5km). The absence of magnetic sources between these faults in the subsurface probably signifies a fluid filled basin bounded by the active faults both the west and the east; these normal faults forms linear structures which bound the basin/graben as seen in the surface.

The existence of very low resistivity from the top of the penetrated depth between the fault splays in the resistivity model confirms upward flow of fluids along the faults. Therefore, the manifestations of the saline hot springs along the margin of the basin both to the west and to the east probably results from the fact that the fluids (hydrothermal) tends to find their way to the surface through the faults splay.

It can be concluded therefore, from the interpreted data, supported by the existing literature and field observations, that the manifestations of hot springs and trona deposit in the south of Lake Magadi are largely supported by the presence of N-S faults in the area.

7.2. Research Limitations

In addition to the field limitations stated in this thesis, lack of deeper resistivity imaging tool prevented deeper investigations of resistivity structures across the tectonic lineaments. The MT equipments deployed to the field was defective and as such could not utilised for deeper resistivity imaging of the subsurface.

7.3. Recommendation

Based on the results obtained and the limitations of this research the following are recommended:

1. As a follow up to the calculated Curie point depth, heat flow values and geothermal gradients should be investigated by using borehole temperature logging; this would further provide detail information on the geothermal potential of Lake Magadi region.
2. A 3D geothermal model could be constructed for Lake Magadi using integrated borehole, temperature and geophysical data.
3. A deeper resistivity imaging such as magnetotelluric should be employed across the established five N-S structures in the south of Lake Magadi to enable deeper imaging of the fluid conduits; this could also be used to confirm the heat source depth and also delineate the hot fluid reservoir.

References

- Abiye, T.A., and Tigistu, H., 2008, Geophysical exploration of the Boku geothermal area, Central Ethiopian Rift: *Geothermics*, v. 37, p. 586-596.
- Adepelumi, A.A., Ako, B.D., Ajayi, T.R., Olorunfemi, A.O., Awoyemi, M.O., and Falebita, D.E., 2008, Integrated geophysical mapping of the Ifewara transcurrent fault system, Nigeria: *Journal of African Earth Sciences*, v. 52, p. 161-166.
- AGI, 2008, Instruction Manual for Earth Imager 2D Version 2.2.8, *in. ed.*: Texas, USA, Advance Geosciences Inc, p. 1-136.
- Aizawa, K., Ogawa, Y., Hashimoto, T., Koyama, T., Kanda, W., Yamaya, Y., Mishina, M., and Kagiya, T., 2008, Shallow resistivity structure of Asama Volcano and its implications for magma ascent process in the 2004 eruption: *Journal of Volcanology and Geothermal Research*, v. 173, p. 165-177.
- Atmaoui, N., and Hollnack, D., 2003, Neotectonics and extension direction of the Southern Kenya Rift, Lake Magadi area: *Tectonophysics*, v. 364, p. 71-83.
- Babiker, M., and Gudmundsson, A., 2004, The effects of dykes and faults on groundwater flow in an arid land: the Red Sea Hills, Sudan: *Journal of Hydrology*, v. 297, p. 256-273.
- Baker, B.H., 1958, *Geology of the Magadi area*, Geological Survey of Kenya, Nairobi.
- , 1987, Outline of the petrology of the Kenya rift alkaline province: *Geological Society, London, Special Publications*, v. 30, p. 293-311.
- Baker, B.H., Williams, L.A.J., Miller, J.A., and Fitch, F.J., 1971, Sequence and geochronology of the Kenya rift volcanics: *Tectonophysics*, v. 11, p. 191-215.
- Bibby, H.M., Risk, G.F., Grant Caldwell, T., and Heise, W., 2009, Investigations of deep resistivity structures at the Wairakei geothermal field: *Geothermics*, v. 38, p. 98-107.
- Björnsson, A., 2008, Temperature of the Icelandic crust: Inferred from electrical conductivity, temperature surface gradient, and maximum depth of earthquakes: *Tectonophysics*, v. 447, p. 136-141.
- Blanco-Montenegro, I., Torta, J.M., García, A., and Araña, V., 2003, Analysis and modelling of the aeromagnetic anomalies of Gran Canaria (Canary Islands): *Earth and Planetary Science Letters*, v. 206, p. 601-616.
- Blewitt, G., Coolbaugh, M., Holt, W., Kreemer, C., Davis, J.L., and Bennett, R.A., 2002, Targeting of Potential Geothermal Resources in the Great Basin from Regional Relationships between Geodetic Strain and Geological Structures: *Transactions Geothermal Resources Council*, v. 26, p. 523-526.
- Boonchaisuk, S., Vachiratienchai, C., and Siripunvaraporn, W., 2008, Two-dimensional direct current (DC) resistivity inversion: Data space Occam's approach: *Physics of the Earth and Planetary Interiors*, v. 168, p. 204-211.
- Bosworth, W., Strecker, M.R., and Blisniuk, P.M., 1992, Integration of East African Paleostress and Present-Day Stress Data: Implications for Continental Stress Field Dynamics: *J. Geophys. Res.*, v. 97.
- Braile, L.W., Wang, B., Daudt, C.R., Keller, G.R., and Patel, J.P., 1994, Modeling the 2-D seismic velocity structure across the Kenya rift: *Tectonophysics*, v. 236, p. 251-269.
- Chorowicz, J., 2005, The East African rift system: *Journal of African Earth Sciences*, v. 43, p. 379-410.
- Clark, D.A., and Emerson, D.W., 1991, Notes on rock magnetization characteristics in applied geophysical studies: *Exploration Geophysics*, v. 22, p. 547-555.
- Colella, A., Lapenna, V., and Rizzo, E., 2004, High-resolution imaging of the High Agri Valley Basin (Southern Italy) with electrical resistivity tomography: *Tectonophysics*, v. 386, p. 29-40.
- Cooper, G.R.J., 2004, Euler deconvolution applied to potential field gradients: *Exploration Geophysics*, v. 35, p. 165-170.
- Cooper, G.R.J., and Cowan, D.R., 2004, Filtering using variable order vertical derivatives: *Computers & Geosciences*, v. 30, p. 455-459.

- Crane, K., and O'Connell, S., 1983, The distribution and implications of heat flow from the Gregory rift in Kenya: *Tectonophysics*, v. 94, p. 253-275.
- El Dawi, M.G., Tianyou, L., Hui, S., and Dapeng, L., 2004, Depth estimation of 2-D magnetic anomalous sources by using Euler deconvolution method: *American Journal of Applied Sciences*
- Espinosa-Cardena, J.M., and Campos-Enriquez, J.O., 2008, Curie point depth from spectral analysis of aeromagnetic data from Cerro Prieto geothermal area, Baja California, México: *Journal of Volcanology and Geothermal Research*, v. 176, p. 601-609.
- Eugster, H.P., 1970, Chemistry and origin of brines of Lake Magadi, Kenya: *Mineral. Soc. Amer. Spec. Paper*, v. No. 3, p. 215 - 235.
- , 1986, Lake Magadi, Kenya: a model for rift valley hydrochemistry and sedimentation?: *Geological Society, London, Special Publications*, v. 25, p. 177-189.
- Garg, S.K., Pritchett, J.W., Wannamaker, P.E., and Combs, J., 2007, Characterization of geothermal reservoirs with electrical surveys: Beowawe geothermal field: *Geothermics*, v. 36, p. 487-517.
- Geosoft, 2005, *Montaj MAGMAP filtering: 2D Frequency Domain Processing of Potential Field Data.*: Toronto, Canada, Geosoft Incorporated, p. 2-72.
- Gudmundsson, A., Berg, S.S., Lyslo, K.B., and Skurtveit, E., 2001, Fracture networks and fluid transport in active fault zones: *Journal of Structural Geology*, v. 23, p. 343-353.
- Gürer, A., and Bayrak, M., 2007, Relation between electrical resistivity and earthquake generation in the crust of West Anatolia, Turkey: *Tectonophysics*, v. 445, p. 49-65.
- Hochstein, M.P., and Soengkono, S., 1997, Magnetic anomalies associated with high temperature reservoirs in the Taupo volcanic zone (New Zealand): *Geothermics*, v. 26, p. 1-24.
- Hunt, T.M., Bromley, C.J., Risk, G.F., Sherburn, S., and Soengkono, S., 2009, Geophysical investigations of the Wairakei Field: *Geothermics*, v. 38, p. 85-97.
- Ibs-von Seht, M., Blumenstein, S., Wagner, R., Hollnack, D., and Wohlenberg, J., 2001, Seismicity, seismotectonics and crustal structure of the southern Kenya Rift- new data from Lake Magadi area: *Geophysical journal Int.*, v. 146, p. 439-453.
- Ibs-von Seht, M., Plenefisch, T., and Klinge, K., 2008, Earthquake swarms in continental rifts -- A comparison of selected cases in America, Africa and Europe: *Tectonophysics*, v. 452, p. 66-77.
- Ito, K., 1999, Seismogenic layer, reflective lower crust, surface heat flow and large inland earthquakes: *Tectonophysics*, v. 306, p. 423-433.
- Jeng, Y., Lee, Y.-L., Chen, C.-Y., and Lin, M.-J., 2003, Integrated signal enhancements in magnetic investigation in archaeology: *Journal of Applied Geophysics*, v. 53, p. 31-48.
- Jessell, M., 2001, Three-dimensional geological modelling of potential-field data: *Computers & Geosciences*, v. 27, p. 455-465.
- Jones, B.F., Eugster, H.P., and Rettig, S.L., 1977, Hydrochemistry of the Lake Magadi basin, Kenya: *Geochimica et Cosmochimica Acta*, v. 41, p. 53-72.
- Kearey, P., and Brooks, M., 1984, *An Introductory to Geophysical Exploration*: Oxford, London, Blackwell Scientific Publications, 171 -199 p.
- Keller, G.R., Mechie, J., Braile, L.W., Mooney, W.D., and Prodehl, C., 1994a, Seismic structure of the uppermost mantle beneath the Kenya rift: *Tectonophysics*, v. 236, p. 201-216.
- Keller, G.R., Prodehl, C., Mechie, J., Fuchs, K., Khan, M.A., Maguire, P.K.H., Mooney, W.D., Achauer, U., Davis, P.M., Meyer, R.P., Braile, L.W., Nyambok, I.O., and Thompson, G.A., 1994b, The East African rift system in the light of KRISP 90: *Tectonophysics*, v. 236, p. 465-483.
- Kodikara, G.R.L., 2009, *Hyperspectral mapping of surface Mineralogy in Lake Magadi Area in Kenya* [Msc thesis]: Enschede, ITC.
- Kuria, Z.N., Woldai, T., Meer, F.D.v.d., and Barongo, J.O., 2009, Active fault segments as potential earthquake sources: Inferences from integrated geophysical mapping of the Magadi fault system, southern Kenya Rift: *Journal of African Earth Sciences*, v. In Press, Corrected Proof.
- Le Turdu, C., Tiercelin, J.J., Richert, J.P., Rolet, J., Xavier, J.P., Renaut, R.W., Lezzar, K.E., and Coussement, C., 1999, Influence of pre-existing oblique discontinuities on the geometry and evolution of extensional fault patterns; Evidence from the Kenya Rift using Spot Imagery. In:

- C.K. Morley (Editor), *Geoscience of Rift systems-Evolution of East Africa: AAPG studies in Geology*, p. 173-191.
- Lerner, E.K.L., and Cengage, B.W.L.G., 2003, *Faults and Fractures*, World of Earth Science.
- MacLeod, I.N., Jones, K., and Dai, T.F., 1993, 3-D analytic signal in the interpretation of total magnetic field data at low magnetic latitudes: *Exploration Geophysics*, v. 24, p. 679-688.
- Maguire, P.K.H., and Long, R.E., 1976, The Structure on the Western Flank of the Gregory Rift (Kenya). Part I. The Crust: *Geophysical Journal of the Royal Astronomical Society*, v. 44, p. 661-675.
- Maguire, P.K.H., Swain, C.J., Masotti, R., and Khan, M.A., 1994, A crustal and uppermost mantle cross-sectional model of the Kenya Rift derived from seismic and gravity data: *Tectonophysics*, v. 236, p. 217-249.
- Mariita, N.O., and Keller, G.R., 2007, An integrated geophysical study of the northern Kenya rift: *Journal of African Earth Sciences*, v. 48, p. 80-94.
- Mary, H.D., and Mario, F., 2004, *What is Geothermal Energy?:* Pisa, Italy, Istituto di Geoscienze e Georisorse, p. 1-61.
- Mechie, J., Keller, G.R., Prodehl, C., Gaciri, S., Braile, L.W., Mooney, W.D., Gajewski, D., and Sandmeier, K.J., 1994, Crustal structure beneath the Kenya Rift from axial profile data: *Tectonophysics*, v. 236, p. 179-200.
- Mechie, J., Keller, G.R., Prodehl, C., Khan, M.A., and Gaciri, S.J., 1997, A model for the structure, composition and evolution of the Kenya rift: *Tectonophysics*, v. 278, p. 95-119.
- Mishina, M., 2009, Distribution of crustal fluids in Northeast Japan as inferred from resistivity surveys: *Gondwana Research*, v. 16, p. 563-571.
- Miyazaki, Y., 1985, Analysis of aeromagnetic anomalies; mapping of Curie isothermal surface at Long Valley, California [Ph. D thesis].
- Molnar, P., and Aggarwal, Y.P., 1971, A microearthquake survey in Kenya: *BULLETIN OF THE SEISMOLOGICAL SOCIETY OF AMERICA*, v. 61, p. 195-201.
- Mushayandevvu, M.F., Driel, P.v., Reid, A.B., and Fairhead, J.D., 2001, Magnetic source parameters of two-dimensional structures using extended Euler deconvolution: *Geophysics*, v. 66, p. 814-823.
- Mwaura, F., 1999, A spatio-chemical survey of hydrogeothermal springs in Lake Elementaita, Kenya: *International Journal of Salt Lake Research*, v. 8, p. 127-138.
- Noorollahi, Y., Itoi, R., Fujii, H., and Tanaka, T., 2007, GIS model for geothermal resource exploration in Akita and Iwate prefectures, northern Japan: *Computers & Geosciences*, v. 33, p. 1008-1021.
- Pelton, W.H., Rijo, L., Swift, C.M.J.R., 1978, Inversion of two-dimensional resistivity and induced-polarization data: *Geophysics*, v. 43, p. 788-803.
- Prodehl, C., Ritter, J.R.R., Mechie, J., Keller, G.R., Khan, M.A., Jacob, B., Fuchs, K., Nyambok, I.O., Obel, J.D., and Riaroh, D., 1997, The KRISP 94 lithospheric investigation of southern Kenya - the experiments and their main results: *Tectonophysics*, v. 278, p. 121-147.
- Riddihough, R.P., 1971, Diurnal Corrections To Magnetic Surveys; An Assessment Of Errors: *Geophysical Prospecting*, v. 19, p. 551-567.
- Risk, G.F., Bibby, H.M., and Caldwell, T.G., 1999, Resistivity structure of the central Taupo Volcanic Zone, New Zealand: *Journal of Volcanology and Geothermal Research*, v. 90, p. 163-181.
- Roest, W.R., Verhoef, J., and Pilkington, M., 1992, Magnetic interpretation using the 3-D analytic signal.: *Geophysics* v. 57, p. 116-125.
- Sequar, G.W., 2009, Neotectonics of the East African rift system : new interpretations from conjunctive analysis of field and remotely sensed datasets in the lake Magadi area, Kenya [Msc thesis]: Enschede, ITC.
- Simiyu, S.M., and Keller, G.R., 1998, Upper crustal structure in the vicinity of Lake Magadi in the Kenya Rift Valley region: *Journal of African Earth Sciences*, v. 27, p. 359-371.
- , 2000, Seismic monitoring of the Olkaria Geothermal area, Kenya Rift valley: *Journal of Volcanology and Geothermal Research*, v. 95, p. 197-208.
- Smith, M., and Mosley, P., 1993, Crustal Heterogeneity and Basement Influence on the Development of the Kenya Rift, East Africa: *Tectonics*, v. 12.

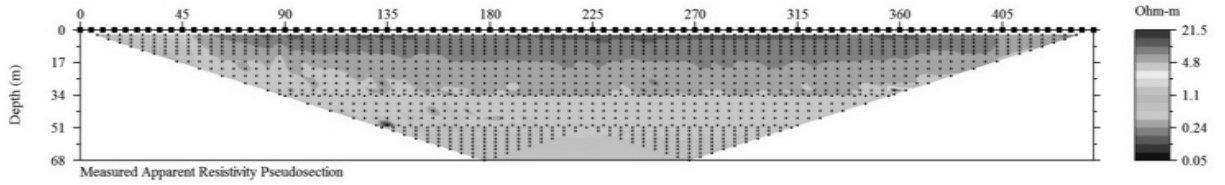
- Spector, A., and Grant, F.S., 1970, Statistical models for interpreting aeromagnetic data: *Geophysics* v. 35, p. 293–302.
- Stampolidis, A., and Tsokas, G.N., 2002, Curie Point Depths of Macedonia and Thrace, N. Greece: *Pure and Applied Geophysics*, v. 159, p. 2659-2671.
- Teichrieb, V., and Kelner, J., 2007, Enhancement of radar based DEMs using 3D techniques, *Geoscience and Remote Sensing Symposium, 2007. IGARSS 2007. IEEE International*, p. 4902-4905.
- Telford, W.M., Geldart, L.P., and Sheriff, R.E., 1976, *Applied Geophysics*, Cambridge University Press, 50-102 p.
- Thurmond, A.K.A.-S., M., Yin, Z., Hassanipak, A., and Ghazi, A.M., 2002, Structural Analysis of the Khoy Ophiolite, NW Iran from ASTER Imagery, *in* Union, A.G., ed., *American Geophysical Union, Spring Meeting 2002*, American Geophysical Union.
- Tripp, A.C., Hohmann, G.W., and Swift, C.M., 1984, Two-dimensional resistivity inversion. : *Geophysics*, v. 49, p. 1708–1717.
- Tüfekçi, N., Lütfi Süzen, M., and Güleç, N., 2010, GIS based geothermal potential assessment: A case study from Western Anatolia, Turkey: *Energy*, v. 35, p. 246-261.
- Unsworth, M., 2002, Role of Crustal Fluids in Strike-slip Tectonics: New Insights from Magnetotelluric Studies: *Turkish Journal of Earth Sciences*, v. 11, p. 193-203.
- Wheildon, J., Morgan, P., Williamson, K.H., Evans, T.R., and Swanberg, C.A., 1994, Heat flow in the Kenya rift zone: *Tectonophysics*, v. 236, p. 131-149.
- Wilson, S.R., Ingham, M., and McConchie, J.A., 2006, The applicability of earth resistivity methods for saline interface definition: *Journal of Hydrology*, v. 316, p. 301-312.
- Yang, X., 2002, *Resistivity Data Processing with Earth Imager*: Austin, Texas, Advance Geosciences Inc, p. 5.
- Yang, X., D. Liu, and Zhang, J., 2008, Ore-search information using aster data in bashibulake uranium deposit area in xinjiang. : *The International Archives of the Photogrammetry, Remote Sensing and Spatial Information Sciences*, v. XXXVI, p. Part B6b.

Appendices

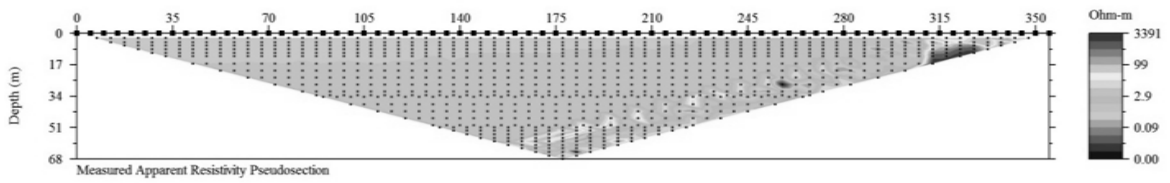
Appendix 01: Apparent resistivity profiles data used for this research.

They show the raw data collected from the study area. The profiles show low resistivity distributions as seen in the inverted resistivity.

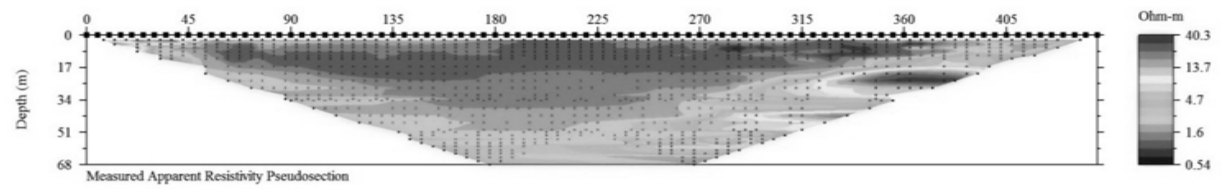
Profile R1



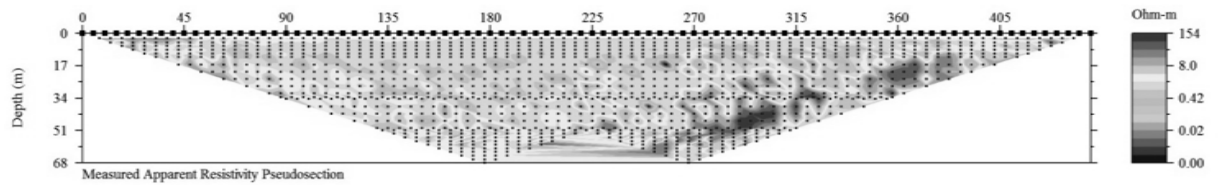
Profile R2



Profile R3

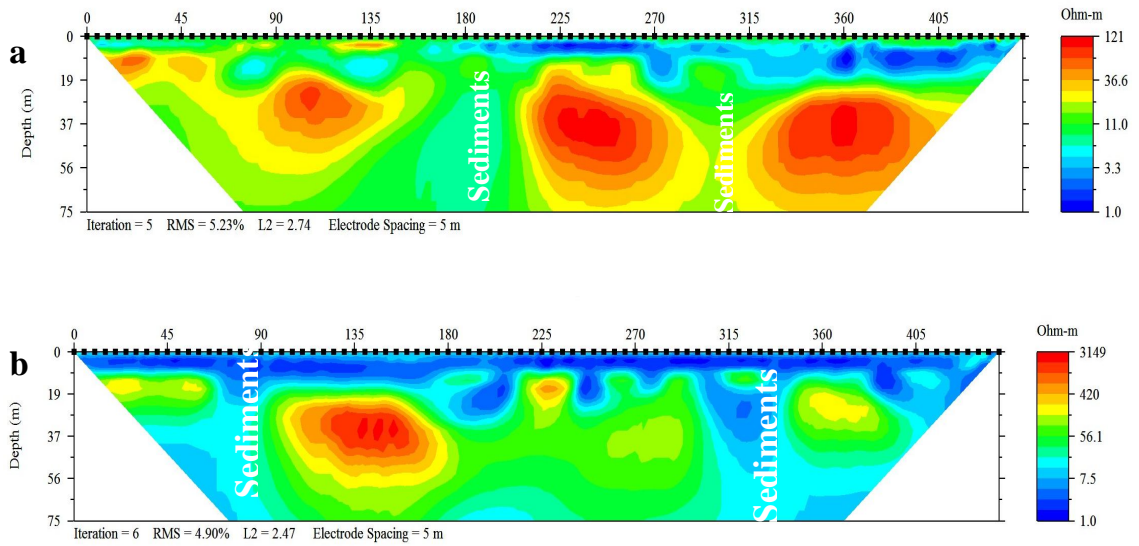


Profile R4



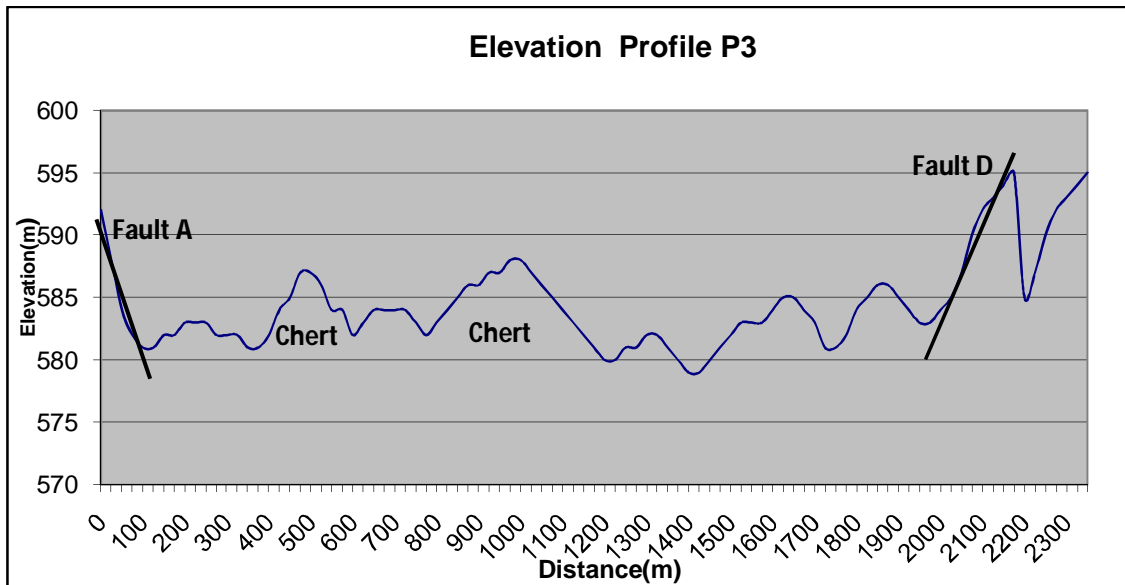
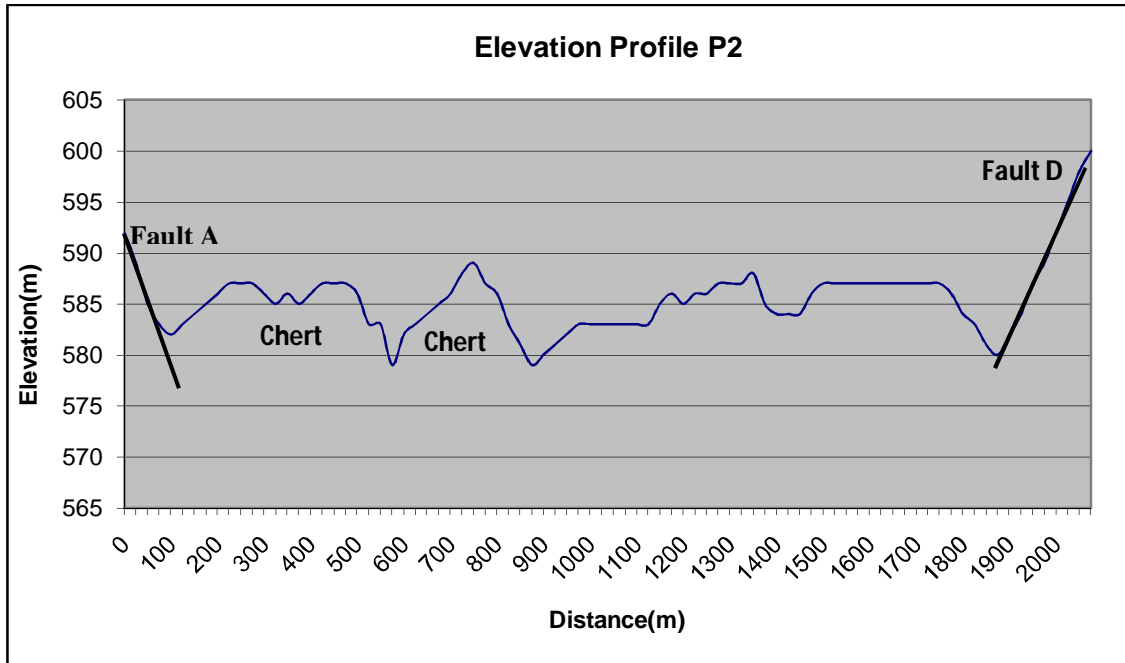
Appendix: 02. Inverted resistivity profiles acquired in the north of the study area by Sequar, (2009)

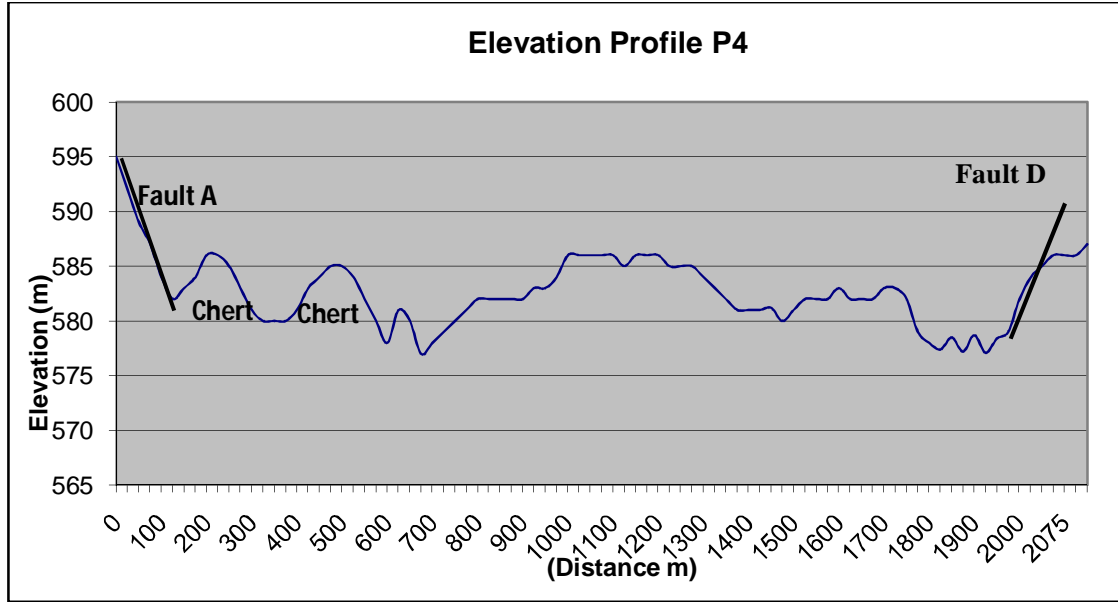
It shows inverted resistivity profiles acquired by Sequar (2009) in the north of Lake Magadi. Profile (a) and Profile (b) were collected in North East (NE) and North West (NW) directions respectively. The high resistivity distributions within the fractured zones are attributed to the existence of sediments. On the contrary, the south profiles in this research show very low resistivity within the faults zones, confirming the presence of saline hydrothermal fluids.



Appendix: 03. Elevation profiles along the ground magnetic profiles P2, P3 and P4.

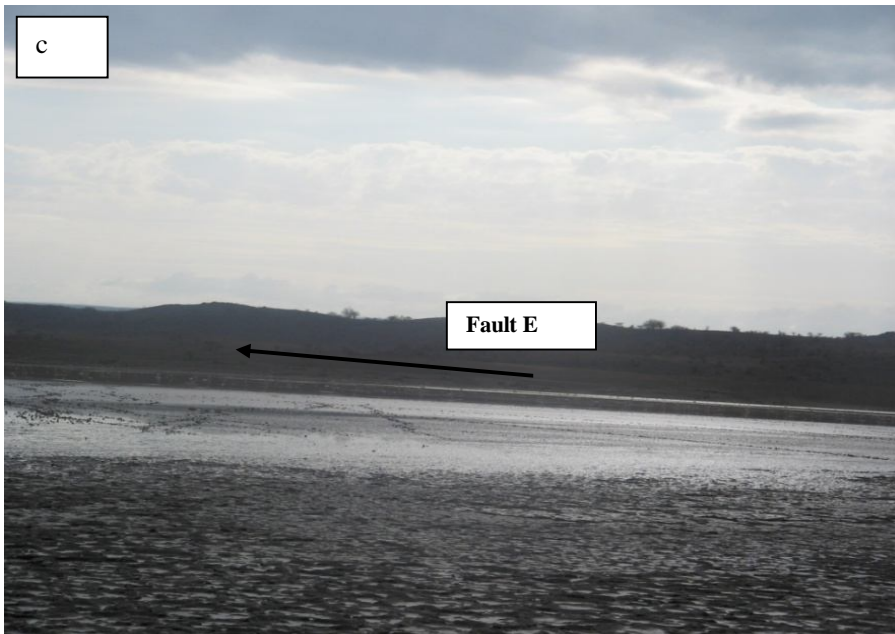
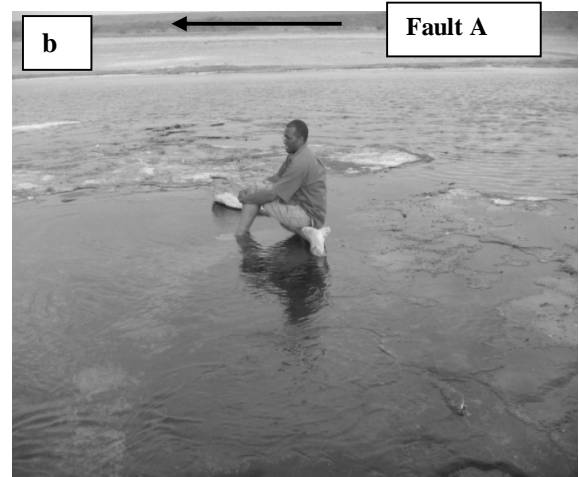
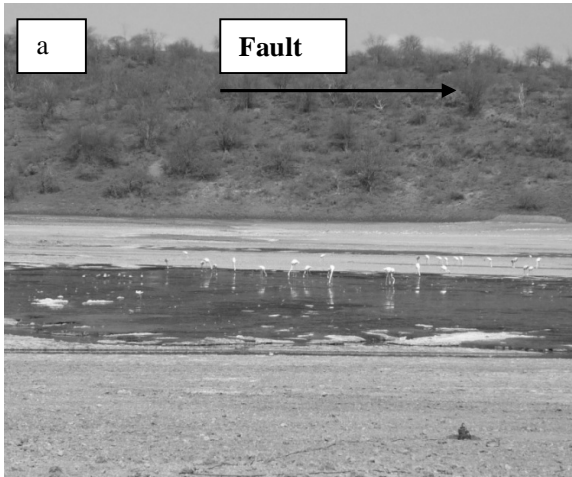
The profiles show the surface expressions of the investigated faults in the study area. The basin is bounded by the faults A and D to the west and to the east.





Appendix: 04. Photos of hot and cold springs along Magadi Lake's margin

Photo **a** and **b** are hot springs locations between Faults A and B in the study area. Photo **b** is a cold saline spring between Faults D and E. The arrows are pointing north. The hotness and saline nature of this zone is probably responsible for the low resistivity observed in resistivity profiles.



Appendix: 05: 2D power spectrum

The grid was generated the log power spectrum in Figure 5.1. It shows the magnetic spectral differences as related to the depth of magnetic sources.

